Nuclear Science
NEA/NSC/R(2021)5
April 2023
www.oecd-nea.org

Benchmark for Uncertainty Analysis in Modelling (UAM) for Design, Operation and Safety Analysis of Light Water Reactors

Volume I. Neutronics Phase (Phase I)

OECD
BETTER POLICIES FOR BETTER LIVES

NEA
NUCLEAR ENERGY AGENCY

Nuclear Energy Agency

NEA/NSC/R(2021)5

Unclassified

English text only

18 April 2023

NUCLEAR ENERGY AGENCY
NUCLEAR SCIENCE COMMITTEE

Benchmark for Uncertainty Analysis in Modelling (UAM) for Design, Operation and Safety Analysis of Light Water Reactors

Volume I. Neutronics Phase (Phase I)

This document is available in PDF format only.

JT03517040

Benchmark for Uncertainty Analysis in Modelling (UAM) for Design, Operation and Safety Analysis of Light Water Reactors

Volume I. Neutronics Phase (Phase I)

G. Delipei, J. Hou, M. Avramova, K. Ivanov

April 2023
Nuclear Energy Agency

ORGANISATION FOR ECONOMIC CO-OPERATION AND DEVELOPMENT

The OECD is a unique forum where the governments of 38 democracies work together to address the economic, social and environmental challenges of globalisation. The OECD is also at the forefront of efforts to understand and to help governments respond to new developments and concerns, such as corporate governance, the information economy and the challenges of an ageing population. The Organisation provides a setting where governments can compare policy experiences, seek answers to common problems, identify good practice and work to co-ordinate domestic and international policies.

The OECD member countries are: Australia, Austria, Belgium, Canada, Chile, Colombia, Costa Rica, the Czech Republic, Denmark, Estonia, Finland, France, Germany, Greece, Hungary, Iceland, Ireland, Israel, Italy, Japan, Korea, Latvia, Lithuania, Luxembourg, Mexico, the Netherlands, New Zealand, Norway, Poland, Portugal, the Slovak Republic, Slovenia, Spain, Sweden, Switzerland, Türkiye, the United Kingdom and the United States. The European Commission takes part in the work of the OECD.

OECD Publishing disseminates widely the results of the Organisation's statistics gathering and research on economic, social and environmental issues, as well as the conventions, guidelines and standards agreed by its members.

NUCLEAR ENERGY AGENCY

The OECD Nuclear Energy Agency (NEA) was established on 1 February 1958. Current NEA membership consists of 34 countries: Argentina, Australia, Austria, Belgium, Bulgaria, Canada, the Czech Republic, Denmark, Finland, France, Germany, Greece, Hungary, Iceland, Ireland, Italy, Japan, Korea, Luxembourg, Mexico, the Netherlands, Norway, Poland, Portugal, Romania, Russia (suspended), the Slovak Republic, Slovenia, Spain, Sweden, Switzerland, Türkiye, the United Kingdom and the United States. The European Commission and the International Atomic Energy Agency also take part in the work of the Agency.

The mission of the NEA is:

– to assist its member countries in maintaining and further developing, through international co-operation, the scientific, technological and legal bases required for a safe, environmentally sound and economical use of nuclear energy for peaceful purposes;

– to provide authoritative assessments and to forge common understandings on key issues as input to government decisions on nuclear energy policy and to broader OECD analyses in areas such as energy and the sustainable development of low-carbon economies.

Specific areas of competence of the NEA include the safety and regulation of nuclear activities, radioactive waste management and decommissioning, radiological protection, nuclear science, economic and technical analyses of the nuclear fuel cycle, nuclear law and liability, and public information. The NEA Data Bank provides nuclear data and computer program services for participating countries.

Foreword

Since the early 2000s there is an increasing demand from nuclear research, industry, safety and regulation for best-estimate predictions to be provided with their confidence bounds. Consequently, an in-depth discussion on uncertainty analysis in modelling was organised at the June 2005 Nuclear Science Committee (NSC) meeting of the Nuclear Energy Agency (NEA). Furthermore, discussions were held at the 2005 International Conference on Mathematics and Computational Methods Applied to Nuclear Science and Engineering (M&C) in Avignon and the Washington American Nuclear Society (ANS) meetings. A workshop on uncertainty analysis in modelling (UAM) was held in April 2006 at the University of Pisa, Italy, to define future actions and a programme of work. This resulted in the endorsement of the NEA Expert Group on Uncertainty Analysis in Modelling (EGUAM) under the auspices of the Working Party on Scientific Issues in Reactor Systems (WPRS) by the NSC at its June 2006 meeting.

Analysis of existing and near-term light water reactors (LWRs) was identified as a high priority. To foster and share best practices on uncertainty analysis studies in modelling in light water systems, the EGUAM created a comprehensive set of benchmark exercises covering pressurised water reactor (PWR), boiling water reactor (BWR) and water-water energetic reactor (VVER) systems. These exercises are separated into three phases: (1) neutronics, (2) core and (3) system, with the ultimate objective of determining the uncertainties in LWR systems arising from all stages of a coupled reactor physics/thermal-hydraulics calculation.

This report summarises the final results of Phase I, which consists of exercises at the three different scales of pin cell, fuel pin lattice, and reactor core with the aim of examining the propagation of neutronics uncertainties from small to full scale modelling. Altogether, 48 results were submitted by 20 organisations, from 12 countries. This extraordinarily large participation reflects the success of the benchmark activity in creating a community of practice that has advanced uncertainty analysis and modelling methods, fulfilling the initial purpose to share best practices and lessons learnt throughout the course of the activity. This report on the Phase 1 results provides important insights into best practices in the domain of uncertainty analysis, and provides important feedback to the nuclear data community in its burgeoning efforts to improve and complement uncertainty information in the nuclear data evaluations.

Acknowledgements

The UAM Phase I final report has benefitted from the contribution of many individuals who provided data analysis and detailed reviews of the final results. In particular, the NEA expresses its sincere gratitude to Grigorios Delipei, Jason Hou, Maria Avramova and Kostadin Ivanov for their preparation of the final manuscript.

Name	Country	Establishment	Contribution
Maria Avramova	United States	North Carolina State University	Final Manuscript Preparation
Oliver Buss		OECD Nuclear Energy Agency	NEA Secretariat
Grigorios Delipei	United States	North Carolina State University	Final Manuscript Preparation
Nuria Garcia-Herranz	Spain	Universidad Politécnica de Madrid	Reviewer
Christopher Gozum	United States	North Carolina State University	Data Processing
Xiaoyu Guo	China	Tsinghua University	Reviewer
Jon Helton	United States	Sandia National Laboratories	Reviewer
Ian Hill		OECD Nuclear Energy Agency	NEA Secretariat
Jason Hou	United States	North Carolina State University	Final Manuscript Preparation
Mathieu Hursin	Switzerland	Paul Scherrer Institute	Reviewer
Kostadin Ivanov	United States	North Carolina State University	Final Manuscript Preparation
Ben Lindley	United Kingdom	Jacobs	Reviewer
Ivan Maldonado	United States	University of Tennessee	Reviewer
Cameron Maras	United States	North Carolina State University	Data Processing
Winfried Zwermann	Germany	Gesellschaft für Anlagen-und Reaktorsicherheit	Reviewer

Table of contents

Tables

Figures

List of abbreviations

AFW	Amec Foster Wheeler
ANS	American Nuclear Society
BEMUSE	Best Estimate Methods Uncertainty and Sensitivity Evaluation
BEPU	Best Estimate Plus Uncertainties
BWR	Boiling water reactor
2D	Two-dimensional
EGUAM	Expert Group on Uncertainty Analysis in Modelling (NEA)
EK	Hungarian Academy of Sciences (Hungary)
ENDF	Evaluated Nuclear Data File (United States)
GRS	Gesellschaft für Anlagen- und Reaktorsicherheit (Germany)
HFP	Hot full power
HZP	Hot zero power
JENDL	Japanese Evaluated Nuclear Data Library (Japan)
KIT	Karlsruher Institut für Technologie (Germany)
KOZ	Kozloduy
LEU	Low enriched uranium
LWR	Light water reactor
M&C	Mathematics and Computational Methods Applied to Nuclear Science and Engineering
MOX	Mixed oxide
NCSU	North Carolina State University (United States)
NDL	Nuclear data library
NEA	Nuclear Energy Agency
NESCA	South African Nuclear Energy Corporation SOC Ltd (South Africa)
NINE	Nuclear and INdustrial Engineering (Italy)
NRA	Nuclear Regulation Authority (Japan)
NSC	Nuclear Science Committee (NEA)
NWU	North-West University (South Africa)
OECD	Organisation for Economic Co-operation and Development
ORNL	Oak Ridge National Laboratory (United States)
PB	Peach Bottom
PREMIUM	Post-BEMUSE Reflood Model Input Uncertainty Methods
PSI	Paul Scherrer Institute (Switzerland)

PT	Perturbation theory
PWR	Pressurised water reactor
RSD	Relative standard deviation
SAPIUM	Systematic APproach for Input Uncertainty quantification Methodology
SNEAK	Fast spectrum zero-power assembly at Karlsruhe, Germany (Schnelle Null-Energie-Anordnung Karlsruhe)
SNU	Seoul National University (Korea)
SOARCA	State-of-the-art reactor consequence analysis
S/U	Sensitivity and uncertainty
THU/REAL	Reactor Engineering Analysis Lab of Tsinghua University, Beijing (China)
TMI	Three Mile Island
UAM	Uncertainty analysis in modelling
UMS	Uncertainty Method Study
UNIST	Ulsan National Institute of Science and Technology (Korea)
UOX	Uranium oxide
UPM	Technical University of Madrid (Universidad Politécnica de Madrid, Spain)
UPV	Valencia Polytechnic University (Universitat Politècnica de València, Spain)
UQ	Uncertainty quantification
VCM	Variance-covariance matrices
VTT	VTT Technical Research Centre (Finland)
VVER	Water-water energetic reactor
WPRS	Working Party on Scientific Issues in Reactor Systems (NEA)

Executive summary

Great efforts have been devoted to light water reactor (LWR) uncertainty quantification (UQ) within the framework of the LWR Uncertainty Analysis in Modelling (UAM) benchmark, which aims to investigate the uncertainty propagation in all modelling stages of the LWRs and guide uncertainty and sensitivity analysis methodology development. The Nuclear Energy Agency (NEA) began the development of the UAM benchmark in 2006 within the Nuclear Science Committee (NSC). The principal objective of the project is to "define, co-ordinate, conduct, and report an international benchmark for uncertainty analysis in best-estimate coupled code calculations for design, operation, and safety analysis of LWRs."

This report summarises the benchmark activities for the standalone neutronics phase (Phase I), which includes three main steps (exercises): Exercise I-1: "Cell Physics," Exercise I-2: "Lattice Physics," and Exercise I-3: "Core Physics." Different LWR types were selected based on previous benchmark work, as well as an abundance of experience and available data. In this report, a comparative analysis of the Phase I submitted results is performed to understand the general trend of the uncertainty of core parameters due to the nuclear data uncertainty. The results cover different LWR reactors: the Three Mile Island Unit 1 (TMI-1) pressurised water reactor (PWR), the Peach Bottom Unit 2 (PB-2) boiling water reactor (BWR), the Kozloduy Unit 6 (KOZ-6) water-water energetic reactor (VVER) and a Generation III reactor.

It was found that for all major exercises the predicted uncertainty of the system eigenvalue is highly dependent on the choice of the covariance libraries used in the UQ process and is less sensitive to the solution method, nuclear data library and UQ method. Comparative analysis produced similar results for all the reactor types studied, with observed uncertainty estimates due to nuclear data in all exercises (pin cell, lattice, and core) having a relative standard deviation of approximately 0.5% $\Delta k/k$. In the pin cell and lattice calculations with MOX fuel this uncertainty increases to 1%. The main reason is the larger ^{239}Pu nu-bar uncertainty compared to the ^{235}U nu-bar. The largest contributors to the eigenvalue uncertainties are the ^{235}U nu-bar and the ^{238}U capture in the UO_2 fuel and the ^{239}Pu nu-bar in the MOX fuel. Further improvement on the nuclear data uncertainties, especially the assessment of ^{235}U nu-bar reaction, is necessary in order to reduce the uncertainty of the reactor simulation results.

In the assembly lattice exercises, higher uncertainties are predicted for the fast group constants compared to the thermal group constants with differences up to one order of magnitude. This is attributed to the fact that most of the cross sections have higher uncertainties in high energies due to the lack of available measurements in these regions, especially if resonances are present. Additionally, the correlation matrices obtained from these exercises share some common major trends such as the high positive correlation between total, absorption and scattering cross sections. However, differences are found in case-by-case comparisons indicating an impact of the selected neutronics modelling and of the selected base nuclear data library.

In the core exercises, the predicted relative standard deviation of the radial and axial power, for most of the cores, is below 10%. An exception is the radial power profile of the Generation III core, when a mixture of UOX/MOX assemblies is considered. Finally, it is important to note that the bias in most of the studies was found to be significant and up to the order of the estimated uncertainty. This indicates a need for better quantification of the bias/variance through more code to code and code to experiments comparisons.

1. Introduction

Much effort has been invested in the last decades to improve the safety assessment of nuclear power plants. The first study of the probabilistic risk assessment (PRA) can be traced back to 1975 (United States Nuclear Regulatory Commission, 1975[1]). The 1979 accident at Three Mile Island motivated the research in improving the PRA methods and together with the development of computer models led to NUREG-1150 (United States Nuclear Regulatory Commission, 1990-1991[2]), an updated PRA for five different nuclear power plants. The continuous improvement in the computer models due to the better understanding of the underlying physical phenomena and the increase of the computational resources lead to the development of Best Estimate Plus Uncertainties (BEPU) approaches (Rohatgi and Kaizer, 2020[3]). In BEPU, best-estimate codes are used in an uncertainty quantification framework in order to better assess the design margins. Various international projects were conducted concerning the system thermal-hydraulics uncertainty quantification such as the Uncertainty Method Study (UMS) for Advanced Best Estimate Thermal Hydraulic Code Applications (NEA, 1998[4]) and the Best Estimate Methods Uncertainty and Sensitivity Evaluation (BEMUSE) (NEA, 2013[5]). One of the main conclusions of these projects was the importance of the input uncertainty quantification. For this reason, the Post-BEMUSE Reflood Model Input Uncertainty Methods (PREMIUM) benchmark (NEA, 2016[6]) was launched highlighting the importance of the user-effect and identifying the need for a more systematic approach. Such an approach was developed through the SAPIUM project (Baccou et al., 2018[7]). Additionally, the SOARCA project (United States Nuclear Regulatory Commission, 2012[8]) developed best estimates for the consequences from potential nuclear power plant severe accidents. These estimates indicated a reduced impact on the public health.

In this general context, the Nuclear Energy Agency (NEA) Benchmark for Uncertainty Analysis in Modelling (UAM) for the Design, Operation and Safety Analysis of Light Water Reactors (LWRs), known as the LWR-UAM benchmark (NEA, 2013[9]), has been established for over a decade to facilitate the development and validation of available sensitivity and uncertainty (S/U) analysis methods for best-estimate LWR design and safety calculations. The high-level approach to the LWR-UAM benchmark involves the full chain of uncertainty propagation from basic data and engineering uncertainties, across different scales (multi-scale) and physics phenomena (multi-physics). Uncertainty propagation methods are tested on a number of benchmark exercises for which experimental data are available and for which the power plant details have been released.

LWR-UAM covers three main domains of nuclear reactor engineering, namely neutronics, thermal-hydraulics, and fuel thermal/mechanical behaviour. The major sources of uncertainty are to be determined from these types of calculations, which may arise from data (nuclear data, geometry, materials), numerical methods and physical models. The benchmark takes into consideration a large amount of pre-existing benchmarking data and engineering experience on LWRs and addresses four types of LWR: PWR, BWR and VVER.

The first phase of the benchmark (Phase I) is dedicated to standalone neutronics problems and is carried out in three steps, each step corresponding to the standard LWR simulation approach: cell physics (to produce multi-group microscopic cross section libraries), lattice physics (to derive multi-group homogenised macroscopic cross section sets), and core physics (to assess full core performance parameters). As a conclusion to the work done for Phase I, this report summarises the results of the comparative analysis of the neutronics solutions across participants for various reactor types, including the PWR, BWR, VVER and Gen-III reactors. The trends in the uncertainty due to nuclear data is the main focus of the analysis due to the relatively abundant results available. Few participants included manufacturing uncertainties, something that does not allow any thorough analysis in this phase. For Phase II and III a larger emphasis should be invested in the manufacturing uncertainties and boundary conditions.

2. LWR-UAM Phase I description

Phase I of the LWR-UAM benchmark consists of different exercises proposed to the participants for both numerical and experimental reactor cores. The exercises span PWR, BWR, VVER and Gen-III types of reactors at three different levels: pin cell, assembly lattice and full core.

Exercise I-1 concerns the pin cell calculations and includes the following studies:

- PWR-TMI-1: Numerical test for a representative pin cell of the Three Mile Island Unit 1 (TMI-1) core at Hot Zero Power (HZP) and Hot Full Power (HFP).
- BWR-PB-2: Numerical test for a representative pin cell of the Peach Bottom Unit 2 (PB-2) core at HZP and HFP.
- VVER-KOZ-6: Numerical test for a representative pin cell of the Kozloduy Unit 6 (KOZ-6) core at HZP and HFP.
- GEN-III: Numerical test for a representative pin cell of a Generation III LWR core at HFP.
- KRITZ-2: Experimental tests for KRITZ-2:1 (UOX), KRITZ-2:13 (UOX) and KRITZ-2:19 (MOX) low enriched uranium (LEU) critical experiments at cold and hot conditions (NEA, 2021[10]).

For all these tests, the participants are requested to provide results for the estimated mean and uncertainty of the *k*-inf, one-group microscopic cross sections and top five neutron-nuclide reactions. To study the uncertainties in fuel pin burn-up calculations, an additional Exercise I-1b was considered where a depletion is studied for a TMI-1 fuel pin. The requested results involve the estimation of the mean and uncertainty of the *k*-inf, collapsed cross sections, reaction rates and major isotopes concentrations for actinides and fission products. The results should be calculated for both the core depletion period up to 60 GWd/t and the cooling period up to 100 years.

Exercise I-2 concerns the assembly lattice calculations and includes the following studies:

- PWR-TMI-1: Numerical test for a representative 2D assembly colourset of the TMI-1 core at HZP and HFP with and without the presence of control rods. Numerical test for 1D assembly/reflector colourset for calculating the discontinuity factors (DF) at HZP and HFP. Numerical test for 2D minicore colourset consisting of 9 TMI-1 fuel assemblies at HZP and HFP.
- BWR-PB-2: Numerical test for a representative 2D assembly colourset of the PB-2 core at HZP and HFP with and without the presence of control rods. Numerical test for 1D assembly/reflector colourset for calculating the discontinuity factors (DF) at HZP and HFP. Numerical test for 2D minicore colourset consisting of 4 PB-2 fuel assemblies at HZP and HFP.
- VVER-KOZ-6: Numerical test for a representative 2D assembly colourset of the KOZ-6 core at HZP and HFP with and without the presence of control rods. Numerical test for 1D assembly/reflector colourset for calculating the discontinuity factors (DF) at HZP and HFP. Numerical test for 2D minicore colourset consisting of 7 KOZ-6 fuel assemblies at HZP and HFP.
- GEN-III: Numerical test for a representative 2D assembly colourset of a Generation III LWR core at HZP and HFP with and without the presence of control rods. A total number of 4 assemblies are studied: UOX without Gd rods (T1), UOX with 12 Gd rods (T2), UOX with 20 Gd rods (T3) and MOX without Gd rods (T4).
- KRITZ-2: Experimental tests for KRITZ-2:1 (UOX), KRITZ-2:13 (UOX) and KRITZ-2:19 (MOX) low enriched uranium (LEU) critical experiments at cold and hot conditions.

For all these studies, the main results requested by the participants are the estimated mean and uncertainty of the *k*-inf, the homogenised two-group macroscopic cross sections, the discontinuity factors and the pin power distribution.

Exercise I-3 concerns the full core calculations and includes the following studies:

- PWR-TMI-1: Numerical test for 3D model of TMI-1 core at HZP.
- BWR-PB-2: Numerical test for 3D model of PB-2 core at HZP.
- VVER-KOZ-6: Numerical test for 3D model of KOZ-6 core at HZP.
- GEN-III: Numerical test for 3D model of one UOX and one UOX/MOX Generation III core at HZP and HFP.
- BWR-QC1: Experimental test for 3D model of Quad Cities unit 1 BWR unit 1 core.
- PWR-B&W: Experimental test for 3D model of B&W research centre core.
- VVER-LR-0: Experimental test for 3D model of LR-0 zero-power reactor core.
- SNEAK: Fast reactor experimental test for 3D model SNEAK 7A & 7B benchmark experiments (NEA, 2021[11]).

For all these studies, the main results requested by the participants are the estimated mean and uncertainty of the *k*-eff, core axial and radial power distribution, relative pin power distribution and assembly reaction rates for selected fuel assemblies.

In general, there are two broad types of uncertainties (Roy and Oberkampf, 2011[12]):

- **Stochastic (aleatoric)** uncertainty**:** Sources of uncertainties due to natural inherent variability that are considered irreducible. This means that for the same conditions the uncertain variables will vary stochastically (e.g. temperature of a room). A common approach to model these uncertainties is by considering the variables as random and characterised by their probability density function (pdf) that can be determined through enough observations.
- **Epistemic uncertainty**: Sources of uncertainties due to lack of knowledge. It is usually related to modelling and it reflects various sources from numerical approximation to physical models. This uncertainty can be reduced by acquiring more insights about the underlying physical phenomena through experiments, improved numerical solutions, etc. A common approach to model these uncertainties is by using intervals. If a pdf is employed, then it corresponds to a degree of belief in a Bayesian context.

The source of the inputs uncertainty considered in Phase I exercises includes the neutron cross section data, supplemented by the variance-covariance matrices (VCMs), and as-built manufacturing uncertainties in material composition and geometric dimensions. All these sources of uncertainties are considered stochastic. The nuclear data are characterised as multivariate normal with their corresponding VCM and the other sources are considered independent and thus characterised by their marginal pdf. Few participants included the manufacturing uncertainties in Phase I and thus the focus of this report is mainly on the nuclear data.

Two sets of uncertainty quantification (UQ) methods were pursued by the participants, namely deterministic and stochastic methods. The deterministic method calculates the sensitivity of the system response R with respect to uncertain input parameter σ using perturbation theory (PT) and computes an estimate for the response variance $Var[R]$ by linearising the response $R \approx S\sigma$. Here, S is the response sensitivity vector that can be calculated using various codes and examples are given

in (Rearden et al., 2009[13]; Pusa, 2012[14]). With the linearisation, the variance of the response can be calculated by folding sensitivities with the VCM of input parameters:

$$\boldsymbol{Var[R] \approx Var[S\sigma] = SCov[\sigma]S^T} \quad \textbf{(1)}$$

where $Cov[\sigma]$ denotes the VCM of the input parameter σ. Eq. (1) is known as the first-order uncertainty propagation formula or the "Sandwich rule". The sampling method relies on sampling the uncertain input parameters using the VCM, assuming usually multivariate normal distribution, and statistically analysing the calculated output responses. The variance is computed using:

$$\boldsymbol{Var[R] = \frac{\sum_{i=1}^{N_s}(R_i - \bar{R})^2}{N_s - 1}} \quad \textbf{(2)}$$

where N_s is the number of samples and $\bar{R}$ is the sample mean of the response. Examples of the implementation of the statistical sampling can be found in (Krzykacz, Hofer and Kloos, 1994[15]; Williams et al., 2013[16]). Both deterministic and sampling methods have advantages and drawbacks. The deterministic method does not need many code evaluations and thus is computationally efficient, but it assumes a linear relationship between the inputs and outputs and requires codes that have the capability of applying PT. The sampling method is black-box with regards to the codes and does not make any approximation for the inputs/outputs relationship, but it requires a larger number of code evaluations in order to estimate the desired statistical quantities.

There are many results that are requested from the participants and in order to facilitate the report structure the most important ones for each exercise are selected and analysed. For Exercise I-1 the report focuses on the *k*-inf uncertainties and the top five reactions contributing to this uncertainty. The focus for Exercise I-2, which is tightly related with the conventional two-step LWR uncertainty propagation approach, is on the *k*-inf uncertainties, some representative two-group macroscopic cross sections, the correlation matrices among the two-group cross sections and the radial power distribution of the minicore coloursets. The section on Exercise I-3 focuses on *k*-eff uncertainties and the radial and axial power distribution in the core. Concerning the five most important neutron-nuclide reactions for the *k*-inf, there is no requirement by the benchmark on the method used to rank the reactions. The results are qualitative, since they do not quantify the importance of each reaction, and the participants could use a variety of available methods such as the correlation coefficients (Iooss and Lemaître, 2015[17]) or the PT sensitivities (Smith, 2013[18]).

A total of 48 submitted results were processed, as can be seen in Table 2.1, from participants using different neutronics codes, nuclear data libraries (NDL), covariance libraries and uncertainty quantification methods. Additional details concerning the submitted results are provided in Annex A. Results were provided for most of the benchmark exercises. For only the I-3 BWR-QC1 and SNEAK experimental studies there were no results and thus they are not included in the following analysis. Most participants focused on the quantification and propagation of nuclear data induced uncertainty, thus the VCM is simply the nuclear data covariance information, available either by processing covariance data files provided by major NDLs or in the SCALE code package (Wieselquist, Lefebvre and Jessee, 2020[19]). Two SCALE VCMs have been proposed for the benchmark: the 44-group library distributed with SCALE 6.0 and 6.1, and the updated library available in SCALE 6.2, which is provided in a 56-group and 252-group structure (Marshall et al., 2015[20]). The former contains uncertainty data for 401 materials with important isotopes taken from high-fidelity nuclear data evaluations including ENDF/B-VII.0, ENDF/B-VI and JENDL-3.3. The latter is based on the ENDF/B-VII.1 data for 187 nuclides, combined with information of ~215 nuclides from the SCALE 6.1 VCM. So-called "low-fidelity" uncertainties from a collaboration of BNL, LANL, and ORNL are also considered (Little et al., 2008[21]). It should be noted here that although the SCALE 6.0 and 6.1 VCMs are identical, in the presented results they are treated as

separate. For facilitating the discussion, all mentions to SCALE 6.0/6.1 will correspond to the 44-group VCM library, while all mentions to SCALE 6.2 will correspond to the 56-group VCM library. In many cases, the SCALE VCMs were transformed into a user-specified energy group structure to satisfy the requirements of the neutronics code used in the UQ process; this can be accomplished with the ANGELO tool (NEA, 2003[22]).

In Chapter 3, a comparative analysis is performed for the numerical exercises organised by type of reactor. First, the results for the PWR I-1, I-2 and I-3 are presented followed by the BWR, VVER and GEN-III corresponding exercises. Chapter 4 provides a comparative analysis for the experimental exercises and Chapter 5 presents a cross-exercise analysis. Lastly, Chapter 6 provides a summary of the main conclusions of the LWR-UAM benchmark Phase I results.

Table 2.1. Summary of submitted benchmark results

Case	Contributor	NDL	Transport Code	VCM	UQ Method	PWR Cases	BWR Cases	VVER Cases	GEN3 Cases	Experi-mental Cases
1	NINE	ENDF/B-VI	SERPENT 2	SCALE 6.0	Deterministic	I-1, I-2	I-1	I-1		
2	NINE	ENDF/B-V	SCALE 6.0	SCALE 6.0	Deterministic					I-1
3	MTA EK	ENDF/B-VI	MULTICELL	SCALE 5.1	Sampling	I-1, I-2	I-1	I-1, I-2		
4	MTA EK	ENDF/B-VI	MULTICELL	SCALE 5.1	Sampling	I-2		I-2		
5	MTA EK	ENDF/B-VI	KIKO3D	SCALE 5.1	Sampling			I-3		
6	KIT	ENDF/B-VII.0	XSDRNPM	SCALE 6.1	Deterministic	I-1	I-1	I-1, I-2	I-1	I-1
7	VTT	ENDF/B-VI	CASMO4/SIMULATE3	SCALE 6.0	Deterministic	I-1, I-2, I-3	I-1, I-2		I-1	
8	PSI	ENDF/B-VII.0	CASMO-5MX	SCALE 5.1	Sampling	I-1	I-1		I-1	I-1
9	NECSA	ENDF/B-VII.0	NEWT	SCALE 6.1	Deterministic	I-1, I-2	I-1			
10	NECSA	ENDF/B-VI	MGRAC	SCALE 6.1	Sampling	I-3				
11	UPM	ENDF/B-VII	MCNP5	SCALE 6.0	Deterministic	I-1	I-1			
12	UPM	ENDF/B-VII.0	NEWT	SCALE 6.1	Deterministic	I-2	I-2			
13	UPM	ENDF/B-VII.0	NEWT	SCALE 6.2	Sampling	I-2				
14	UPM	ENDF/B-VII.1	COBAYA	SCALE 6.2	Sampling	I-3				
15	UPM	ENDF/B-VII.1	COBAYA	SCALE 6.2	Sampling	I-3				
16	UPM	ENDF/B-VII.1	COBAYA	SCALE 6.2	Sampling	I-3				
17	UPM	ENDF/B-VII.1	COBAYA	SCALE 6.2	Sampling	I-3				
18	McMaster	ENDF/B-VII.1	POLARIS	SCALE 6.2	Sampling	I-1	I-1			
19	McMaster	ENDF/B-VII.1	NEWT	SCALE 6.2	Sampling	I-1	I-1			
20	McMaster	ENDF/B-VII.0	NEWT	SCALE 6.2	Sampling	I-1	I-1			
21	NRA	JENDL-4.0	CASMO5/SIMULATE5	JENDL-4.0	Sampling	I-1, I-2, I-3	I-1, I-2, I-3			
22	NWU	ENDF/B-VII.0	NEWT	SCALE 6.2	Deterministic			I-1		
23	NWU	ENDF/B-VII.0	NEWT	SCALE 6.2	Deterministic			I-1		
24	NWU	ENDF/B-VII.0	NEWT	SCALE 6.2	Deterministic			I-2		
25	SNU	ENDF/B-VII.1	McCARD	ENDF/B-VII.1	Deterministic	I-1	I-1	I-1		
26	UNIST	ENDF/B-VII.1	MCS	ENDF/B-VII.1	Deterministic	I-1				
27	UNIST	ENDF/B-VII.1	MCS	SCALE 6.1	Deterministic	I-1				
28	UNIST	ENDF/B-VII.1	MCS	ENDF/B-VII.1	Deterministic	I-1, I-2, I-3				
29	UNIST	ENDF/B-VII.1	MCS	SCALE 6.1	Deterministic	I-1, I-2, I-3				
30	UNIST	ENDF/B-VII.1	STREAM	SCALE 6.2	Deterministic	I-1				
31	UNIST	ENDF/B-VII.1	STREAM	ENDF/B-VII.1	Deterministic	I-1				
32	UNIST	ENDF/B-VII.1	STREAM	ENDF/B-VII.1	Sampling	I-1				
33	GRS	ENDF/B-VII.0	NEWT/SCALE	SCALE 6.1	Deterministic	I-1, I-2	I-1, I-2	I-1, I-2	I-1, I-2, I-3	I-1, I-2, I-3
34	GRS	ENDF/B-VII.1	NEWT/SCALE	SCALE 6.2	Deterministic	I-1, I-2	I-1, I-2	I-1, I-2	I-1, I-2, I-3	I-1, I-2, I-3
35	GRS	ENDF/B-VII.1	HELIOS2	SCALE 6.1	Sampling	I-1, I-2	I-1, I-2	I-1, I-2	I-1, I-2,	I-1
36	GRS	ENDF/B-VII.0	NEWT/SCALE	SCALE 6.1	Sampling	I-1, I-2	I-1, I-2	I-1, I-2	I-1, I-2, I-3	I-1, I-2, I-3
37	GRS	ENDF/B-VII.1	NEWT/SCALE	SCALE 6.2	Sampling	I-1, I-2	I-1, I-2	I-1, I-2	I-1, I-2, I-3	I-1, I-2, I-3
38	ORNL	ENDF/B-VI	NEWT/SCALE	SCALE 6.1	Deterministic	I-1, I-2	I-1, I-2			I-3

Table 2.2. Summary of submitted benchmark results (Continued)

Case	Contributor	NDL	Transport Code	VCM	UQ Method	PWR Cases	BWR Cases	VVER Cases	GEN3 Cases	Experi-mental Cases
39	JACOBS	JEFF-3.1.2	WIMS	WIMS[1]	Sampling		I-1, I-2			
40	UPV	ENDF/B-VII.0	NEWT	SCALE 6.2	Sampling	I-2	I-2			
41	UPV	ENDF/B-VII.0	NEWT	SCALE 6.2	Sampling	I-2	I-2			
42	JACOBS	JEFF-3.1.2	WIMS/PANTHER	WIMS[1]	Sampling	I-2	I-3			
43	JACOBS	JEFF-3.1.2	WIMS	WIMS[1]	Sampling	I-2				
44	JACOBS	JEFF-3.1.2	WIMS	WIMS[1]	Sampling	I-2				
45	THU	ENDF/B VII.0	RMC	SCALE 6.2/6.12	Sampling	I-1b[2], I-3	I-3			
46	NCSU	ENDF/B-VII.1	POLARIS/PARCS	SCALE 6.2	Sampling	I-3				
47	NCSU	ENDF/B-VII.1	MPACT	ENDF/B-VII.1	Sampling	I-1, I-2	I-1, I-2			
48	Framatome GmbH	ENDF/B-VII.1	SCALE 6.0	ENDF/B-VII.1	Sampling	I-1b[3]				

Source: NEA data, 2021

[1]Covariance data were collected from various sources, including JEFF-3.2, ENDF/BV-II.1, JENDL-4.0 and TENDL-2011. For the comparison purposes it will be considered as ENDF/B-VII.1.

[2]SCALE 6.2 is used for the PWR exercises and SCALE 6.1 for the BWR exercises.

[3]Results provided only for I-1b case and not any other I-1 case.

3. Comparative analysis of numerical results

This chapter presents the results obtained for the numerical exercises and the main conclusions drawn concerning the uncertainty quantification. There are different numerical exercises spanning PWR, BWR, VVER and GEN-III type reactors at the levels of pin cell (Exercise I-1), assembly (Exercise I-2) and full core (Exercise I-3). For each exercise, a variety of results were requested from the participants with the main ones being the uncertainty of the multiplication factor, homogenised macroscopic cross sections and power distribution.

3.1. Pressurised water reactor exercises: TMI-1

3.1.1. Exercise I-1: Cell physics

For each study in Exercise I-1, the following results were requested from the participants: calculated *k*-inf and its associated uncertainty, top five neutron-nuclide reactions that contribute the most uncertainty to *k*-inf, and covariances of selected one-group cross sections generated in the pin cell calculation.

A 2D model adopted from the TMI-1 reactor was chosen as the representative PWR test problem. It is fuelled with 4.85% enriched UO2 fuel, and both HZP and HFP conditions were specified. In total, 23 sets of results have been submitted for the HZP condition, from which calculation-related information was collected to facilitate the comparative analysis of the results in order to reveal the relation between the choice of calculation parameters (e.g. transport solution method, covariance library, UQ method) and output uncertainties. Figure 3.1.a shows the predicted *k*-inf and associated uncertainties for HZP. The nominal value of *k*-inf spans a range of ~1 200 pcm, which primarily is caused by the use of different methods (i.e. deterministic vs. Monte Carlo methods based on various degree of modelling simplification), transport codes and NDLs. The averaged nominal value and relative standard deviation (RSD), or $\Delta k/k$, of all predicted *k*-inf values are 1.430 and 0.529%, respectively.

A more detailed analysis was performed to determine the correlation between each of the calculation parameters. The uncertainty of *k*-inf and the results indicate that the choice of the covariance library strongly impacts the RSD of *k*-inf, as shown in Figure 3.1.b, while other parameters have limited influence. The average RSD of *k*-inf calculated using the SCALE 6.0/6.1 covariance libraries is 0.47%, while the value corresponding to SCALE 6.2 is 0.54%. Only two datasets were submitted using the SCALE 5.1 and one using JENDL-4.0 covariance libraries and both RSDs are ~0.5%. The ENDF/B-VII.1 covariance data yields the highest *k*-inf RSD of 0.61%, despite the fact that one dataset with an extremely low uncertainty is included. Similar behaviour is observed also for the HFP condition with an average *k*-inf of 1.413 and RSD of 0.55% as can be seen in Figure 3.2. More information about the estimated mean and RSD for each covariance library can be found in Table B.1 of Appendix B.

Figure 3.1. Calculated k-inf of TMI-1 HZP unit cell physics case: (a) mean value with uncertainties, b) relative uncertainty grouped by covariance libraries utilised

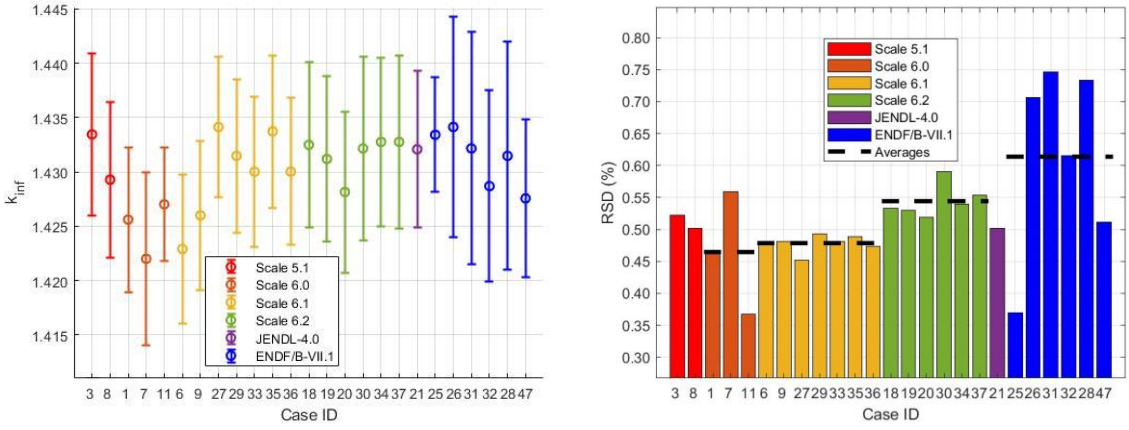

(a) (b)

Source: NEA data, 2021

Figure 3.2. Calculated k-inf for I-1 PWR-TMI-1 at HFP: (a) mean value with uncertainties, (b) RSD grouped by covariance libraries utilised.

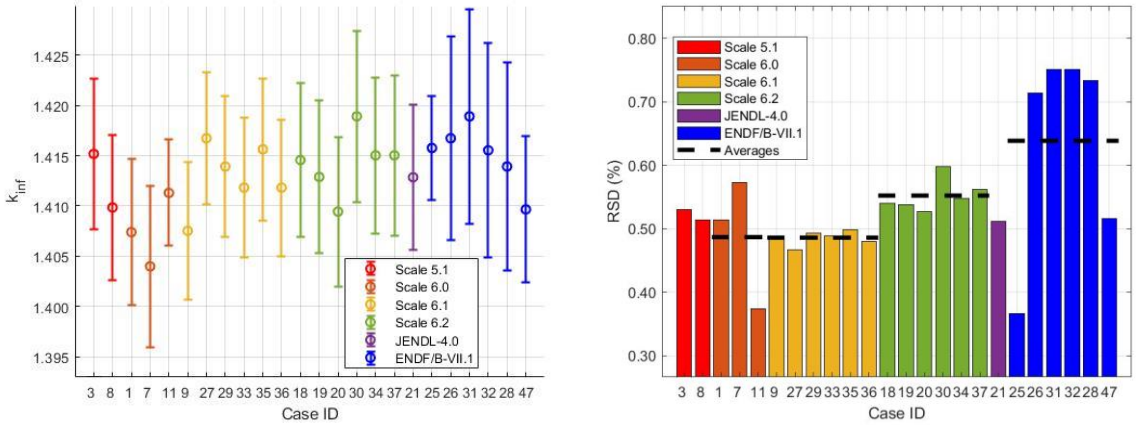

(a) (b)

Source: NEA data, 2021

The trends observed in Figure 3.1 and Figure 3.2 can be explained by the difference of the nuclear data covariance information in various sources. In one instance, the covariance data in the ENDF evaluations are generated as part of the cross section evaluation process and represent uncertainties and correlations in differential data, semi integral data and nuclear modelling. The use of this covariance to calculate uncertainties for integral quantities such as *k*-inf will usually result in an overestimation of the uncertainty as discussed in (Sobes et al., 2019[23]). Conversely, in the next instance, a range of different tests, such as the critical benchmark experiments, are performed to investigate and verify the new covariance data from the NDL before being incorporated into the SCALE covariance libraries (Marshall et al., 2013[24]). For example, two of the changes that have significant impact on many experiments are the modifications made to the covariance data for nu-bar (average number of neutrons per fission reaction $\bar{\nu}$) of ^{235}U and ^{239}Pu, with the first one being relevant to the case study shown in this report. The uncertainty of ^{235}U nu-bar in the thermal range increases from 0.31% in SCALE 6.1 to 0.7% in ENDF/B-VII.1, which is responsible for differences exhibited in the covariance testing in the low enriched, water moderated uranium oxide pin array systems (NEA, 2021[10]). Subsequently, it was reduced to 0.39% in the SCALE 6.2 library, which is consistent with the value in JENDL-3.3 (Marshall et al., 2015[20]). This explains why the calculated RSD of *k*-inf using SCALE 6.2 data is slightly higher than that using SCALE 6.0/6.1, while the value corresponding to ENDF/B-VII.1 is the largest. It is important to note that in the ENDF/B-VII.1 VCM there is a mismatch between the ^{235}U nu-bar and the ^{235}U prompt nu-bar, when they should be almost identical. In the thermal region of interest for LWR, the RSD of the ^{235}U prompt nu-bar is significantly lower ~0.15%. If the ^{235}U prompt nu-bar is used by the participants, which is in principle correct, it could lead to reduced uncertainties in the *k-inf*. This could explain partly why some participants using ENDF/B-VII.1 VCM obtained significantly lower uncertainties. For the context of this benchmark, the multi-group cross sections uncertainties are the focus, but in future studies other sources of uncertainties such as fission yields or the angular flux distribution (Fiorito, Dyrda and Fleming, 2019[25]) should be considered as well.

It is computationally efficient to use the PT method to compute the sensitivity coefficients of output variables with respect to nuclear data as compared with the sampling approach, thus making it possible to determine the most influential nuclide-reaction pair to the predicted *k*-inf uncertainties by sorting them from greatest to lowest variance fraction. For the TMI-1 HZP study, 13 sets of submitted results include such information and Figure 3.3 shows the occurrence of various nuclide-reaction pairs as the top five contributors. Although a certain degree of diversity can be found in the ranking, as it includes up to 10 nuclide-reaction pairs, some reactions dominate the contribution to the uncertainty of *k*-inf, such as ^{238}U capture, ^{235}U nu-bar and ^{235}U capture.

By definition, these main contributors to the uncertainty are identifiable due to: 1) the highest sensitivities associated with such reactions, or 2) the highest value of the associated covariances, or 3) a combination of both. For example, *k*-inf is quite sensitive to the ^{238}U capture cross section, especially in the unresolved resonance regions, where the evaluated cross sections exhibit large uncertainties (Trkov et al., 2005[26]). This is why, in one case, ^{238}U capture reaction is the predominant component of the total uncertainty when covariance libraries of SCALE 5.1/6.0/6.1 are utilised. While in other cases, ^{235}U nu-bar tops the ranking if the SCALE 6.2 or ENDF/B-VII.1 covariance library is used, which is in line with the analysis of the ENDF/B-VII.1 ^{235}U nu-bar uncertainty described above. The ^{235}U capture is another important contributor. It almost always ranks third regardless of which covariance library is used. Notably, some nuclide-reaction pairs only associate with the ENDF/B-VII.1 covariance library, including the ^{1}H capture, ^{238}U nu-bar and ^{238}U elastic scattering, which can also be explained by the difference in covariance libraries. For example, the ^{1}H thermal capture in the SCALE covariance library is adopted from JENDL 3.3 (Members of JNDC, 1992[27]), which is lower than that in ENDF/B-VII.1 by a factor of five.

Figure 3.3. Ranking of the five nuclide-reaction pairs with the highest contribution to the k-inf uncertainty

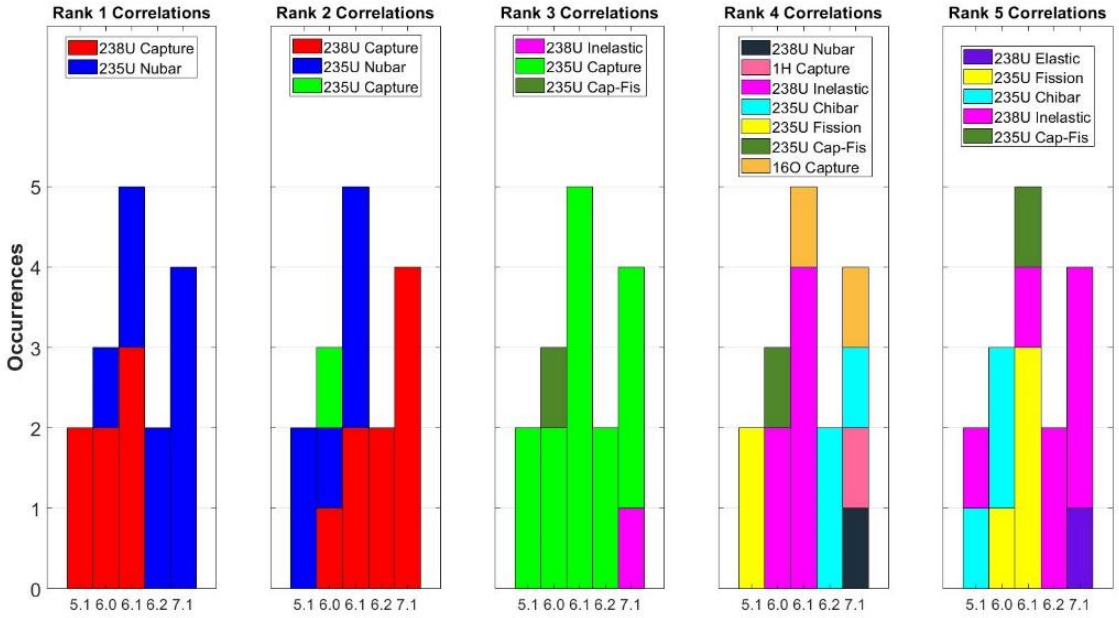

Source: NEA data, 2021

Note: SX = SCALE X covariance library, E7.1 = ENDF/B-VII.1 covariance library.

3.1.2. Exercise I-1b: Cell physics depletion

The uncertainties in the depletion calculation due to the basic nuclear data as well as the impact of processing the nuclear and covariance data were considered through an extension to Exercise I-1 denoted as I-1b. The geometry is a typical TMI-1 pin cell at HFP and the exercise is focused on propagating the uncertainties to different quantities of interest for the whole depletion up to 60 GWd/t at incremental burn-up steps of 10 GWd/t and for the cooling period up to 100 years. The quantities of interest requested by the participants are the *k-inf*, reaction rates for the major nuclides, the collapsed two-group macroscopic cross sections and the densities of isotopes of interest including actinides and fission products. A total of five participants provided results for this exercise and while all of them provided the results for the core depletion period, only one provided results for the cooling period as well. This small participation does not allow making general comparisons between the covariances and the different uncertainty propagation methods and restricts us to only preliminary analysis. It is important to mention that in these results only the cross sections uncertainties are considered. For depletion calculations, uncertainties of fission yields, decay constants and branching ratios are important as well, as highlighted in (Cabellos, 2013[28]), and should be considered in future studies. Figure 3.4 and Figure 3.5 show the results for the *k*-inf for the core depletion and cooling periods respectively. In the core depletion period, a constant increase of the RSD with burn-up from 0.5% up to 0.8% is observed. This can be attributed to the ^{239}Pu build-up because its nu-bar RSD in SCALE 6.1 44G covariance is at the order of 1% while for ^{235}U is 0.31%. Additionally, the build-up of neutron poisons such as ^{135}Xe and ^{149}Sm can also be a reason, since their neutron capture cross section in SCALE 6.1 has a much larger uncertainty compared to ^{238}U capture.

The latter reason could also explain the continuing increase of the *k*-inf RSD in the cooling period due to the accumulation of fission products that have larger neutron capture cross sections

uncertainties. Figure 3.6 and Figure 3.7 show the evolution of the ^{235}U concentration and ^{239}Pu respectively. The obtained RSD increase for both nuclides with burn-up, reaching up to 2% at the end of the irradiation. Since the nuclide concentration depends on the neutron population, this behaviour can be attributed to the same reasons with *k-inf*.

Figure 3.4. Calculated k-inf for I-1b PWR-TMI-1 at HFP core depletion period: (a) mean, (b) RSD

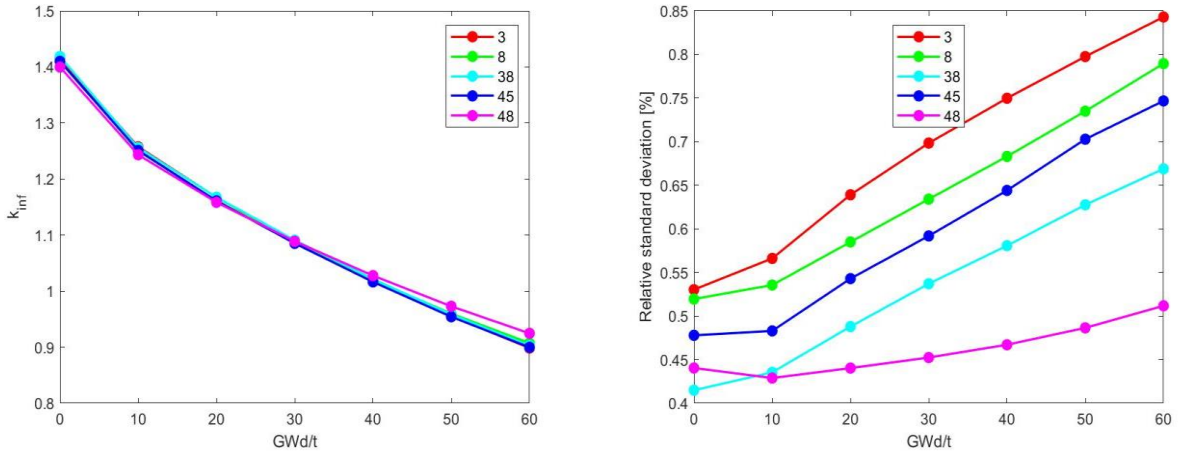

(a) (b)

Source: NEA data, 2021

Figure 3.5. Calculated k-inf for I-1b PWR-TMI-1 at HFP cooling period: (a) mean value, (b) RSD

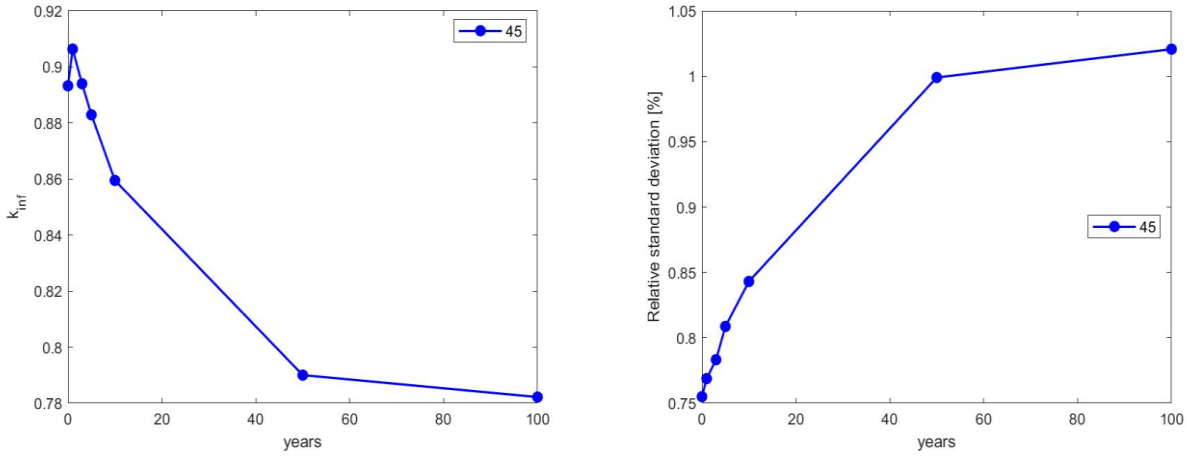

(a) (b)

Source: NEA data, 2021

Figure 3.6. Calculated concentration of 235U for I-1b PWR-TMI-1 at HFP core depletions: (a) mean value, (b) RSD

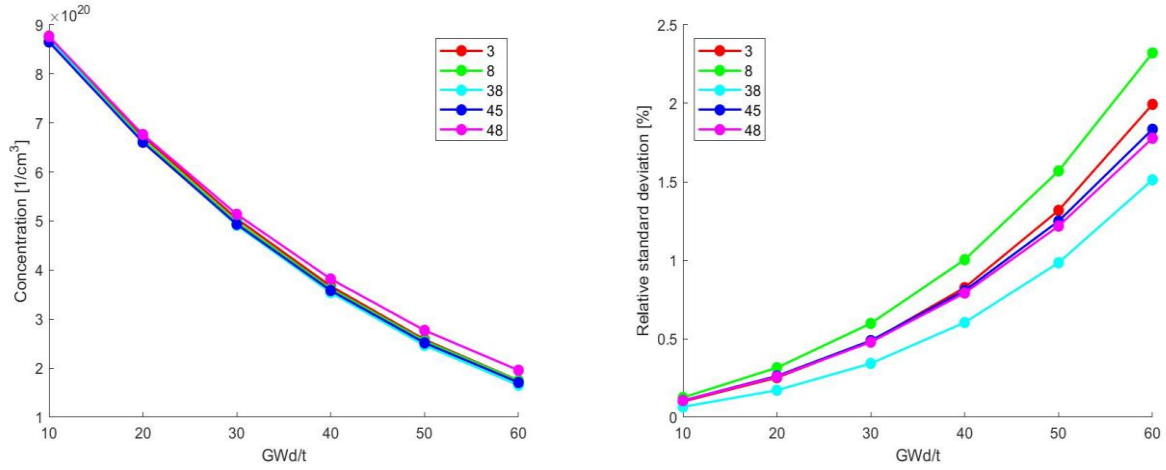

(a) (b)

Source: NEA data, 2021

Figure 3.7. Calculated concentration of 239Pu for I-1b PWR-TMI-1 at HFP core depletion: (a) mean value, (b) RSD

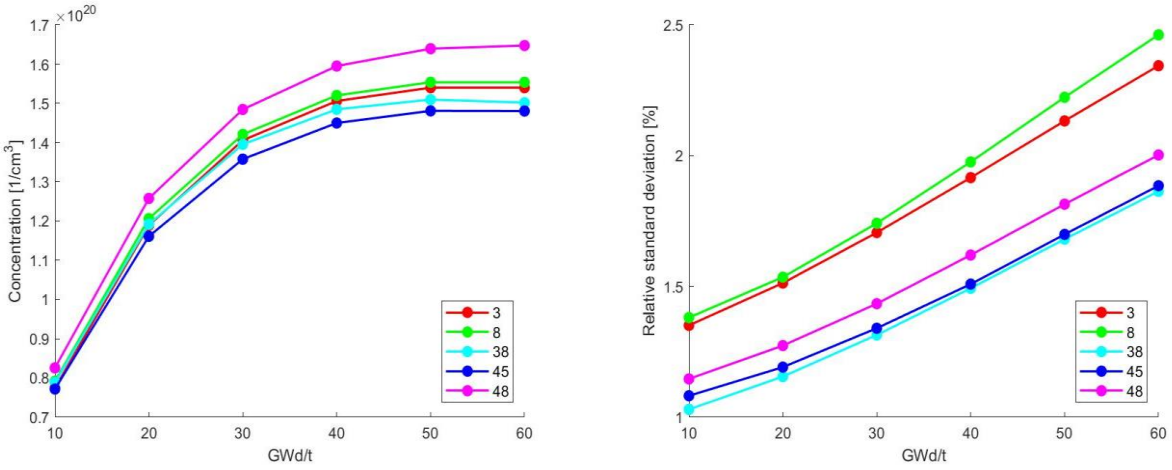

(a) (b)

Source: NEA data, 2021

Important isotopes responsible for long-term radiation after the end of a reactor's life are ^{137}Cs and ^{99}Tc. Figure 3.8 and Figure 3.9 show the evolution of the ^{137}Cs concentration with a half-life of 30 years during the core depletion and cooling periods respectively. Figure 3.10 and Figure 3.11 show the corresponding results for ^{99}Tc that has a half-life of 211 100 years.

In the core depletion period, a similar behaviour is observed for the two isotopes with a linear increase in the concentration. The RSD evolution is relatively constant with 4 cases calculating it below 1.5% while for the case 8 a much larger RSD is obtained of around 3.5%. The latter behaviour can be case specific since the case 3 uses the same covariance library (SCALE 5.1).

Figure 3.8. Calculated concentration of ^{137}Cs for I-1b PWR-TMI-1 at HFP core depletion: (a) mean value, (b) RSD

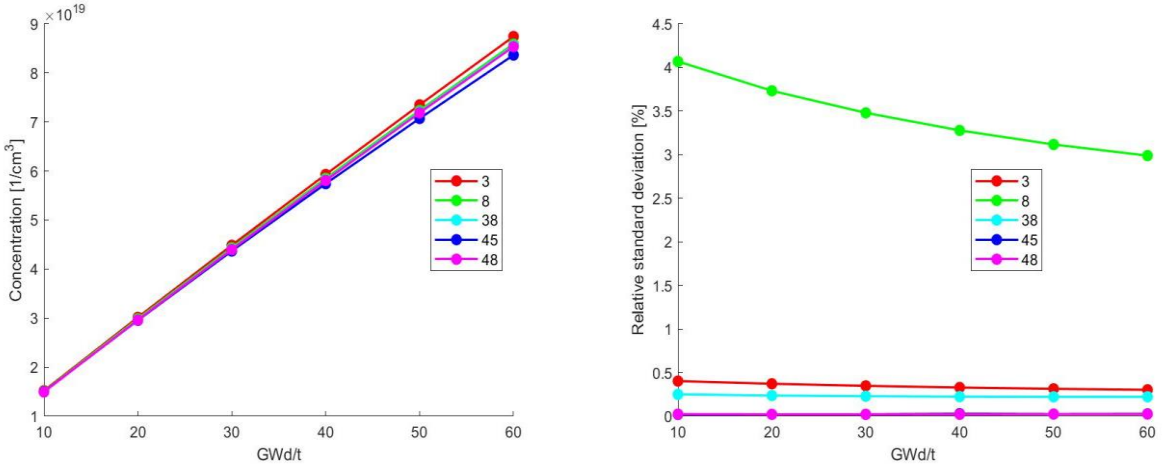

(a) (b)

Source: NEA data, 2021

Figure 3.9. Calculated concentration of 137Cs for I-1b PWR-TMI-1 at HFP cooling period: (a) mean value, (b) RSD

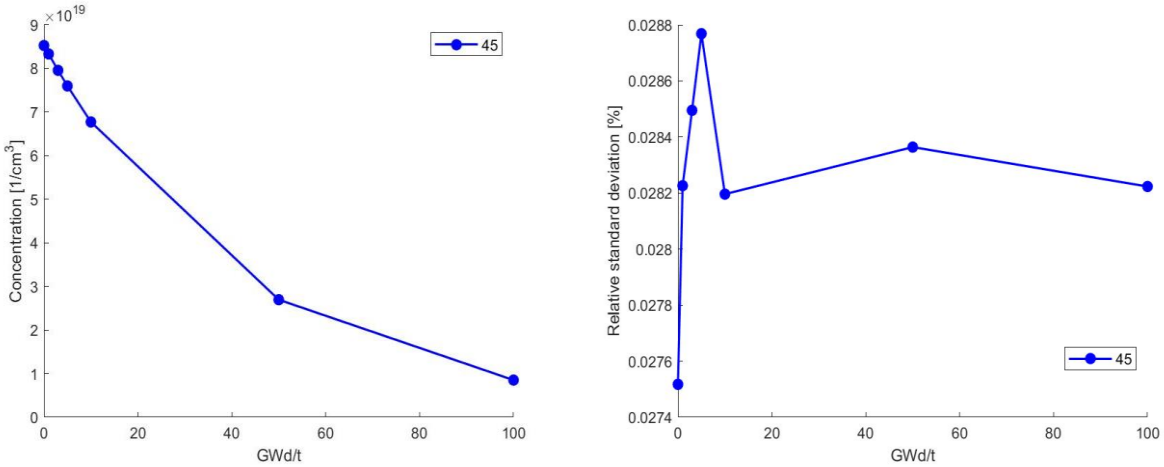

(a) (b)

Source: NEA data, 2021

Figure 3.10. Calculated concentration of ^{99}Tc for I-1b PWR-TMI-1 at HFP core depletion: (a) mean value, (b) RSD

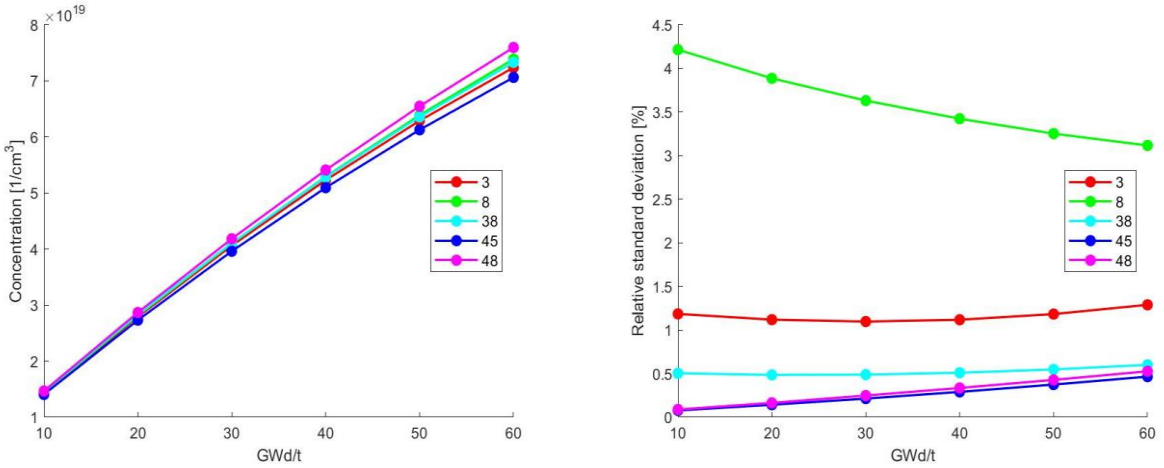

(a) (b)

Source: NEA data, 2021

Figure 3.11. Calculated concentration of ^{99}Tc for I-1b PWR-TMI-1 at HFP cooling period: (a) mean value, (b) RSD

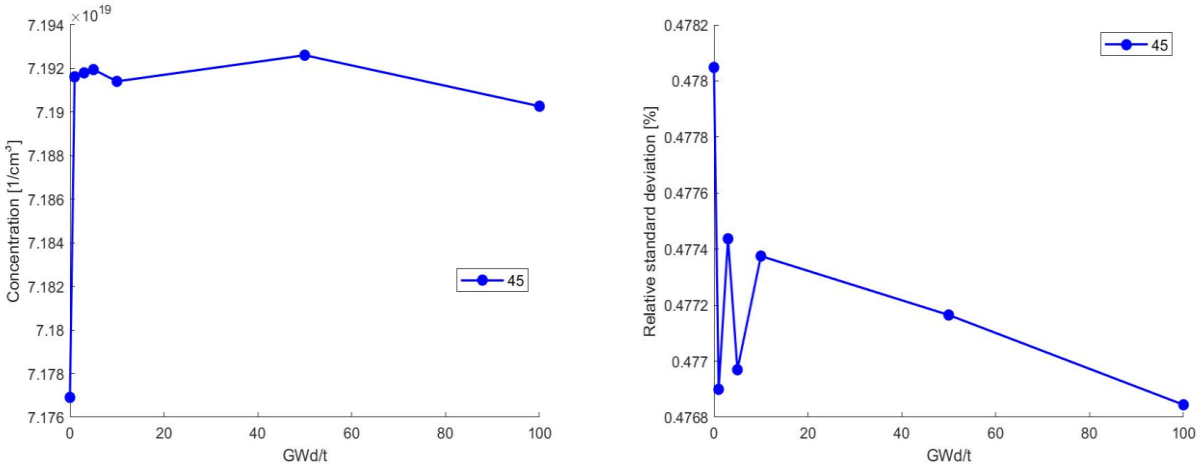

(a) (b)

Source: NEA data, 2021

In the cooling period, as expected, the concentration of ^{137}Cs decreases according to its half-life while ^{99}Tc remains constant due to its very high half-life. Both RSDs are practically constant with values of 0.028% and 0.47% respectively.

3.1.3. Exercise I-2: Lattice physics

The main focus of this exercise is the propagation of nuclear data uncertainties through lattice calculations to the uncertainty of target output variables, primarily the two-group constants. The other sources of uncertainty considered in this exercise are the uncertainties associated with methods and modelling approximations embedded in the lattice codes.

The PWR lattice model is a 2D fuel assembly of 15×15 rods with 1 central instrumental tube, 16 guide tubes and 4 corner Gd pins containing integral Gd burnable poison. The exercise is modelled under both unrodded and rodded conditions at HZP and HFP. There are 18 and 14 sets of results submitted for the HZP unrodded and rodded studies, respectively. There are 17 and 13 sets of results for the HFP unrodded and rodded studies, respectively. Figure 3.12 compares the predicted *k*-inf uncertainty of the HZP study, from which it can be seen that there are no significant differences in the RSD between the unrodded and rodded study. The RSD is at the order of 0.5% for *k-inf*. One can observe a similar trend as in I-1 PWR-TMI-1 exercise with the ENDF/B-VII.1 VCM showing larger RSD compared to the other libraries due to the larger uncertainty in ^{235}U nu-bar. What seems to be more impacted by the presence of the rod is the mean value of *k-inf*, since in the unrodded study a spread of 1 200 pcm is observed while in the rodded study it increases to 2 200 pcm. This larger difference might be related to larger differences in the cross section libraries impacting the control rod absorption and to the more complex neutron transport in the rodded studies. Further investigation needs to be performed in order to understand the source of these discrepancies. The corresponding results for the HFP studies are shown in Figure 3.13. Similar trends are obtained for both the mean and RSD of *k-inf*. More information about the estimated mean and RSD for each covariance library can be found in Table B.2 of Annex B.

Figure 3.12. Calculated k-inf for I-2 PWR-TMI-1 at HZP: (a) mean value with uncertainties for unrodded, (b) RSD for unrodded (c) mean value with uncertainties for rodded, (d) RSD for rodded

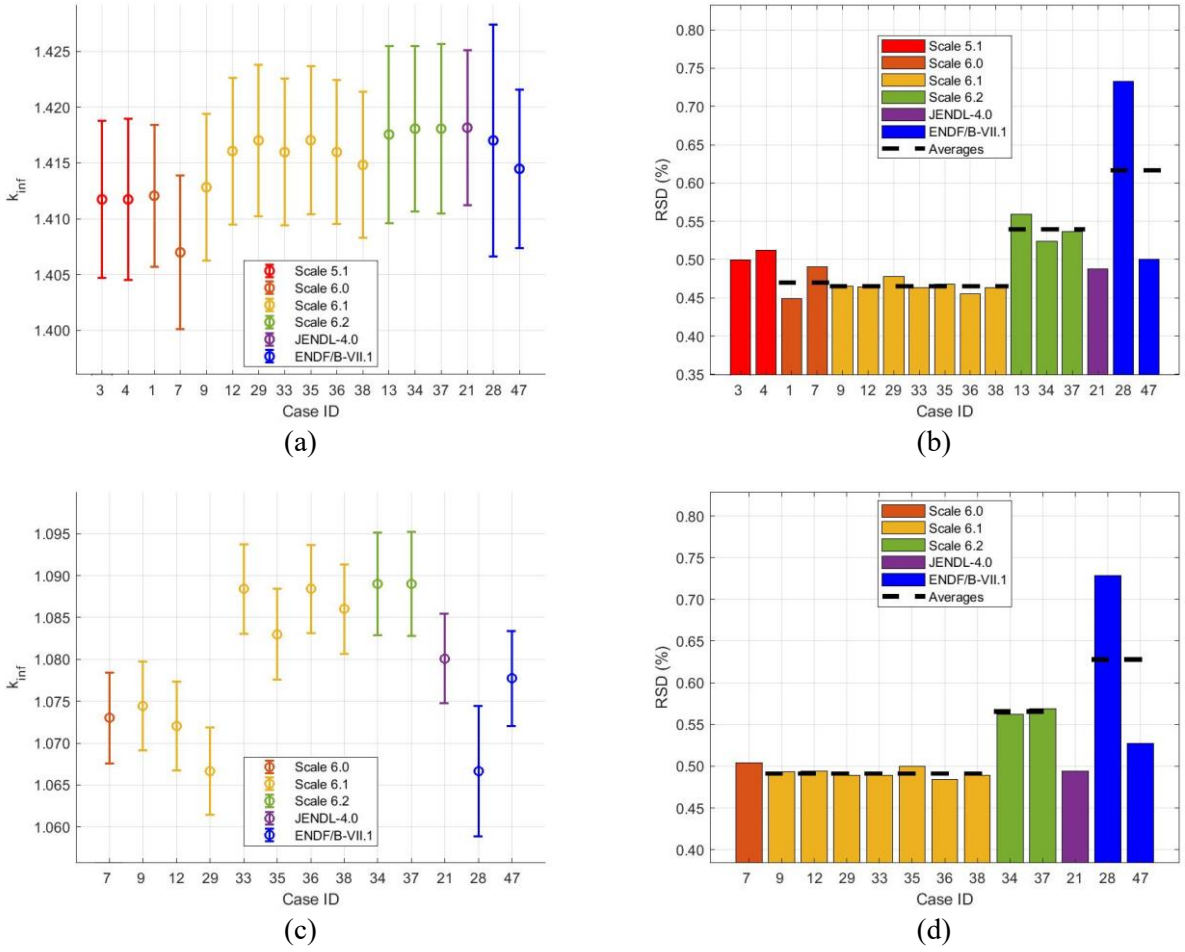

Source: NEA data, 2021

Figure 3.13. Calculated *k*-inf for I-2 PWR-TMI-1 at HFP: (a) mean value with uncertainties for unrodded, (b) RSD for unrodded (c) mean value with uncertainties for rodded, (d) RSD for rodded

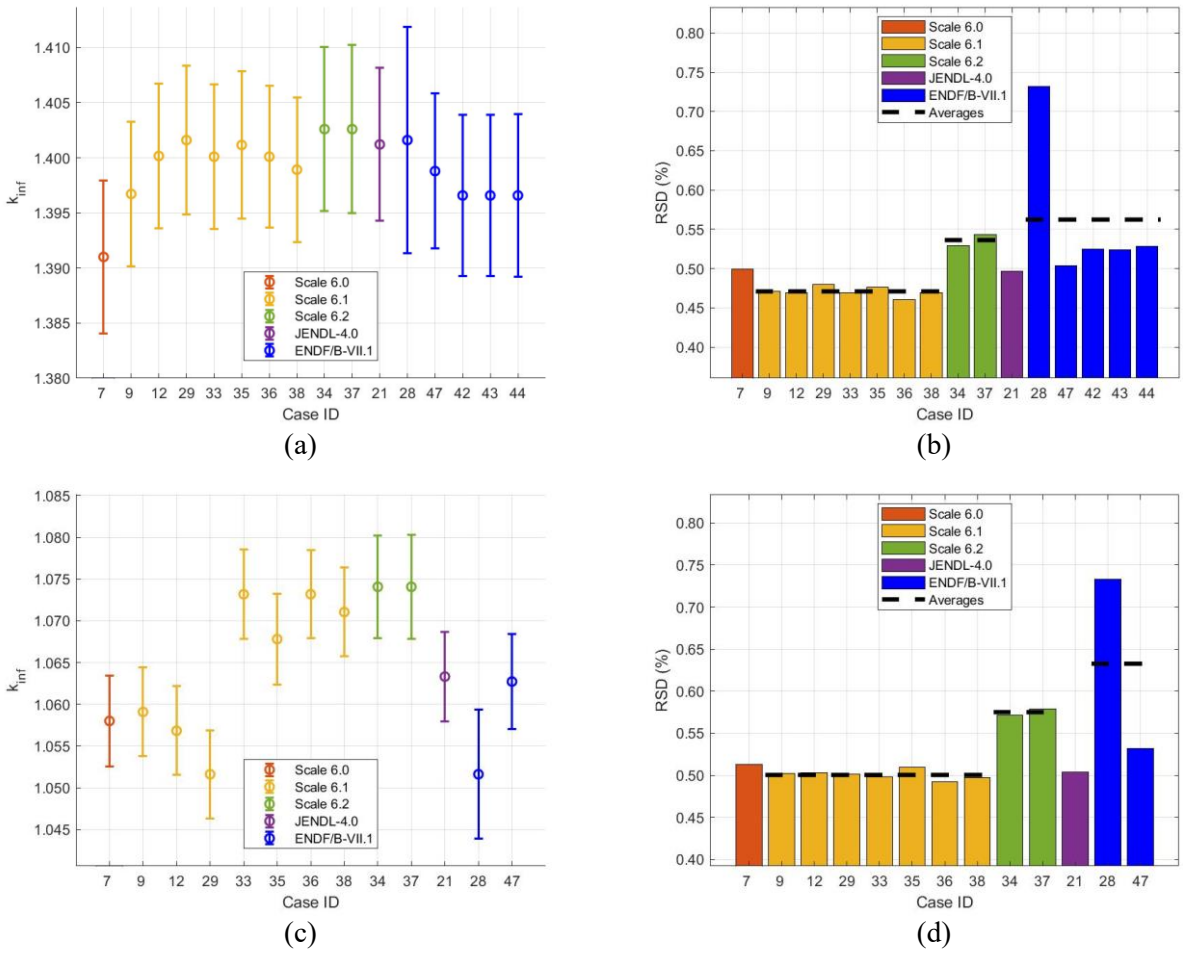

Source: NEA data, 2021

The ranking of the main contributors to the *k*-inf uncertainty follows the I-1 ranking of Figure 3.3, where the most important cross sections are the ^{235}U nu-bar and ^{238}U capture. This conclusion holds for all the studied conditions.

The uncertainties of the homogenised two-group nu-fission cross sections are compared based on the VCM, as shown in Figure 3.14 for the unrodded HFP study. Again, the higher nuclear data uncertainty of the nu-bar reaction in ENDF/B-VII.1 is responsible for the larger uncertainties. It can also be found that the uncertainty of homogenised nu-fission is larger in the fast group than the thermal group for most of the covariance libraries. For example, the value is ~1.58% in the fast group versus ~1.30% in the thermal group in case 44. The case 44 is of particular interest because it differs from case 43 in the fact that uncertainties from fuel pellet densities were also propagated. This allows assessing the strong impact of the densities, since the uncertainty increases from ~0.62% to ~1.58% in the fast group. In Figure 3.15 the corresponding results of the diffusion coefficient for unrodded HFP study are presented. Here the difference in the uncertainties between the fast and thermal group is larger. In fact, this trend is found to be more general, since for all the main group constants and for all the studied conditions (i.e. HFP, HZP, unrodded, rodded) the fast group uncertainty is larger than the thermal one. This can be attributed to the fact that for most cross sections the uncertainties are larger in the epithermal and fast groups due to the increased difficulty in obtaining accurate measurements. More information about the average RSD for each covariance

library can be found in Table B.4 and Table B.5 of Appendix B. In Figure 3.16 and Figure 3.17, shows a plot of the relative standard deviations of ^{235}U nu-bar, ^{235}U fission, ^{235}U capture and ^{238}U capture from the SCALE 6.1 44G covariance. We can clearly see that beyond the cutoff threshold of 0.625 eV the uncertainty increases significantly.

Figure 3.14. RSD of predicted $\nu\Sigma_f$ for I-2 PWR-TMI-1 at HFP unrodded study: (a) fast group, (b) thermal group

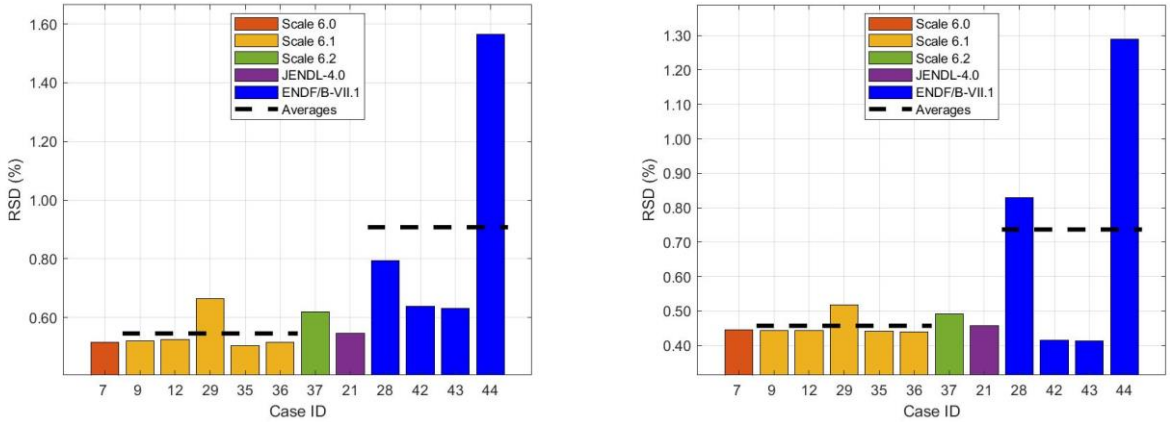

(a) (b)

Source: NEA data, 2021

Figure 3.15. RSD of predicted D for I-2 PWR-TMI-1 at HFP unrodded study: (a) fast group, (b) thermal group

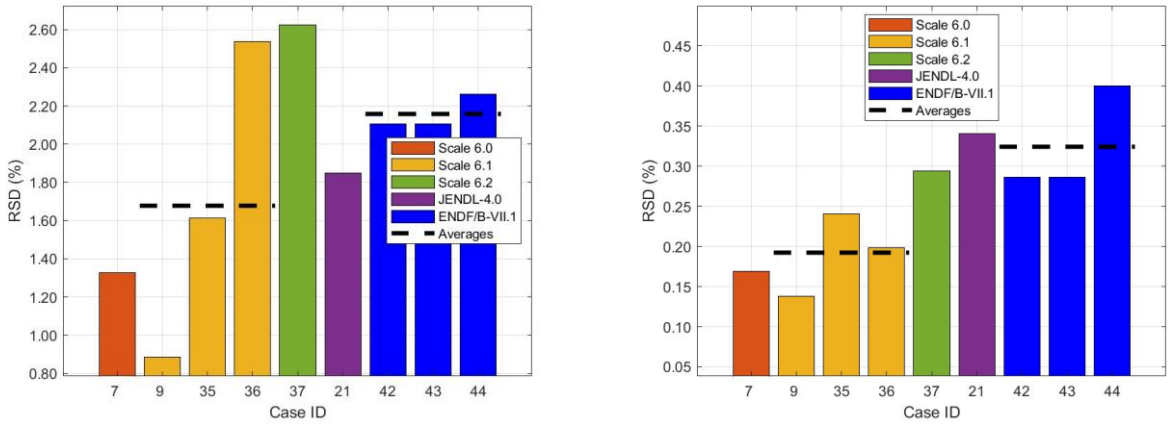

(a) (b)

Source: NEA data, 2021

Figure 3.16. RSD of ^{235}U fission and nu-bar multi-group cross sections from SCALE 6.1 44G covariance library

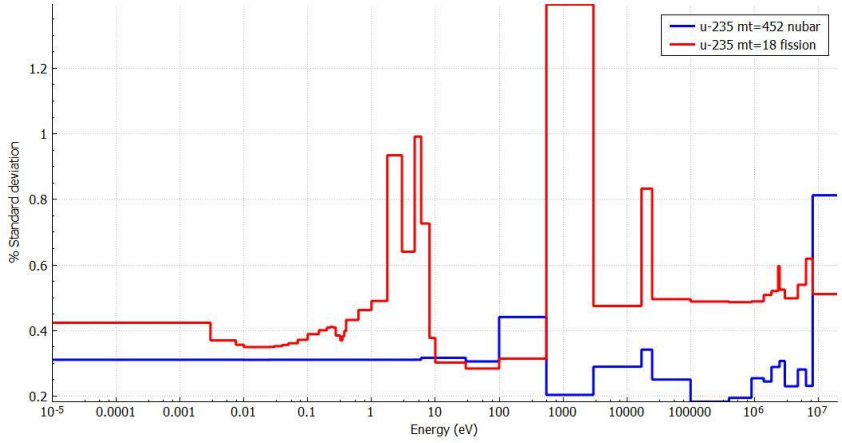

Source: NEA data, 2021

Figure 3.17. RSD of ^{235}U and ^{238}U capture multi-group cross sections from SCALE 6.1 44G covariance library

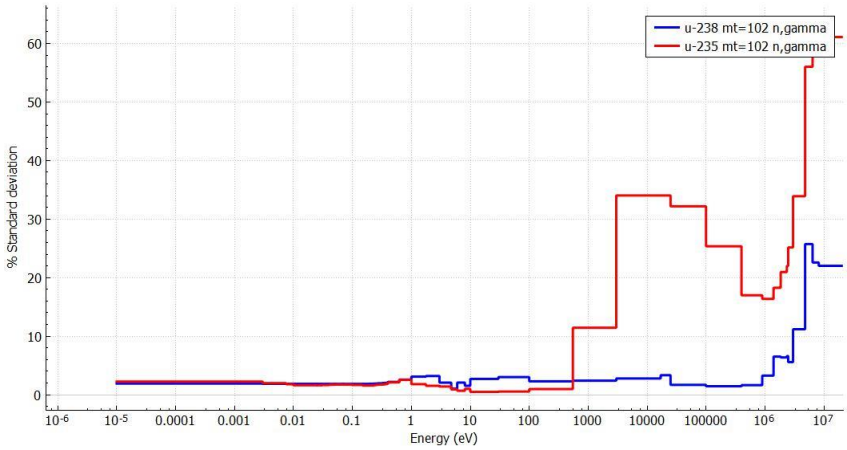

Source: NEA data, 2021

The relationship between the *k*-inf, flux, and group constants (cross sections, diffusion coefficients, and assembly discontinuity factors) in the two-group representation can be determined by calculating the correlation coefficients between variables. The correlations and the corresponding covariances are very important for the uncertainty propagation in the conventional LWR two-step approach as will be detailed in the next section. Selected correlation coefficient matrices from different cases are depicted in Figure 3.18, in which red and blue represent positive and negative correlations, respectively, between two parameters, while white represents correlation close to zero. Intermediate shades of light red or light blue represent varying degrees of positive or negative correlations, respectively.

Figure 3.18. Correlation coefficient matrix of the two-group homogenised cross sections of the unrodded lattice from (a) case 21 (HZP) with JENDL-4.0 (b) case 36 (HZP) with SCALE 6.1, (c) case 37 (HZP) with SCALE 6.2, and (d) case 42 (HFP) with ENDF/B-VII.1

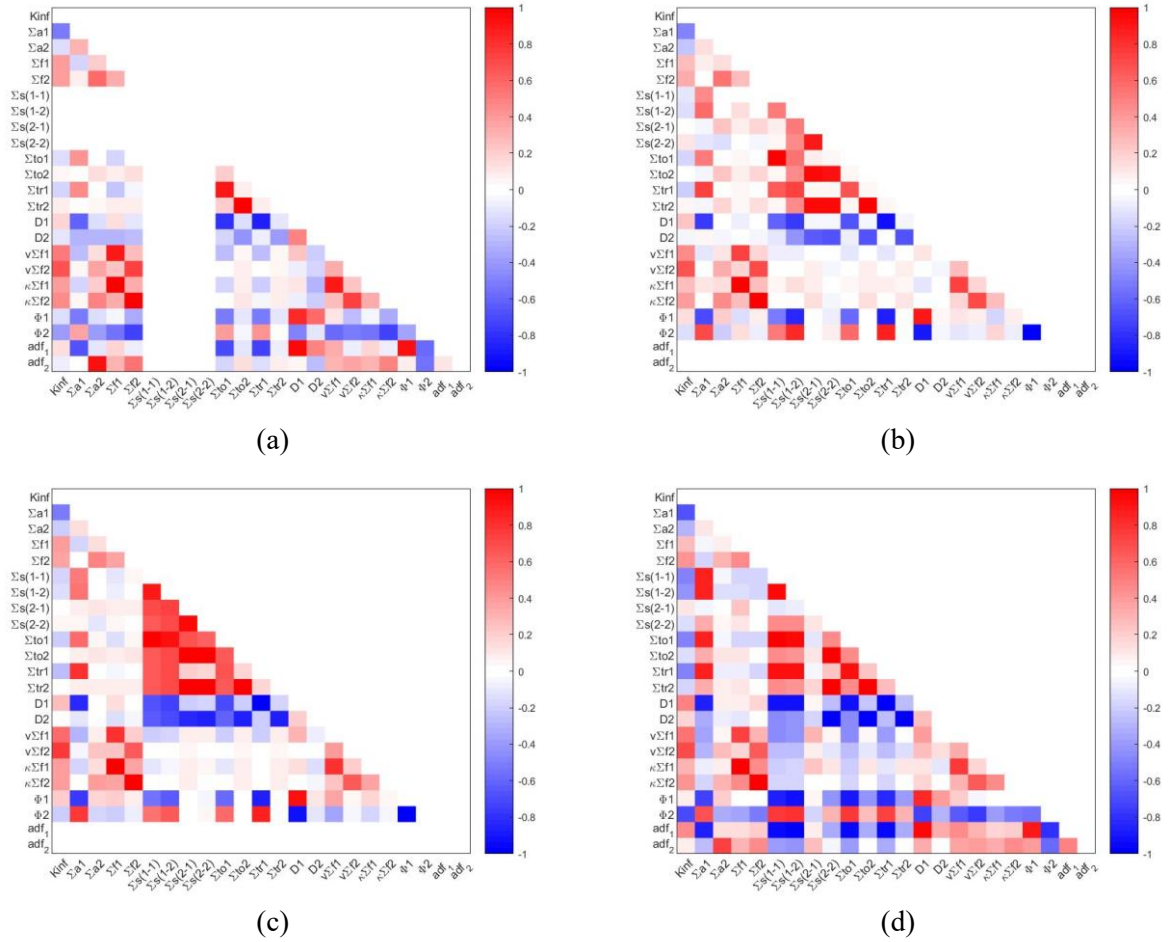

Source: NEA data, 2021

It is important to mention that not all the cases estimated correlations for all the two-group constants. Case 21 did not estimate correlations for the scattering cross sections, while cases 36 and 37 did not consider the assembly discontinuity factors. The main conclusion that can be drawn by examining the matrices is that they agree reasonably well with each other in the sense that similar trends are observed. For example, the fast flux is negatively correlated, and the thermal flux is positively correlated, with the Group 1 absorption, scattering and transport cross sections. A strong positive correlation is found between *k*-inf and Group 2 nu-fission cross section across all the matrices and correspondingly a strong negative correlation between *k*-inf and Group 1 absorption. On the other hand, some unique features are also observed in case 37, with strong cross-correlations between the scattering, transport and total cross sections of both thermal and fast group.

The assembly discontinuity factors (ADF) were also requested at the boundaries with the reflector. Only one participant (case 21) provided results. The results show a very large relative standard deviation of 34% for the thermal group ADF while 1% for the fast group ADF. This behaviour was observed for both HZP and HFP. More investigation needs to be done in order to understand if this is related to the particular case or if it is a general result of the uncertainty propagation.

Finally, a last set of results was requested from the participants for a minicore colourset lattice calculation at HZP and HFP. The minicore is a 3×3 lattice of TMI-1 fuel assemblies where the

central one is rodded and all the others are unrodded. The uncertainties of *k*-inf and pin power are of particular interest in this study. For this exercise, 6 participants provided results. The *k*-inf results are shown in Figure 3.19 and Figure 3.20. The mean value is 1.387 for HZP and 1.371 for HFP with RSD at the order of 0.5%, similar to all the previous studies. More information about the estimated mean and RSD for each covariance library can be found in Table B.3 of Appendix B.

The results of the participants for the pin distributions agree with each other and show RSD less than 1.3% in all the pins with higher relative uncertainties in the Gd pins and in the pins of the central rodded assembly. In general, larger relative uncertainties are observed in the pins with lower power something that can be attributed to the additional uncertainty coming from either the control rod or the Gd presence. Representative results for one case at HFP are shown in the Figure 3.21. Similar conclusions are drawn for the HZP case as well.

Figure 3.19. Calculated *k*-inf for I-2 PWR-TMI-1 minicore colourset at HZP: (a) mean value with uncertainties, (b) RSD grouped by covariance libraries utilised

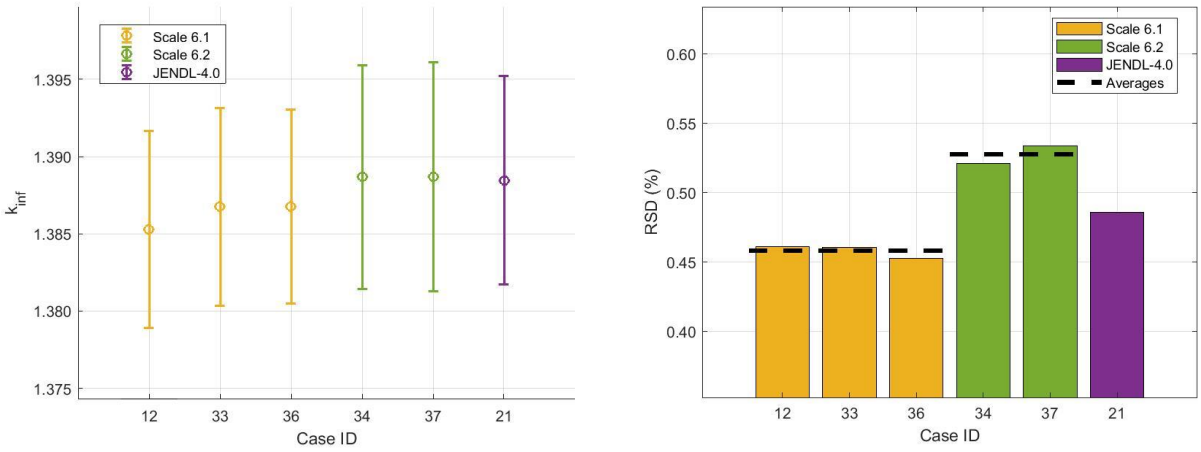

Source: NEA data, 2021

Figure 3.20. Calculated *k*-inf for I-2 PWR-TMI-1 minicore colourset at HFP: (a) mean value with uncertainties, (b) RSD grouped by covariance libraries utilised

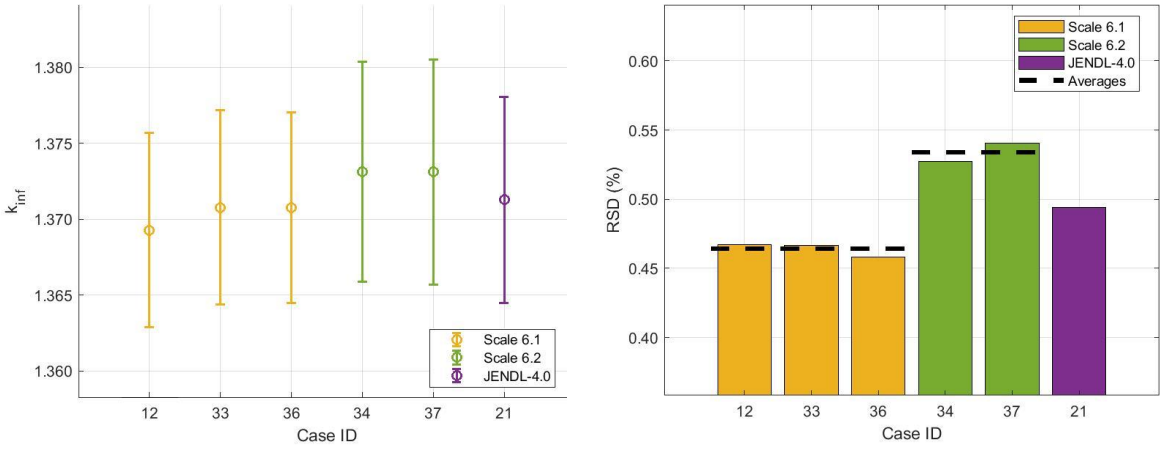

(a) (b)

Source: NEA data, 2021

Figure 3.21. Calculated pin power distribution for I-2 PWR-TMI-1 minicore colourset at HFP (a) case 36 mean, (b) case 36 RSD

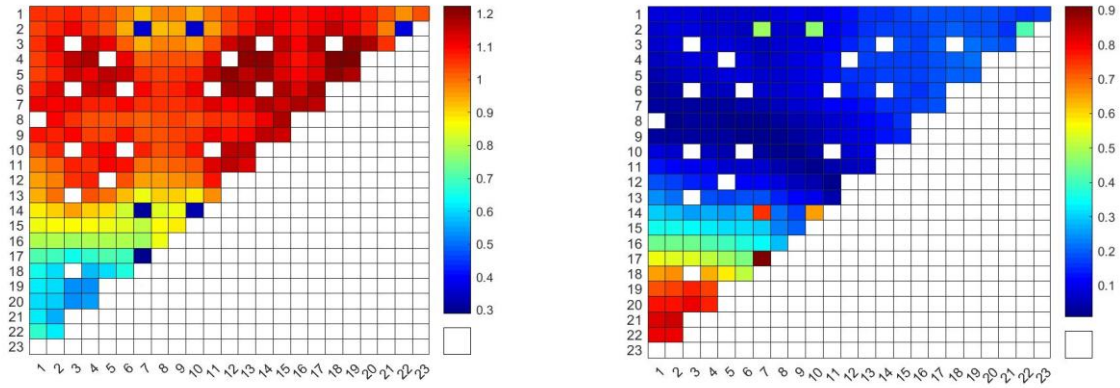

(a) (b)

Source: NEA data, 2021

3.1.4. Exercise I-3: Core physics

The uncertainties of the few-group cross sections evaluated in Exercise I-2 are to be propagated through the standalone neutronics core calculation in Exercise I-3 to the parameters of interest such as the core *k*-eff and power distribution. Various uncertainty propagation methodologies can be used, as summarised in Table 3.1 (Castro et al., 2018[29]). In the full deterministic approach, the PT calculation is performed at both lattice and core level, and the VCM of the few-group homogenised constants generated in the lattice calculation is used to evaluate the uncertainty of core responses. This approach assumes linearity between the inputs and outputs and is computationally very efficient when adjoint calculations can be performed for the output quantities of interest. This might not always be the case, as in transient or multi-physics calculations. The one-step approach relies on the stochastic sampling method at both lattice and core levels and is named as such because it involves a one-to-one connection between lattice calculations to generate the few-group cross sections random libraries and the core calculation that reads this library as input (Yankov et al., 2012[30]). This approach alleviates the linearity constraint of the fully deterministic method but it is computationally more expensive since it requires a large number of lattice calculations. Finally, the two-step approach combines the stochastic sampling and deterministic methods in order to find a balance between the computational cost and the statistical approximations. This method is the one usually used for transient calculations with multi-physics coupling. Detailed explanation and a complete list of references can be found in (Castro et al., 2018[29]). These methodologies can be used with both deterministic and Monte Carlo codes, although usually deterministic codes are used due to the smaller computational cost, especially when a large number of samples is required.

Table 3.1. Uncertainty propagation methodologies in reactor full core simulations

.	Cell/lattice calculation	Intermediate data	Core simulation
Fully deterministic	Deterministic	VCM	Deterministic
One-step	Sampling	Random libraries	Sampling
Two-step	Deterministic	VCM and random libraries	Sampling
	Sampling	VCM	Deterministic

Source: Castro, E. et al. (2018[29]).

It should be noted that all the aforementioned approaches, when used with deterministic codes, follow the standard reactor simulation procedure, which involves the generation of homogenised group constants, simplification of core geometry, and application of lower-order solvers such as the nodal diffusion method. The major modelling difference occurs on whether the spatial homogenisation is performed over the assembly or pin cell. Either way, this procedure will inevitably introduce additional discrepancies to the calculated uncertainty of core responses.

The PWR model defined in the core physics is the PWR-TMI-1 fresh core at HZP state with all control rods fully inserted. In total, 11 sets of results have been collected. Most results were obtained using the one-step and two-step approaches mentioned in Table 3.1, such as in (Zeng et al., 2019[31]), except for few cases (e.g. case 45), where the full core geometry was explicitly modelled using a Monte Carlo code. The estimated relative uncertainties of the core eigenvalue are shown in Figure 3.22 with two outliers being excluded. The mean value shows a discrepancy up to 700 pcm from the critical state and a RSD at the order of 0.5%, similar to that observed in the pin cell and lattice calculations. Also similar to the previous studies is the dependency of the uncertainty on the VCM choice, that is, the calculation using the SCALE 6.2 VCM tends to yield higher uncertainties compared to SCALE 6.0 and 6.1 and the calculation using ENDF/B-VII.1 exhibits the largest uncertainties ~0.7%, primarily due to the large uncertainty in the neutron production rate. More information about the estimated mean and RSD for each covariance library can be found in Table B.6 of Appendix B.

The radial power distributions across the participants show generally a good agreement. To illustrate the results, the normalised radial assembly power and the associated RSD of case 46 are shown in Figure 3.23. The maximum assembly power is observed at (4, 9) and (6, 11) due to the absence of control rods in neighbouring assemblies, and the value and its uncertainty are 1.68±0.55%. In general, the relative uncertainty of the assembly power is higher at low power regions such as the core centre.

Figure 3.22. Calculated *k*-inf for I-3 PWR-TMI-1 full core at HZP: (a) mean value with uncertainties, (b) RSD grouped by covariance libraries utilised

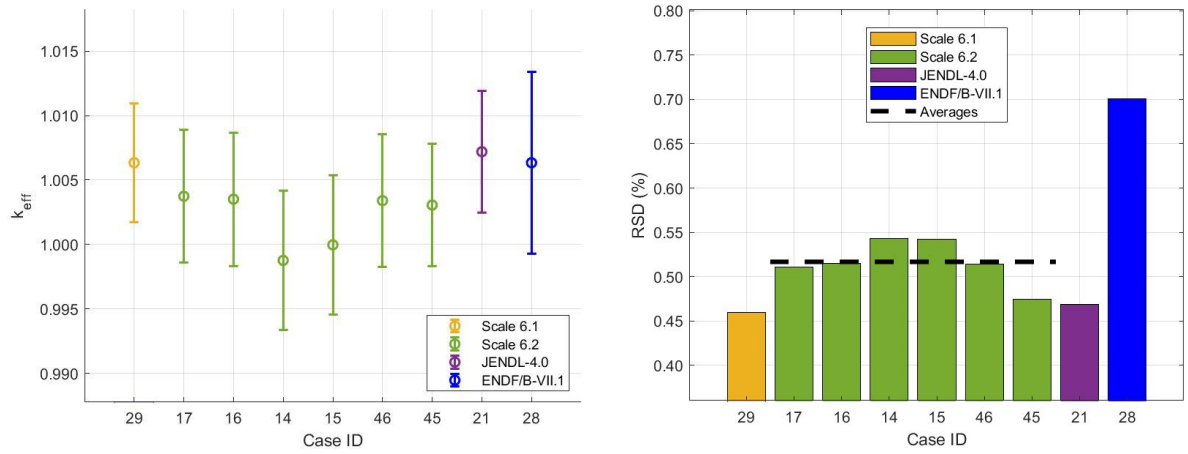

(a) (b)

Source: NEA data, 2021

Figure 3.23. Calculated radial assembly power distribution for I-3 PWR-TMI-1 full core at HZP for case 46 (a) mean and (b) RSD

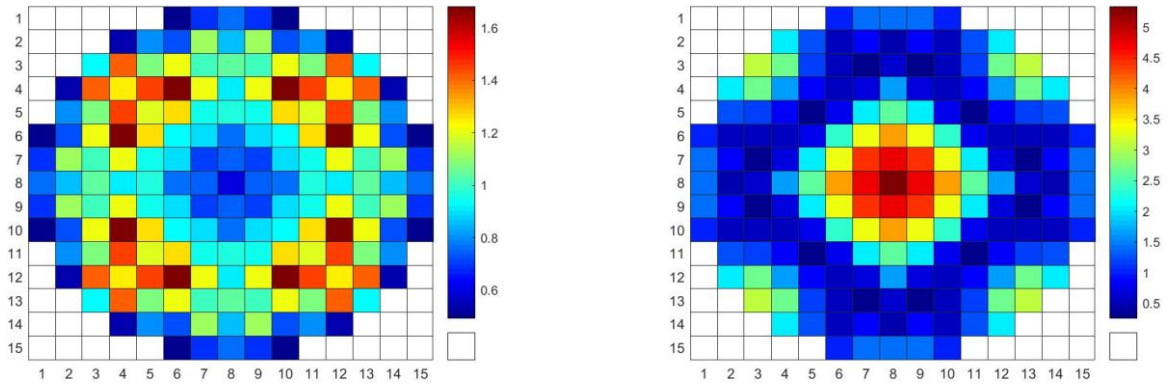

(a) (b)

Source: NEA data, 2021

Finally, in Figure 3.24. the core axial power evolution and the associated uncertainties are plotted for the different results provided by the participants, where the active core height has been divided into 16 axial nodes. On one hand, the mean power profiles exhibit the expected classic cosine shape, although the degree of skewness varies from case to case, which indicates possible differences in the few-group constants, control rod position and solution methods. The uncertainties of the core

axial power on the other hand, demonstrate larger discrepancies in both magnitude and shape, which is difficult to explain without further investigation. The RSD of the node power is below 1.0% in all but one result. In general, the relative uncertainty is smaller in power peaking nodes or the core axial centre, and larger in the vicinity of top and bottom reflectors. The cases 14 and 15 superimpose each other because they use the same code and covariance libraries with only difference the assembly discontinuous factors, that are considered only in case 15.

Figure 3.24. Calculated axial core power distribution for I-3 PWR-TMI-1 full core at HZP (a) mean and (b) RSD

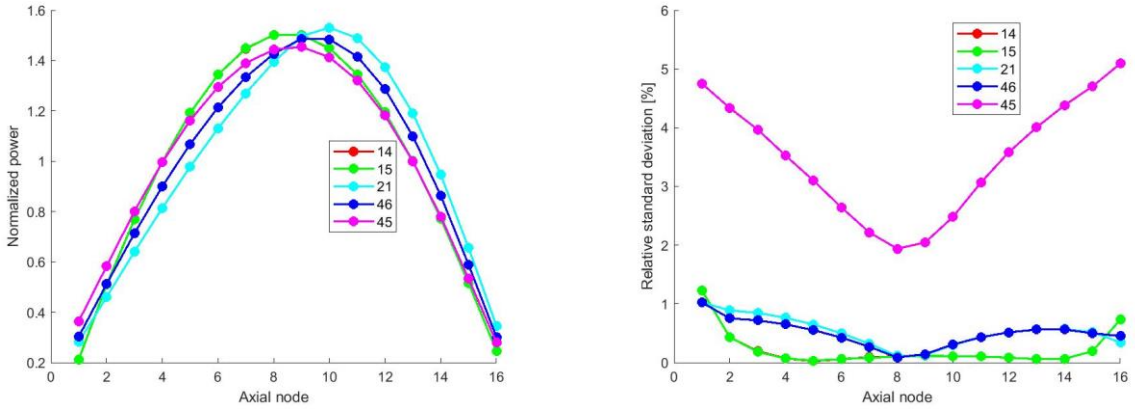

(a) (b)

Source: NEA data, 2021

3.2. Boiling water reactor exercises: PB-2

3.2.1. Exercise I-1: Cell physics

In a similar way to 3.1.1, for each study in Exercise I-1 of the BWR pin cell, the following results are requested from the participants: calculated *k*-inf and its associated uncertainty, the top five neutron-nuclide reactions that contribute the most uncertainty to *k*-inf, and covariances of selected one-group cross sections generated in the pin cell calculations.

The 2D fuel pin cell model was adopted from PB-2 reactor and was chosen as the representative BWR test problem, being analysed under both HFP and HZP conditions. The fuel is UO_2 with 2.93% enrichment. The submitted results included 20 sets of HZP and 18 sets of HFP calculations, from which specific information was extracted in order to perform a comparative analysis of the results. One important operational difference for the BWR, in particular, was the 0% and 40% void fractions applied for the HZP and HFP conditions, respectively. This was done to reflect the operational differences in BWR parameters, as well as to provide varying neutron spectra for the calculations. As in the PWR section, the target of the analysis was to reveal the relation between the choice of calculation approach (e.g. transport solution method, covariance library, UQ method) and output uncertainties. Figure 3.25 and Figure 3.26 show summaries of the results for the predicted *k*-inf and the associated uncertainties for the HZP and HFP conditions, which indicate a mean *k*-inf range of ~1000-1500 pcm. This is likely a result of differences in the transport codes and base NDLs utilised in the calculation, as well as inconsistencies in modelling approaches. The mean value and RSD at HZP are 1.345 and 0.54%, respectively. The mean and RSD at HFP are 1.232 and 0.63%, respectively. The significantly lower *k*-inf mean at HFP is due to the thermal-hydraulics feedbacks, such as the Doppler and moderator effects. A possible reason for the larger RSD compared to the PWR I-1 exercise is the lower enrichment in the BWR fuel decreasing the sensitivity of the ^{235}U nu-bar and thus increasing the importance of the ^{238}U capture which in general has larger uncertainties. Another reason can be the hardening of the neutron spectrum due to the void presence increasing

the significance of ^{238}U capture in epithermal and fast regions where the ^{238}U capture has higher uncertainties as can be seen in Figure 3.17.

Figure 3.25. Calculated *k*-inf for I-1 BWR-PB-2 at HZP: (a) mean value with uncertainties, (b) RSD grouped by covariance libraries utilised

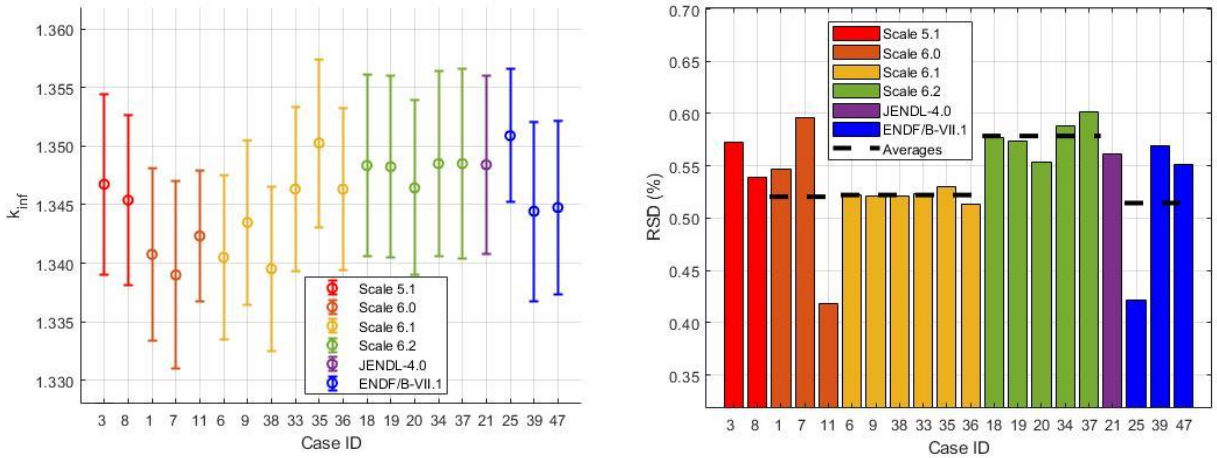

(a) (b)

Source: NEA data, 2021

Figure 3.26. Calculated *k*-inf for I-1 BWR-PB-2 at HFP: (a) mean value with uncertainties, (b) RSD grouped by covariance libraries utilised

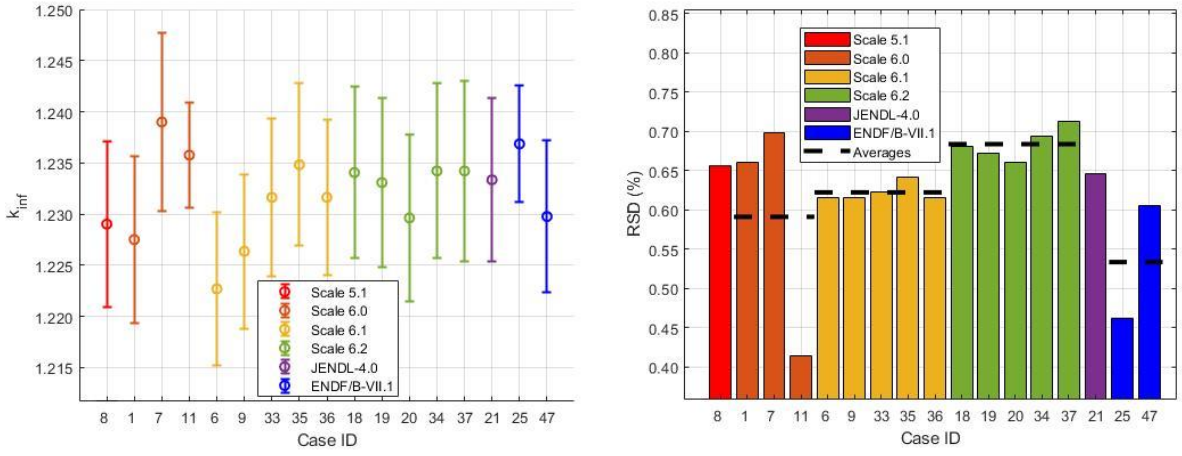

(a) (b)

Source: NEA data, 2021

The BWR case results for *k*-inf indicate that covariance library choice has a noticeable impact on the RSD of *k*-inf. This is seen in both Figure 3.25 and Figure 3.26, which show similar response for HZP and HFP studies. For the SCALE 6.0/6.1 covariance libraries, the average computed RSD for of *k*-inf was found to be 0.52% for HZP. The SCALE 6.2 covariance library yielded an average value of 0.58% for HZP. Other HZP results included three cases using the ENDF/B-VII.1 and one using JENDL-4.0 covariance libraries with RSDs near 0.51% (average of three values) and 0.56% (single value) respectively. Additionally, two cases used SCALE 5.1 with a RSD of 0.56%.

For the SCALE 6.0/6.1 covariance libraries, the average computed RSD for *k*-inf was found to be 0.61% for HFP. The SCALE 6.2 covariance library yielded an average value of almost 0.69% for

HFP. Other HFP results included two cases using the ENDF/B-VII.1 and one using the JENDL-4.0 covariance libraries with RSDs near 0.53% (average of two values) and 0.65% (single value), respectively. All the results regarding the estimated *k*-inf mean and RSD for each covariance library are gathered in Table B.1 of Appendix B.

Similar to the PWR trends shown in 3.1.1, the trends for the BWR I-1 results can also be explained by understanding the differences between sources of uncertainties and their covariance information. It is important to remember that additional verification is performed to understand and modify any new covariance data from NDLs before use in SCALE libraries (Marshall et al., 2013[24]). As mentioned previously, the changes from those verifications to the covariance data for nu-bar (average number of neutrons per fission reaction $\bar{\nu}$) for that of ^{235}U and ^{239}Pu can have strong impacts on the LWR cell physics results.

The different uncertainty of ^{235}U nu-bar in the thermal range in different SCALE versions (0.31% in SCALE 6.0/6.1, 0.39% in SCALE 6.2) explains why the calculated RSD of *k*-inf using SCALE 6.2 data is once again slightly higher than that using SCALE 6.0/6.1. However, in this case no increased uncertainty for ENDF/B-VII.1 is observed. This can be attributed to the lack of available results, the hardened neutron flux spectrum and lower enrichment in the BWR pin cell and the mismatch between prompt nu-bar and nu-bar in ENDF/B-VII.1, as explained in the corresponding PWR exercise. The neutron flux spectrum and fuel enrichment effects, compared to the PWR pin cell, might lead to a decrease in the importance of ^{235}U nu-bar and increase of the importance of the ^{238}U capture.

One advantage from using the PT method compared to the sampling approach is that the sensitivity coefficients of certain output variables with respect to the nuclear data can be computed efficiently, allowing for the analysis of the most influential nuclide reaction to the calculated *k*-inf uncertainties. The influential nuclide-reaction pairs can be sorted from greatest to lowest variance fraction and presented in terms of the covariance library used. For the HZP study, 11 sets of the submitted results included the ranking information while for the HFP study, 9 results were submitted. The results for the top five uncertainty-contributing nuclide-reaction pairs are gathered in Figure 3.27 and Figure 3.28 for HZP and HFP studies respectively.

Although the most important reactions are ^{238}U capture, ^{235}U nu-bar and ^{235}U capture, and thus are the same with the PWR pin cell, there is a small change related to the BWR pin cell. In the PWR pin cell the first rank was almost equally split between ^{235}U nu-bar and ^{238}U capture depending on the covariance libraries, but in the BWR pin cell the ^{238}U capture ranks always first in both HZP and HFP except only one submitted result. This occurs, as explained previously, due to the lower enrichment in the BWR pin cell and due to the hardening of the spectrum that renders ^{238}U capture more effective since there are more neutrons in the epithermal energy spectrum where the cross section is larger and more uncertain. For the HZP study with 0% void fraction the former is the reason of the increased ^{238}U capture importance. For the HFP study with 40% void fraction a combination of both is the reason. This is highlighted by the fact that the only result ranking first the ^{235}U nu-bar in HZP study, it ranks first the ^{238}U capture in the HFP study. Apart from this difference, the explanation of the main contributors to the *k*-inf are identifiable, once again, by the 1) highest sensitivities associated with such reactions, 2) the highest value of the associated covariances, or 3) a combination of both. The ^{238}U capture cross section has a strong effect on *k*-inf, especially in the unresolved resonance regions, while the evaluated cross sections exhibit large uncertainties (Trkov et al., 2005[26]). For the HZP study, ^{235}U capture appears as another important contributor to the uncertainty consistently ranking third, independent of covariance library. Additionally, some less influential nuclide-reaction pairs that occur a few times, like ^{238}U nu-bar and ^{238}U elastic scattering, are solely found within the ENDF/B-VII.1 covariance library and can be explained by the differences in the covariance libraries themselves. For the HFP study, the most noticeable difference from the HZP exercise in the lower rankings is the switching of positions of ^{235}U capture and ^{238}U inelastic scattering for most results.

One of the driving phenomena differentiating the BWR from the PWR exercise is the spectrum shift, more specifically the spectrum hardening effect, due to the 40% void fraction in the coolant for the HFP cases. The contribution of thermal neutrons becomes relatively less important when the degree of moderation decreases in the HFP condition, reflected by the suppression of the sensitivity profile in the thermal energy range, as can be seen in Figure 3.29 for the ^{235}U capture reaction. For nuclide-reaction pairs of which the variance peaks in the thermal range, such as ^{235}U capture, this means the decrease of the contribution to the total *k*-inf uncertainty. In the case of ^{238}U inelastic scattering, which primarily affects the number of fast fission neutrons, the opposite effect occurs because its variance peaks at a much higher energy range.

Figure 3.27. Ranking of the five nuclide-reaction pairs with the highest contribution to the *k*-inf uncertainty for I-1 BWR-PB-2 at HZP [7.1= ENDF/B-VII.1 and the rest X.Y = SCALE X.Y covariance libraries]

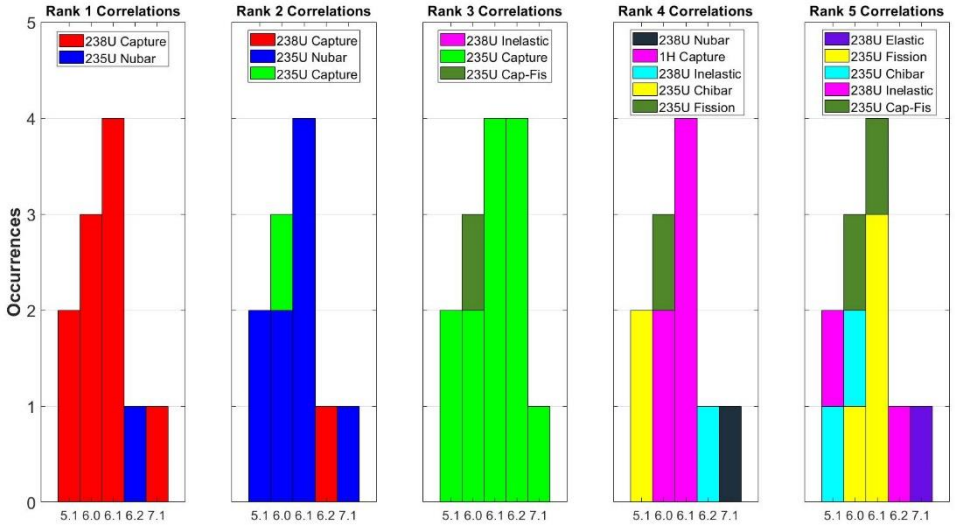

Source: NEA data, 2021
Note: SX = SCALE X covariance library, E7.1 = ENDF/B-VII.1 covariance library.

Figure 3.28. Ranking of the five nuclide-reaction pairs with the highest contribution to the k-inf uncertainty for I-1 BWR-PB-2 at HFP [7.1= ENDF/B-VII.1 and the rest X.Y =SCALE X.Y covariance libraries]

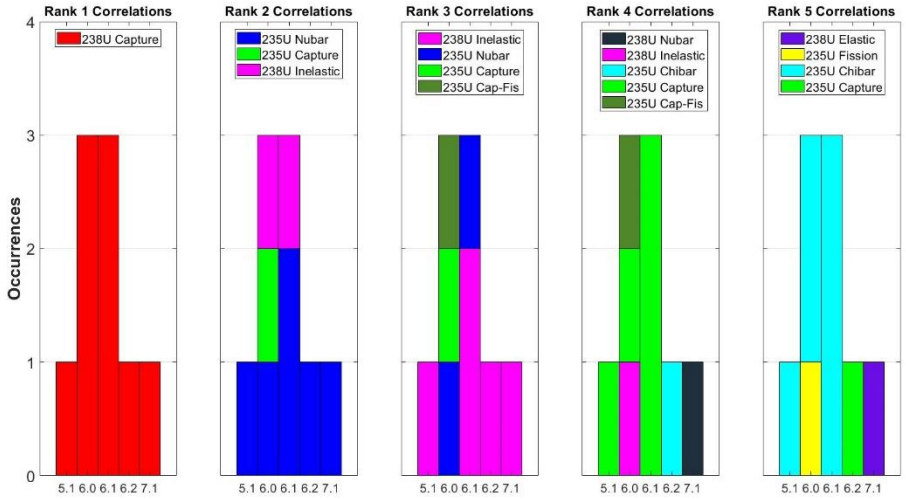

Source: NEA data, 2021
Note: SX = SCALE X covariance library, E7.1 = ENDF/B-VII.1 covariance library.

Figure 3.29. Comparison of the sensitivity profile for 235U capture cross section

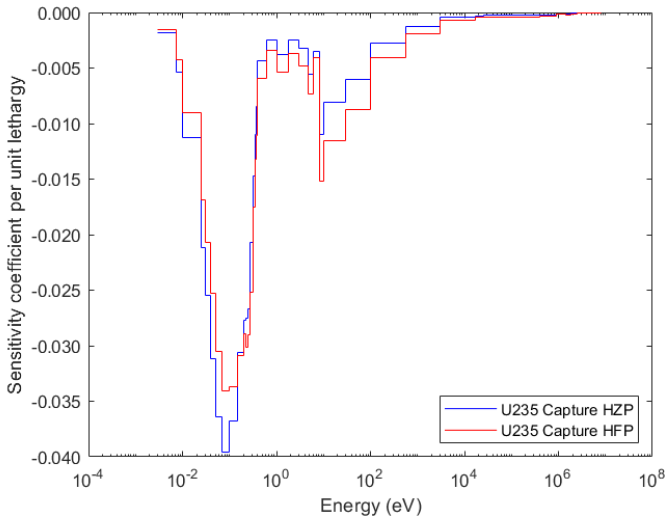

Source: NEA data, 2021

3.2.2. Exercise I-2: Lattice physics

The next BWR exercise focuses on propagating the uncertainties of the nuclear data through lattice calculations to determine the uncertainty of specific output variables including the *k-inf*, group constants like cross sections, diffusion coefficients and discontinuity factors. The correlations between the obtained group constants are important to be quantified, since they will be used afterwards in the full core calculations if a two-step uncertainty propagation method is employed or used directly for a core calculation. Additionally, lattice calculations are performed on larger coloursets of a BWR minicore with main quantities of interest the *k*-inf and the pin power distribution uncertainties.

The BWR lattice is a 2D fuel assembly model consisting of 7×7 fuel rods with 4 burnable poison locations using integral Gd burnable poisons (Gd_2O_3). Lattice cells in a BWR consist of four fuel assemblies separated by a control blade. The exercise is once again modelled under conditions of HZP and HFP with corresponding void coefficients of 0% and 40% and as unrodded and rodded. There are 12 (with one outlier excluded) sets of submitted results for the HZP unrodded study and 9 sets for the rodded study. There are 11 (with one outlier excluded) sets of submitted results for the HFP unrodded study and 8 sets for the rodded study. For these four studies the predicted uncertainties in *k*-inf are presented in Figure 3.30. and Figure 3.31. The mean value at HZP unrodded study has a spread of ~1 000 pcm, which increases to 1 500 pcm for the HZP rodded study and even further to ~2 500 pcm for the HFP unrodded and rodded studies. The large spreads are obtained from few outlier cases. The remaining spread if these outliers are neglected is at the same order of the PWR exercises and I-1 BWR exercise and is attributed to the same reasons, mainly the differences in the base NDLs and transport codes utilised in the calculation, as well as inconsistencies in the modelling approaches. Concerning the predicted RSD of *k*-inf and the effect of the choice of the VCM, similar conclusions to the previous Exercise I-1 can be drawn. The SCALE 6.2 library seems to exhibit the largest uncertainties, if one outlier is neglected, something related to the increased uncertainty of ^{235}U nu-bar compared to SCALE 6.0/6.1 library. The ^{235}U nu-bar uncertainty is even larger in the ENDF/B-VII.1 library but as explained previously in the BWR case the ^{238}U capture is more significant. The comparison between the cases shows that at HZP the RSD is similar for both unrodded and rodded studies with a value of ~0.54%. However, the uncertainty increases to ~0.57% for the HFP unrodded study and up to ~0.61% for the HFP rodded. The increase between HZP and HFP can be attributed to the hardening of the spectrum and thus the presence of more neutrons in higher energy regions where the ^{238}U capture cross sections has larger uncertainties. The increased uncertainty in the HFP study can be attributed to the additional uncertainty added by the absorbent material in the control rod. Unfortunately, there is an imbalance in the number of submitted results across the BWR I-2 exercise, adding to the difficulty of generalising these observations. More information about the estimated mean and RSD for each covariance library can be found in Table B.2 of Appendix B.

Figure 3.30. Calculated k-inf for I-2 BWR-PB-2 at HZP: (a) mean value with uncertainties for unrodded, (b) RSD for unrodded (c) mean value with uncertainties for rodded, (d) RSD for rodded

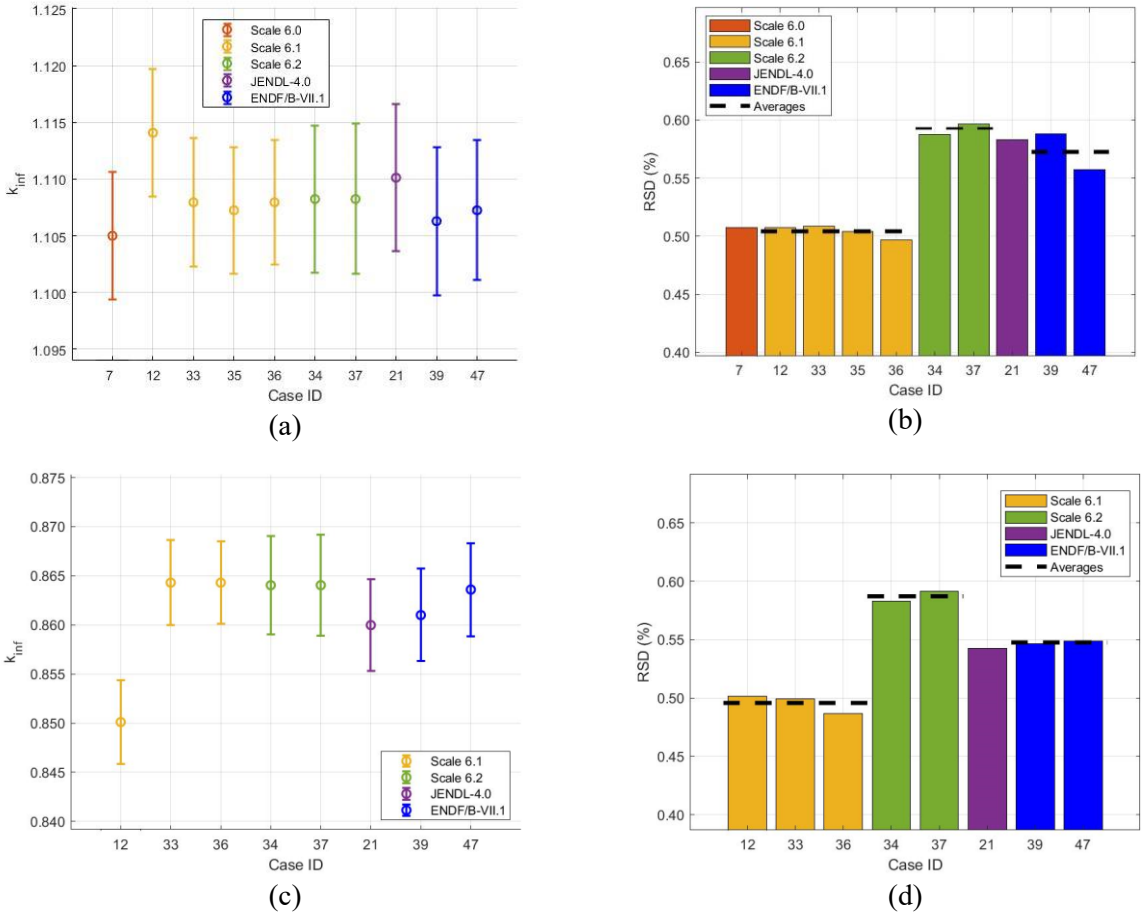

Source: NEA data, 2021

Figure 3.31. Calculated k-inf for I-2 BWR-PB-2 at HFP: (a) mean value with uncertainties for unrodded, (b) RSD for unrodded (c) mean value with uncertainties for rodded, (d) RSD for rodded

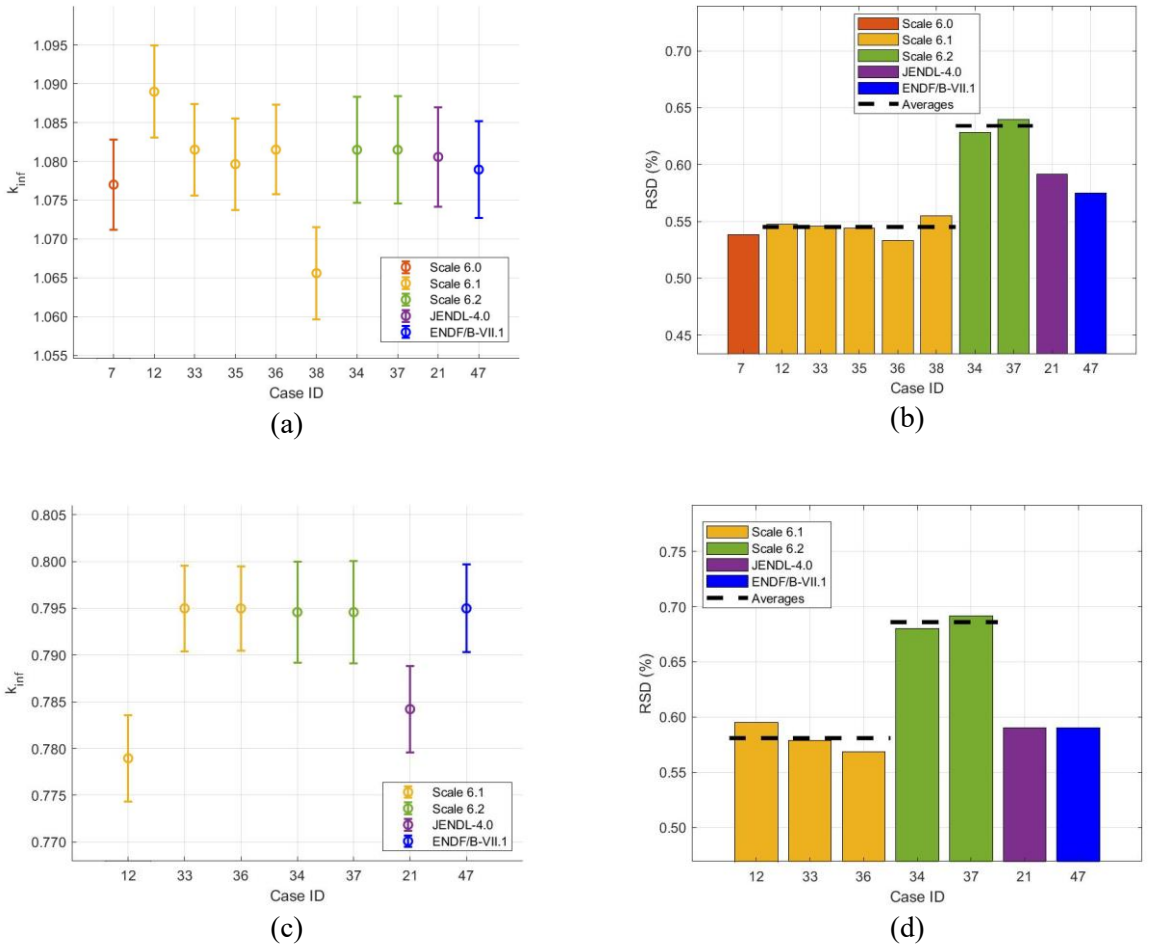

Source: NEA data, 2021

Again, the uncertainties of the homogenised two-group nu-fission cross sections are compared based on the VCM, as shown in Figure 3.32. for the unrodded HFP study. Again, the higher nuclear data uncertainty of the nu-bar reaction in SCALE 6.2 VCM is responsible for the larger uncertainties. Similar to the PWR exercise, it can be found that the uncertainty of homogenised nu-fission is more profound in the fast group than the thermal group for most of the covariance libraries. For example, the value is ~1.1% in the fast group for versus ~0.46% in the thermal group. The ^{235}U nu-bar uncertainty is lower in the epithermal and fast energies but the ^{235}U fission uncertainty is higher. The combination of the two leads to this increased uncertainty in the fast group. In Figure 3.33 the corresponding results of the diffusion coefficient for unrodded HFP study are presented. Here the difference in the uncertainties between the fast and thermal group is larger. In fact, as for the PWR exercise, this trend is found to be more general, since for all the main group constants and for all the studied conditions (i.e. HFP, HZP, unrodded, rodded) the fast group uncertainty is larger than the thermal one. This can be attributed to the fact that for most cross sections the uncertainties are larger in the epithermal and fast groups due to the increased difficulty in obtaining accurate measurements. More information about the average RSD for each covariance library can be found in Table B.4 and Table B.5 of Appendix B.

Figure 3.32. RSD of predicted $\nu\Sigma_f$ for I-2 BWR-PB-2 at HFP unrodded study: (a) fast group, (b) thermal group

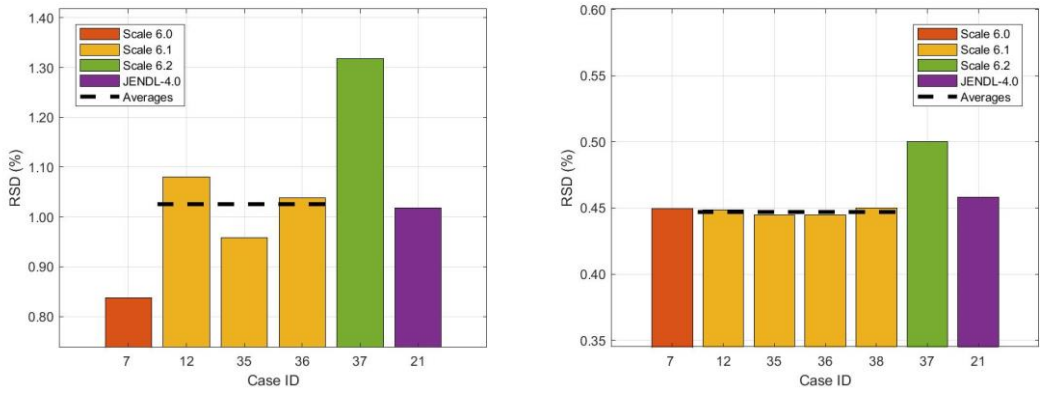

(a) (b)

Source: NEA data, 2021

Figure 3.33. RSD of predicted D for I-2 BWR-PB-2 at HFP unrodded study: (a) fast group, (b) thermal group

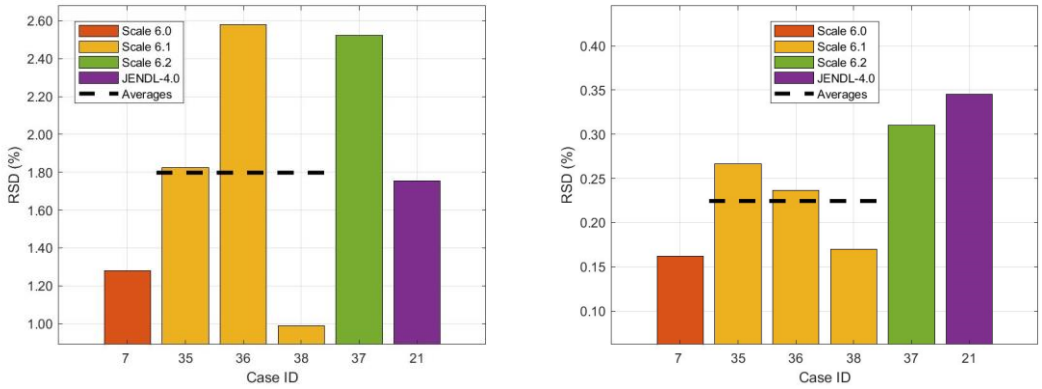

(a) (b)

Source: NEA data, 2021

For the parameters of interest such as *k*-inf, flux, and group constants (cross sections and diffusion coefficients), the relationship between them in the two-group representation can be understood by computing the correlation coefficients between variables. Similar to the PWR results, specific correlation coefficient matrices are presented in Figure 3.34 for the HZP unrodded lattice calculations, in which red and blue represent positive and negative correlations, respectively, between two parameters, while white represents correlations close to zero. Intermediate shades of light red or light blue represent varying degrees of positive or negative correlations, respectively.

Figure 3.34. Correlation coefficient matrix of the two-group homogenised cross sections of the BWR unrodded lattice from (a) case 21 with JENDL-4.0, (b) case 36 with SCALE 6.1, (c) case 37 with SCALE 6.2 and (d) case 39 with ENDF/B-VII.1

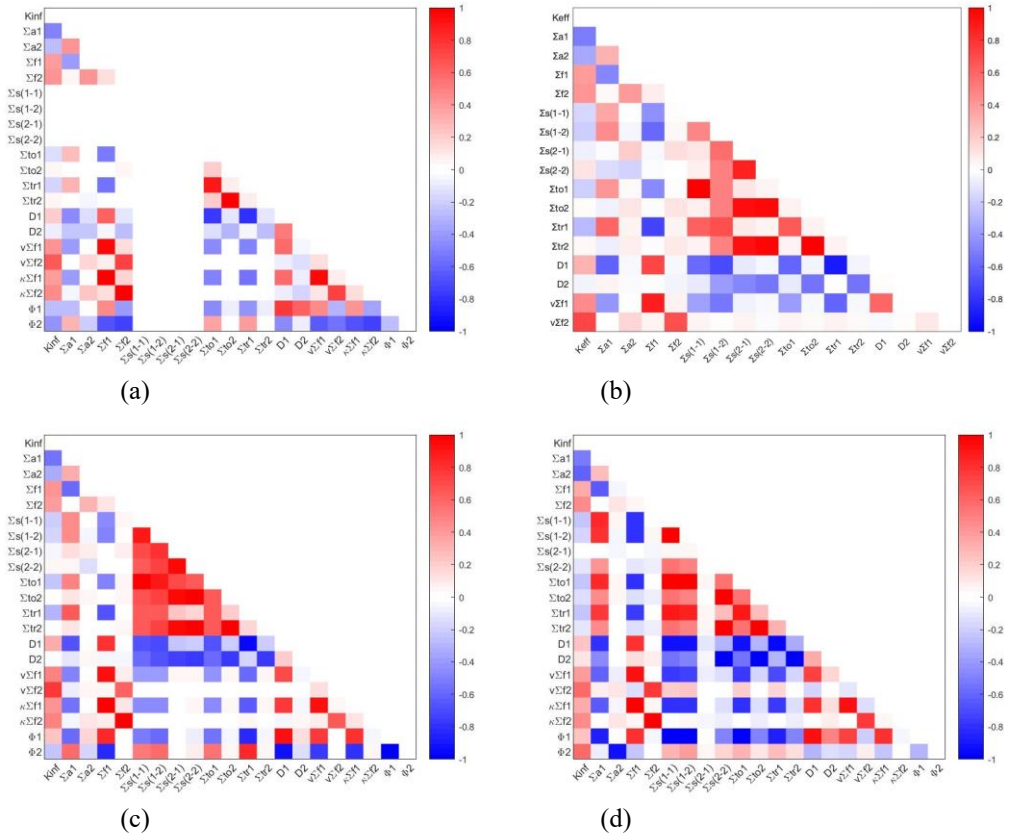

(a) (b)

(c) (d)

Source: NEA data, 2021

The correlation coefficient matrices seem to show reasonable agreement, with similar trends appearing in all four of the selected cases. It should be noted that for case 21 there were no scattering cross sections in the correlation matrix and hence a zero value is used in the figure. One important expected trend is the negative correlation between the Group 1 absorption and the *k*-inf, as well as the positive correlation between *k*-inf and the Group 2 nu-fission cross section, which is observed in all the cases. There are some unique trends than can be observed as well, like case 37, with strong positive correlation between the scattering and transport cross sections of both thermal and fast group. In general, it is difficult to have an intuitive understanding of what should be expected for the scattering cross sections since the scattering cross sections that have positive and negative contribution to the *k*-inf are strongly correlated. Once again, the PB-2 I-2 results submitted are less complete than the TMI-I counterparts, resulting in a less than optimal set of data for analysis. Additional investigations and analysis are suggested with more complete correlation coefficient matrices to identify causes for certain features and to determine the impact of the VCM choice used in the lattice calculations. The variations in the group constants are likely to propagate to the core calculations in I-3 and impact the uncertainty of full core parameters.

The assembly discontinuity factors (ADF) were also requested at the boundaries with the reflector using a 1D model. Only one participant (case 21) provided results. The results show a small RSD of ~0.24% for the fast group ADF and of ~0.36% for the thermal ADF. This behaviour was observed for both HZP and HFP. There is a significant decrease compared to the uncertainties in the thermal group in the PWR exercise.

Finally, a last set of results was requested from the participants for a minicore colourset lattice calculation at HZP and HFP. The minicore is a 2×2 lattice of PB-2 fuel assemblies where two diagonal assemblies are rodded and the others unrodded. The uncertainties of *k*-inf and pin power are of particular interest in this study. For this exercise, 4 participants provided results. The *k*-inf results are shown in Figure 3.35 and Figure 3.36. The mean value is 0.995 for HZP and 0.945 for HFP with RSD at the order of 0.5-0.6%. For similar reasons to the previous BWR cases the uncertainties for the HFP are slightly higher than the HZP study. More information about the estimated mean and RSD for each covariance library can be found in Table B.3 of Appendix B.

Figure 3.35. Calculated k-inf for I-2 BWR-PB-2 minicore colourset at HZP: (a) mean value with uncertainties, (b) RSD grouped by covariance libraries utilised

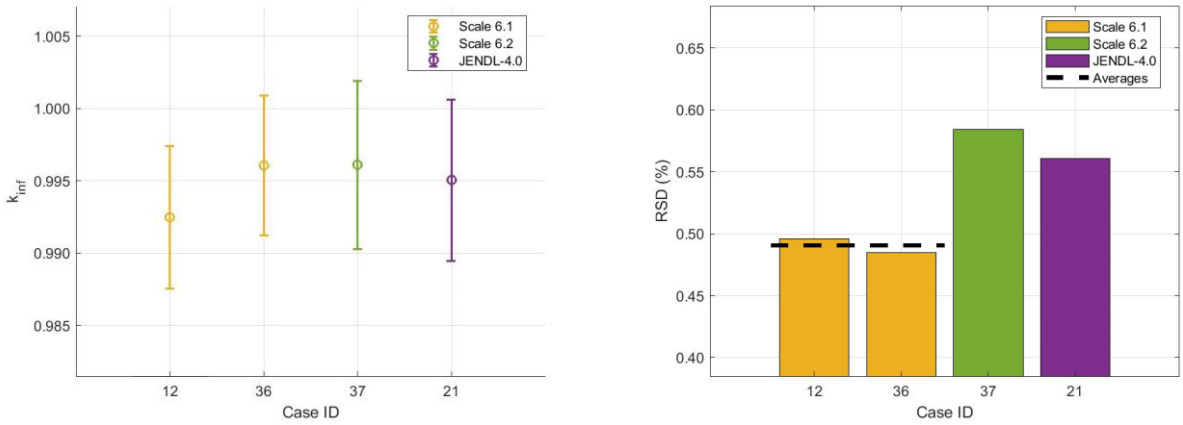

Source: NEA data, 2021

Figure 3.36. RSD of predicted *D* for I-2 BWR-PB-2 at HFP unrodded study: (a) fast group, (b) thermal group

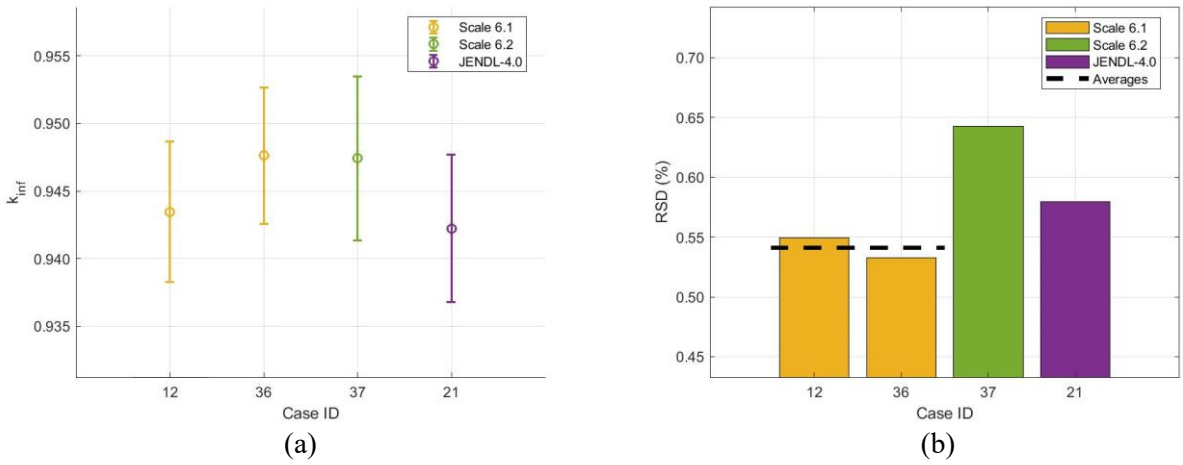

Source: NEA data, 2021

The results of the participants for the pin distributions agree with each other and show RSD less than 1.4% in all the pins. In general, larger relative uncertainties are observed in the pins with lower power something that can be attributed the additional uncertainty coming from either the control rod or Gd presence. Representative results for one case at HFP are shown in Figure 3.37. The left half of the figure is a rodded assembly while the right an unrodded. The fuel pin with the largest RSD is

located in the rodded assembly at location (3,3). Similar behaviour is obtained for the HZP case as well.

Figure 3.37. RSD of predicted *D* for I-2 BWR-PB-2 at HFP unrodded study: (a) fast group, (b) thermal group

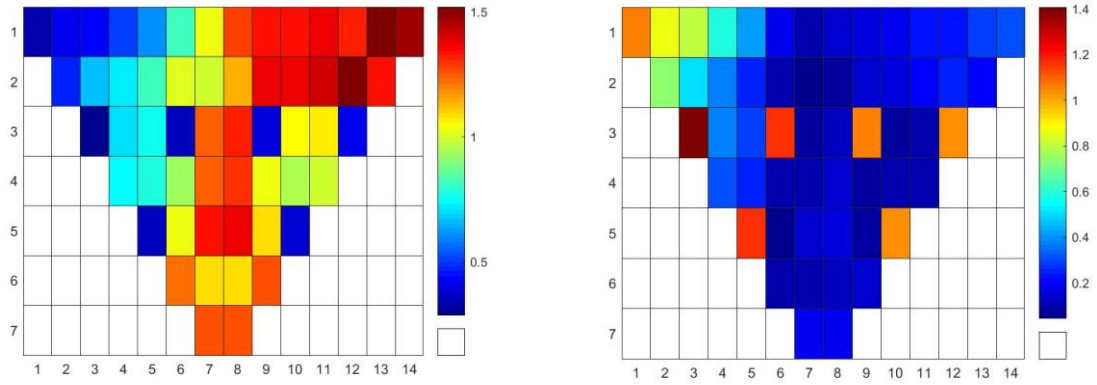

(a) (b)

Source: NEA data, 2021

3.2.3. Exercise I-3: Core physics

As described in Section 3.1.3, the computed uncertainties of the few-group cross sections found in Exercise I-2 are propagated through the neutronics full core calculation in Exercise I-3 to the parameters of interest such as the core *k*-eff and power distribution. This is the final exercise of Phase I, which attempts to understand the uncertainty in key output reactor core parameters and how changes in input parameters can be made to help guide appropriate design decisions in steady-state simulations. The same uncertainty propagation methodologies were used as with the PWR exercise (see Table 3.1). A more thorough explanation and full list of references for these approaches can be found in (Castro et al., 2018[29]).

It should be noted that all of the mentioned propagation methodologies approaches follow a fairly typical reactor simulation methodology, which generates homogenised constants, simplifies core geometry (spatial discretisation), and the application of lower-order neutronic solvers such as nodal diffusion. One of the main differences that occurs in full core simulation depends on whether spatial homogenisation is done over the entire fuel assembly or by pin cell. Each method introduces additional differences in the computed uncertainties of the core parameters of interest, such as *k*-eff and power distribution.

The BWR core physics model is defined as the PB-2 fresh core with 764 fuel assemblies at the HZP conditions (NEA, 2013[9]). In total, 3 sets of submitted results were analysed for PB-2. Of the 3 sets of results, case 21 and 42 utilised a deterministic two-step approach, while case 45 used a Monte Carlo code and modelled the geometry of the core explicitly. Figure 3.38 provides the predicted uncertainties in the core eigenvalue (k_{eff}), which indicates a mean value across the 3 sets of 0. 977 and an RSD of 0.56%. This RSD is comparable to the results found from the HZP pin cell and lattice calculations. More information about the estimated mean and RSD for each covariance library can be found in Table B.6 of Annex B. As in previous analysis, the variation in the uncertainty seems to be directly tied to the VCM choice, as seen from case 21 and 42 that have higher k_{eff} uncertainties compared to case 45. Their choice of using JENDL-4.0 and WIMS (considered as ENDF/B-VII.1), versus case 45's SCALE 6.1 results in slightly higher uncertainties. This is most likely due to the variations between the covariance libraries themselves and specific differences in certain few-group constants uncertainties.

Figure 3.38. RSD of predicted *k*-eff of PB-2 core simulation at HZP

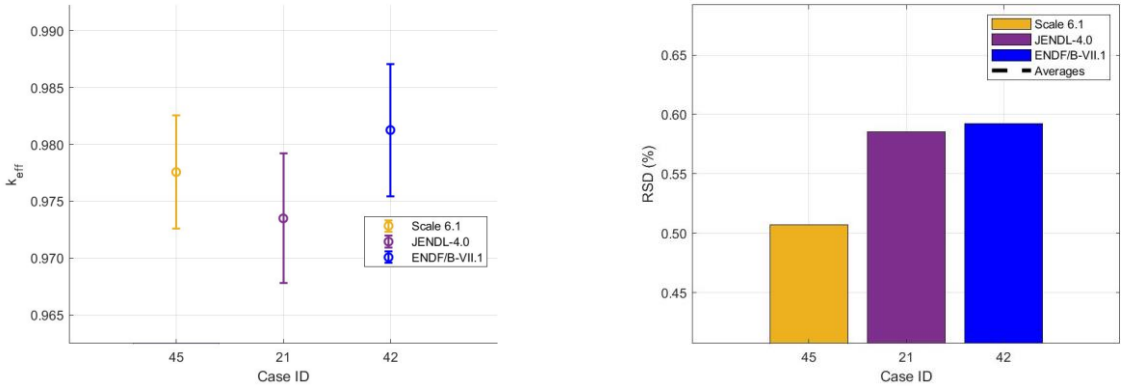

(a) (b)

Source: NEA data, 2021

Using a sampling-based method or perturbation methods allows for estimating uncertainties of many different output variables such as the radial core power distribution. The averaged fuel assembly power and associated RSD from two of the submitted cases (case 21 and case 45) are presented in Figure 3.39 and Figure 3.40. A relatively similar trend in the power distribution trend can be observed between the two cases, with the higher power assemblies near the centre of the core and the low power at periphery. There is also an asymmetry in the power distribution arising from the asymmetric specifications for the BWR-PB-2 exercise (NEA, 2013[9]). However, large differences are observed in the RSD with almost double uncertainty for case 45. The maximum assembly power in the cases are 1.97± 0.30% and 2.36± 4.45%, respectively. As shown, case 45 has some high uncertainties in the radial power, often > 5%.

Figure 3.39. Radial power distribution (1/4 core) with associated uncertainty from Case 11 of PB-2 core at HZP

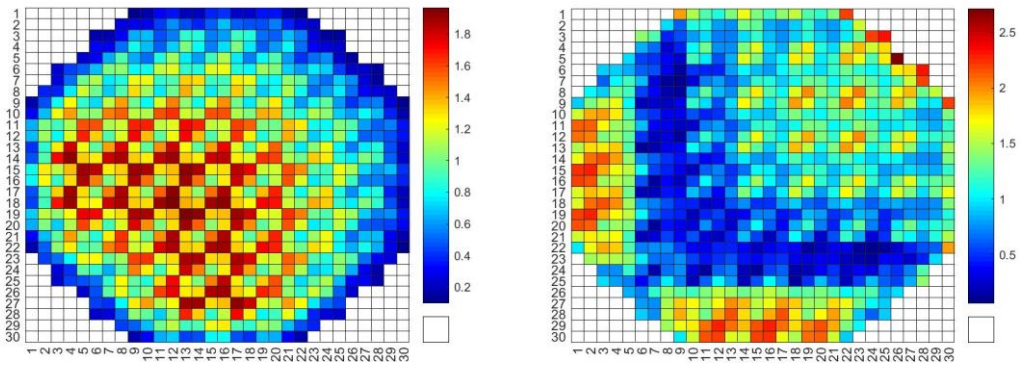

(a) (b)

Source: NEA data, 2021

Figure 3.40. Radial power distribution (1/4 core) with associated uncertainty from Case 11 of PB-2 core at HZP

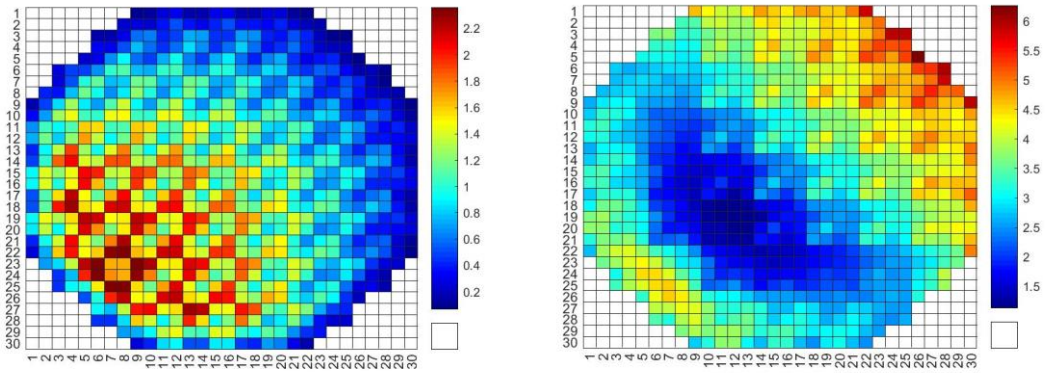

(a) (b)

Source: NEA data, 2021

Figure 3.41 shows the axial power distribution and the associated uncertainties, with a discretisation of 24 axial nodes that divide the BWR core height. The axial power profiles display the shifted cosine shapes typical of boiling water reactors, with a strong bottom-peaking effect. Small differences between them may be due to group constants, control rod worth and the solution methods applied. The associated relative uncertainties of the axial power show a similar behaviour, with matching trends of varying magnitude. In general, the RSD swings from as high as 10% down to 1% across the different cases. The RSD seems to inversely follow the power peaking of the axial nodes, as it is less extreme at high power axial nodes, while peaking near the reactor's top and bottom reflectors.

Figure 3.41. Axial power distribution of PB-2 core at HZP

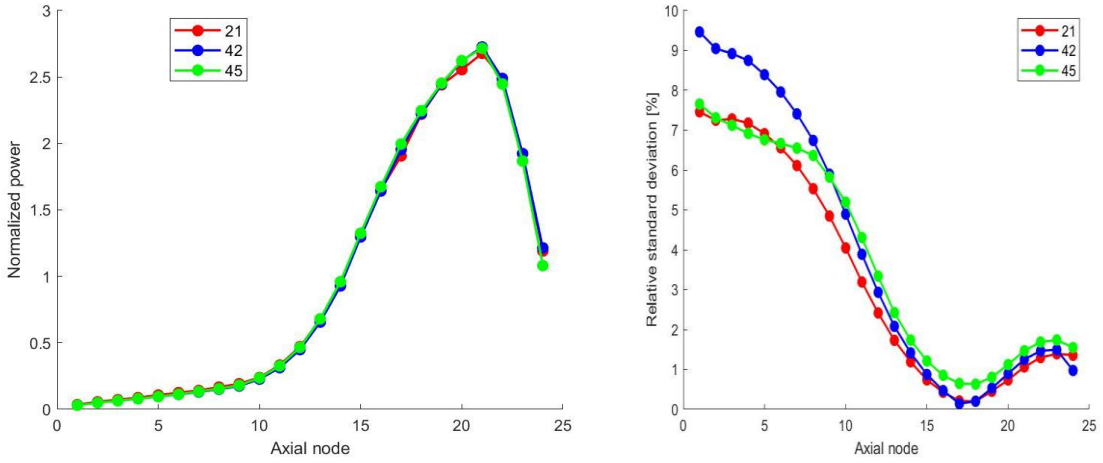

Source: NEA data, 2021

3.3. Water-water energetic reactor (VVER) exercises: KOZ-6

3.3.1. Exercise I-1: Cell physics

For the third reactor design evaluated, the Russian-design VVER, similar results are required as for the other reactors. The calculated *k*-inf and associated uncertainty, the top five neutron-nuclide reactions, and covariances of selected one-group cross sections were collected and analysed.

For the pin cell tests, the 2D model was developed from the Kozloduy-6 (KOZ-6) reactor and used as the representative VVER test problem. The cylindrical fuel pins are within hexagonal cells and are fuelled with 3.3% enriched UO_2 fuel. Unlike the PWR and BWR exercises, which used a square pitch, the VVER exercise uses a triangular pitch for the layout of the fuel and has a hole in the centre of the fuel pin. Similar to the PWR and BWR tests, the VVER was analysed at HZP and HFP conditions. A total of 10 cases were submitted for the HZP condition, while 9 cases were submitted for the HFP condition. One outlier from each case was excluded. The results from these calculations were collected and investigated to determine relations between the choice of calculation parameters (e.g. transport solution method, covariance library, UQ method) and output uncertainties.

Figure 3.42 and Figure 3.43 show the predicted *k*-inf and associated uncertainties for the pin cell KOZ-6 results at HZP and HFP respectively. The nominal value of *k*-inf spans a range of ~1 000 pcm, which primarily is a result of the differences existing among transport codes and base NDLs. The averaged mean value and RSD, of all predicted k-inf are 1.349 and 0.53% for HZP and 1.332 and 0.53% for HFP.

Figure 3.42. Calculated *k*-inf for I-1 VVER-KOZ-6 at HZP: (a) mean value with uncertainties, (b) RSD grouped by covariance libraries utilised

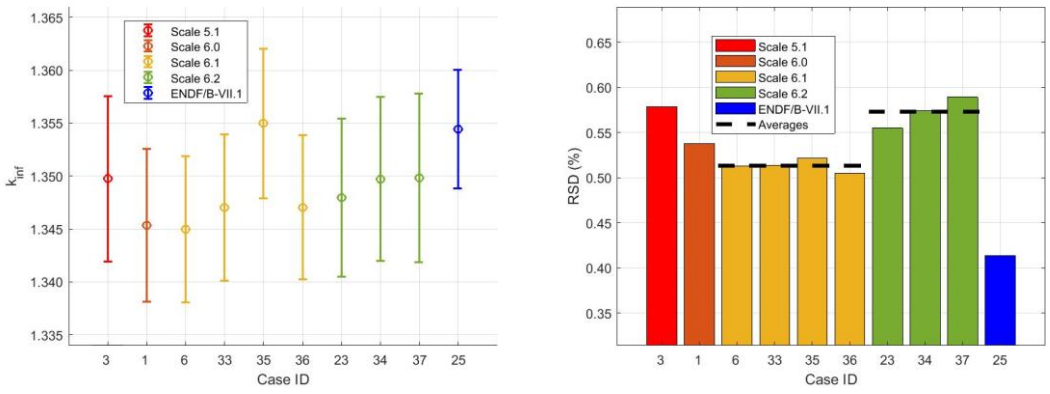

(a) (b)

Source: NEA data, 2021

Figure 3.43. Calculated *k*-inf for I-1 VVER-KOZ-6 at HFP: (a) mean value with uncertainties, (b) RSD grouped by covariance libraries utilised

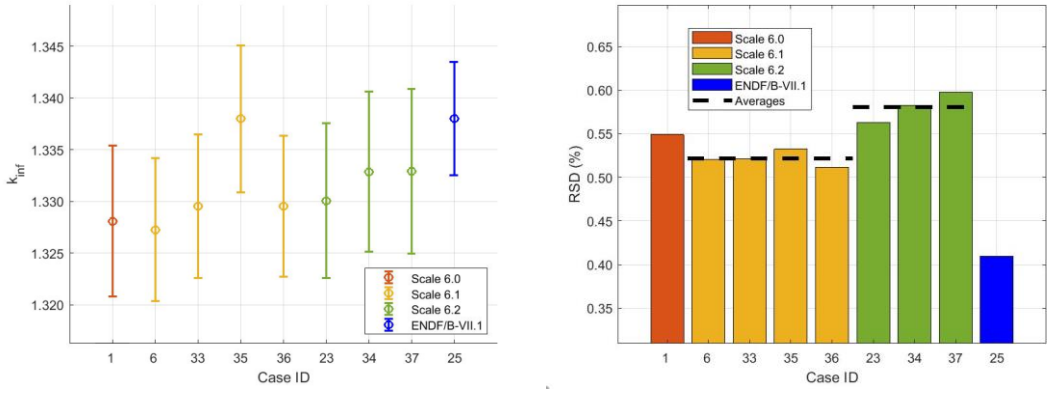

(a) (b)

Source: NEA data, 2021

As in the previous studies, more detailed analyses were performed to determine the correlation of the calculation parameters to output variables. The uncertainty of *k*-inf and the results indicate, once again, that the choice of the covariance library impacts the RSD of *k*-inf. The RSD of *k*-inf calculated using the SCALE 6.0/6.1 covariance libraries is 0.52%. The value corresponding to SCALE 6.2 is approximately 0.58%. Only one data set was submitted using the SCALE 5.1 and ENDF/B-VII.1 covariance libraries restricting general conclusions for these libraries. More information about the estimated mean and RSD for each covariance library can be found in Table B.1 of Appendix B.

Similar to the PWR and BWR trends shown in Sections 3.1.1 and 3.2.1, the trends for the VVER I-1 results can also be explained by understanding the differences between sources and their covariance information. The uncertainty of ^{235}U nu-bar in the thermal range increases from 0.31% in SCALE 6.1 to 0.39% in SCALE 6.2 library. This explains why the calculated RSD of *k*-inf using SCALE 6.2 data is once again slightly higher than that using SCALE 6.0/6.1. The uncertainty of ^{235}U nu-bar is increased to 0.7% in the ENDF/B-VII.1, but this is not reflected in the results as in the PWR exercise. In the BWR exercise this did not occur, probably due to the reduced enrichment of the fuel pin reducing the importance of the ^{235}U nu-bar. In this exercise, the enrichment is also reduced compared to the PWR exercise but this is not the primary reason of the obtained results of case 25, since this case for all the pin cell exercises predicts low uncertainties. This could be attributed to the unusual small uncertainty in the ^{235}U prompt nu-bar in the ENDF/B-VII.1 library, that the participants might have used, as explained in the PWR I-1 exercise.

By using the PT method compared to the sampling approach, the sensitivity coefficients of certain output variables with respect to the nuclear data can be computed efficiently, allowing for the analysis of the most influential nuclide reaction to the calculated *k*-inf uncertainties. Similar to the previous LWR I-1 exercises, the influential nuclide-reaction pairs can be sorted from greatest to least variance fraction and presented in terms of the covariance library used. Figure 3.44 shows a histogram of the top five uncertainty-contributing nuclide-reaction pairs for the VVER-KOZ-6 HZP study.

Figure 3.44. Ranking of the five nuclide-reaction pairs with the highest contribution to the *k*-inf uncertainty for I-1 VVER-KOZ-6 at HZP [7.1= ENDF/B-VII.1 and the rest X.Y = SCALE X.Y covariance libraries]

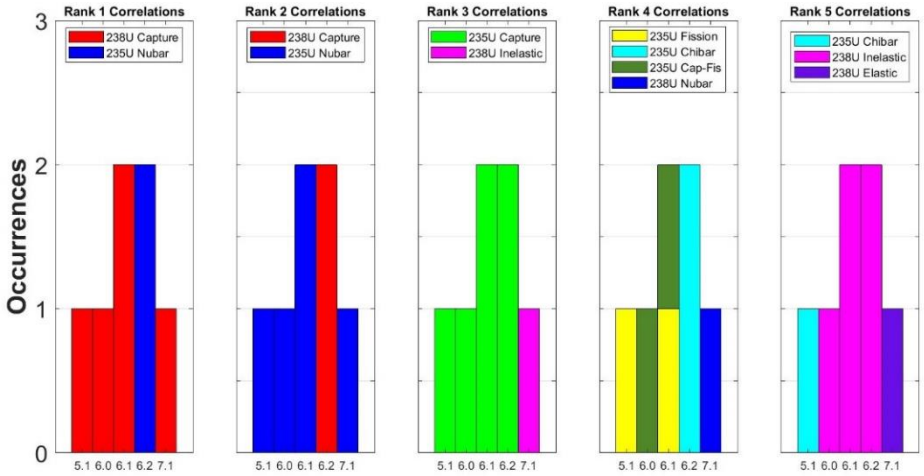

Source: NEA data, 2021

Although there are some deviations, the figure is very similar to the HZP results for TMI-1 and PB-2 with a few of the reaction-pairs especially contributing uncertainty to *k*-inf, which are ^{238}U capture, ^{235}U nu-bar and ^{235}U capture. These main contributors for *k*-inf are identifiable, once again, by the 1) highest sensitivities associated with such reactions, 2) the highest value of the associated covariances, or 3) a combination of both. For the HZP study with 3.3% enrichment, it is expected the sensitivity of *k*-inf to be most similar to the PB-2 HZP. In fact, this is what is observed, since the ^{238}U capture cross section is ranked first in most of the cases. The results differ compared to the TMI-1 HZP because of the lower enrichment reducing the importance of ^{235}U nu-bar. Only for the submitted results using SCALE 6.2, where the ^{235}U nu-bar uncertainty is larger, the ^{235}U nu-bar was ranked first. For the HZP cases, ^{235}U capture appears as another important contributor to uncertainty that is consistently ranked third most influential. Additionally, some less influential nuclide-reaction pairs, like ^{235}U chi-bar and ^{238}U inelastic scattering, are found in lower ranks. Once again, some of these variations can be explained by the differences in the libraries themselves. The HFP ranking results are similar, for the higher rankings, to the HZP results in this exercise. This indicates a deviation compared to the PB-2 HFP were even the cases using SCALE 6.2 ranked first the ^{238}U capture. This happens because in the VVER-KOZ-6 there is no hardening of the spectrum at HFP and thus in this aspect is closer to the TMI-1 HFP.

3.3.2. Exercise I-2: Lattice physics

The I-2 exercise focuses on propagating nuclear data uncertainties through lattice calculations to determine the uncertainty of specific output variables such as *k-inf*, group constants like cross sections, diffusion coefficients and discontinuity factors (when available).

The VVER lattice is a 2D hexagonal fuel assembly model consisting of 312 fuel rods with 18 control rod guide tubes, 1 water rod, and a combination of 3.0% and 3.3% enriched fuel. There are nine sets of submitted results for the HZP unrodded and six results were submitted for the rodded. For the HFP unrodded six results were submitted, while five results for the HFP rodded. Figure 3.45 and Figure 3.46 show the predicted uncertainty in *k*-inf for HZP and HFP studies respectively. The RSD is consistent between data in both sets and follows the general trend of LWR studied so far. The HZP cases show a large spread of the mean value related mainly by cases 3, 4 and 24 that seem to underpredict significantly the *k*-inf in the unrodded study and overpredict in the rodded study. When

neglecting these submitted results for the HZP, the spread is at the order of ~1 000 pcm, similar to the spreads for the other reactors. This is also obtained for the HFP cases where the outliers are not present. More information about the estimated mean and RSD for each covariance library can be found in Table B.2 of Annex B.

The trend for the RSD is typical of what has been seen so far in previous LWR exercises. The RSD in the unrodded study is slightly lower than that of the rodded study, regardless of the choice of VCM. This can be attributed to the more complex neutron transport behaviour with more spatial and energy gradients in the presence of control rods. Again there is a higher predicted uncertainty by the SCALE 6.2 library due to the increased uncertainty of the ^{235}U nu-bar cross section. Concerning the ranking of the important reactions, similar results with the VVER I-1 exercise are obtained, with the most important reactions being first the ^{238}U capture, then the ^{235}U nu-bar (ranked first for the SCALE 6.2 library only) and third the ^{235}U capture.

Figure 3.45. Calculated *k*-inf for I-2 VVER-KOZ-6 at HZP: (a) mean value with uncertainties for unrodded, (b) RSD for unrodded (c) mean value with uncertainties for rodded, (d) RSD for rodded

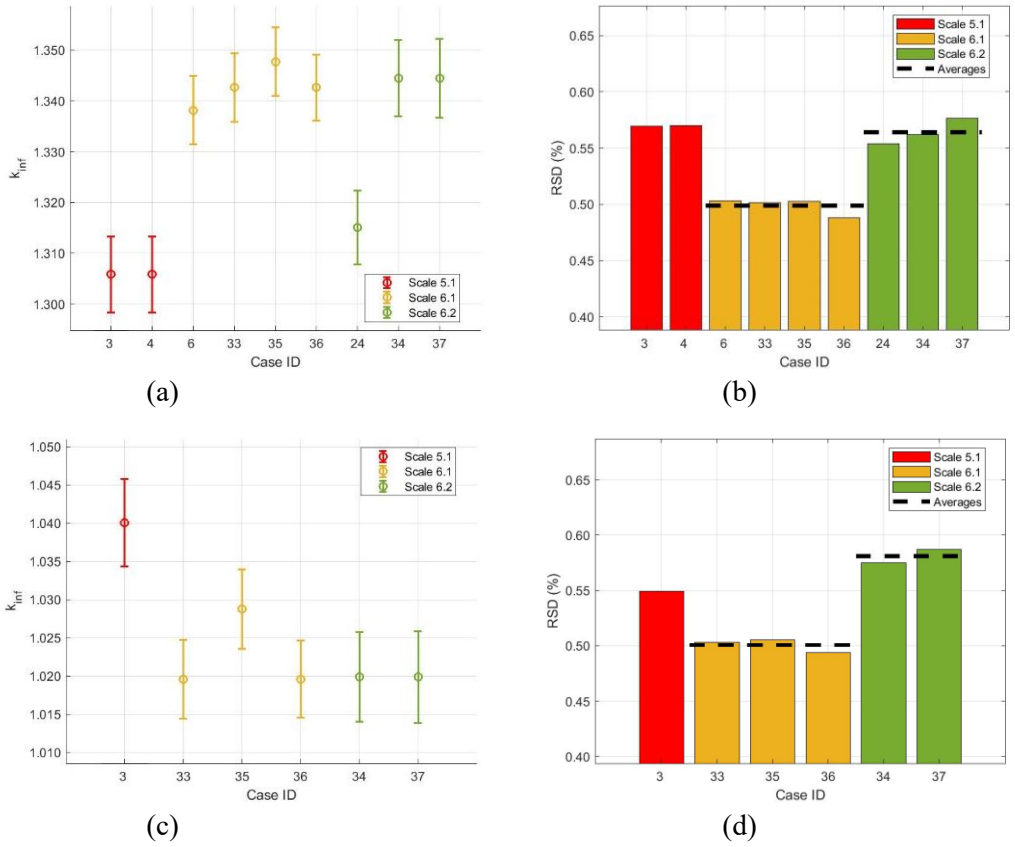

Source: NEA data, 2021

Figure 3.46. Calculated *k*-inf for I-2 VVER-KOZ-6 at HFP: (a) mean value with uncertainties for unrodded, (b) RSD for unrodded (c) mean value with uncertainties for rodded, (d) RSD for rodded

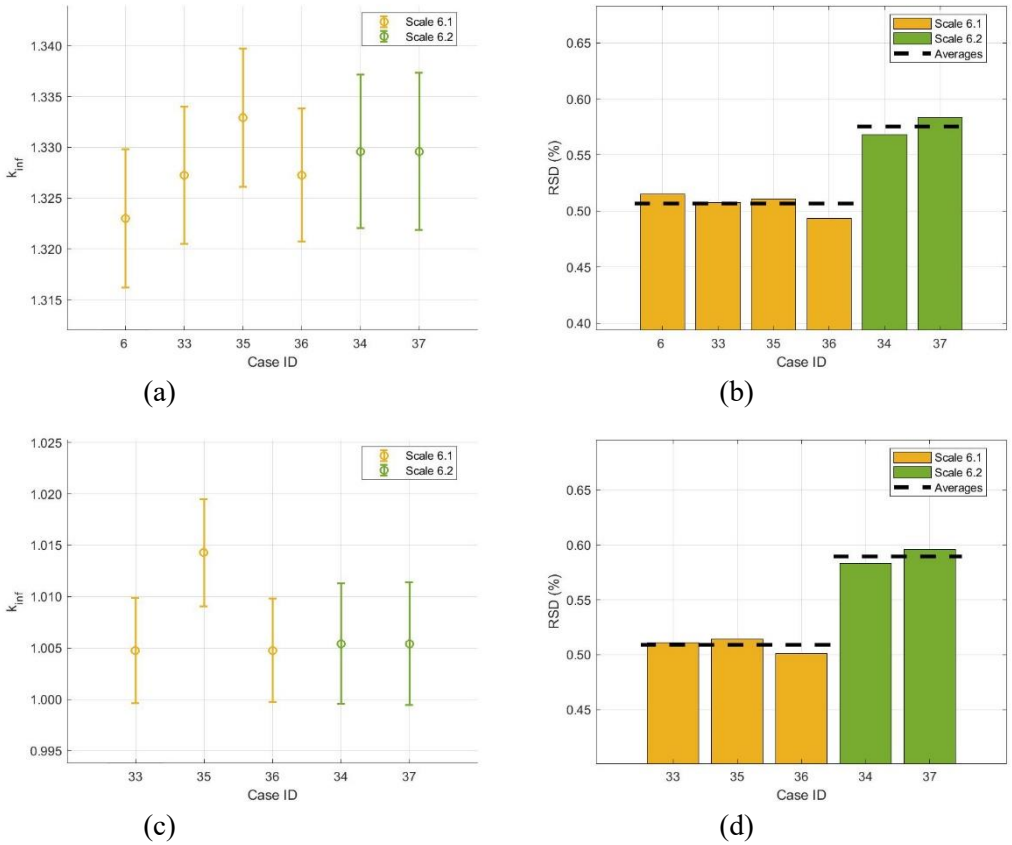

Source: NEA data, 2021

As in the other LWR exercises, the homogenised two-group nu-fission cross sections and the diffusion coefficients are analysed and organised by the choice of VCM, as seen in Figure 3.47 and Figure 3.48 for the HZP unrodded study. The general trend found in the other LWR is observed here as well with higher uncertainties for the fast group constants. For nu-fission cross section it is interesting that for the thermal group there is no variation between the different LWR exercises. However, for the fast group there is a significant difference. For example, for the PWR exercise the RSD of case 36 is 0.52%, for the BWR exercise is 0.98% and here for the VVER is 0.70%. Similar variations are obtained for the other submitted cases as well. This can be related to the enrichment of the fuel because the reduction of the number of ^{235}U nuclei increases the probability of fission in the fast group through ^{238}U, where its nu-bar and fission uncertainties in the epithermal and fast energies is much higher than the ^{235}U. This can explain why the BWR exercise, which has the lowest enrichment, exhibits the largest nu-fission fast group RSD followed by this VVER exercise. For the diffusion coefficient, the differences between the fast group and thermal group are larger with an RSD of 2.3% in the fast group and 0.27% in the thermal group. This behaviour is observed across the different LWR exercises and the different cases. One interesting aspect is the reduced uncertainty of case 35, found mainly for the fast group diffusion coefficient and not the other group constants. The difference between case 35 and 36 is the code used for the lattice calculation and the NDL library, indicating that one of these or a combination of them is responsible for this discrepancy. More information about the average RSD for each covariance library can be found in Table B.4 and Table B.5 of Annex B.

Figure 3.47. RSD of predicted $\nu\Sigma_f$ for I-2 VVER-KOZ-6 at HZP unrodded study: (a) fast group, (b) thermal group

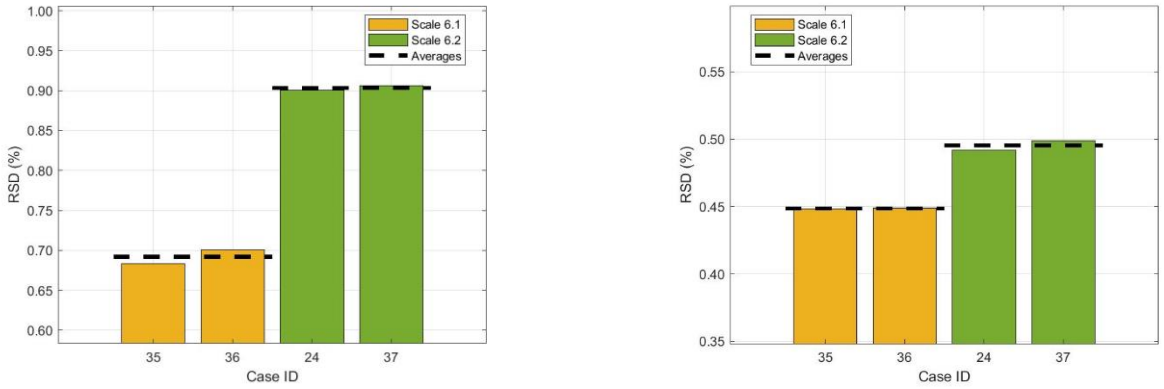

Source: NEA data, 2021

Figure 3.48. RSD of predicted *D* for I-2 VVER-KOZ-6 at HZP unrodded study: (a) fast group, (b) thermal group

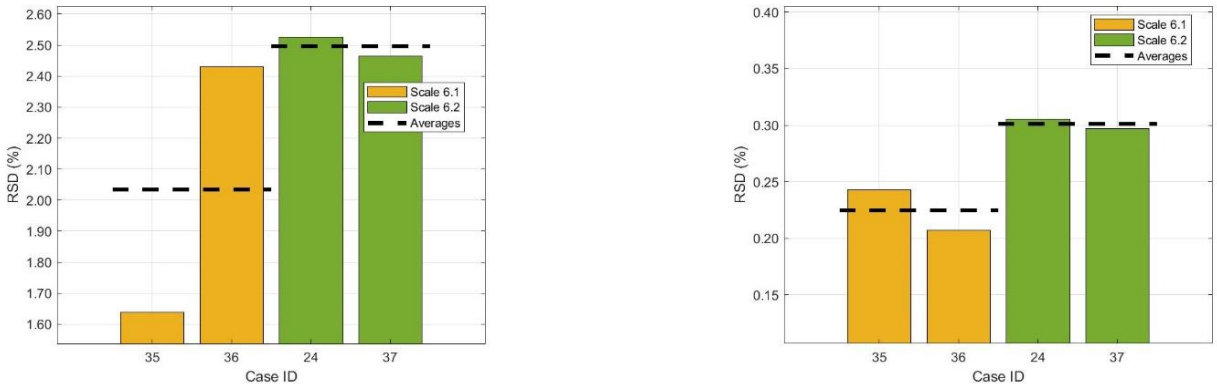

Source: NEA data, 2021

For the parameters of interest such as *k-inf*, flux, and group constants (cross sections, diffusion coefficients, etc.), the relationship between them in the two-group representation can be understood by computing the correlation coefficients between variables. Similar to the PWR and BWR results, specific correlation coefficient matrices are presented in Figure 3.49 for the HZP unrodded lattice calculations, where red and blue represent positive and negative correlations, respectively, between two parameters, while white represents correlations close to zero. Intermediate shades of light red or light blue represent varying degrees of positive or negative correlations, respectively.

Figure 3.49. Correlation coefficient matrix of the two-group homogenised cross sections of the unrodded HZP lattice from (a) case 36 with SCALE 6.1 and (b) case 37 with SCALE 6.2

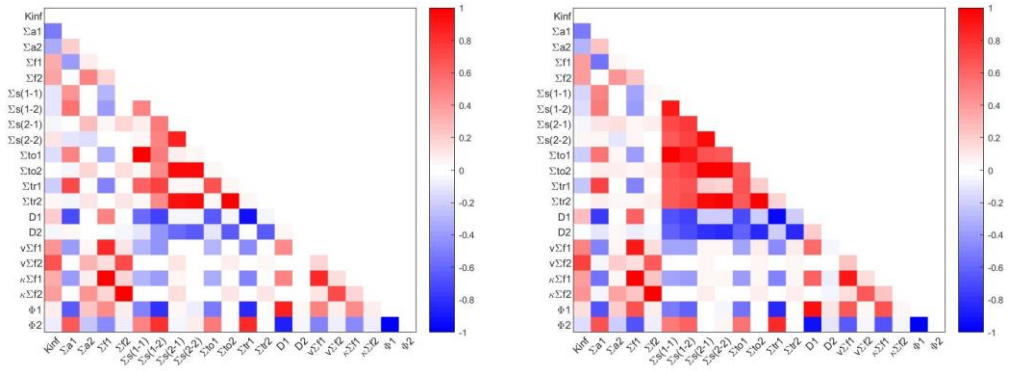

(a) (b)

Source: NEA data, 2021

The correlation coefficient matrices seem to show reasonable agreement, with some main common trends appearing in both of the selected cases. This can be observed by noting the negative correlation between the Group 1 absorption and the *k*-inf, as well as the positive correlation between *k*-inf and the Group 2 nu-fission cross section. There are some unique trends than can be observed for case 37, as in the other LWR exercises, with a strong positive correlation between the scattering and transport cross sections of both thermal and fast group. One conclusion, that applies to previous LWR exercises as well, is that the choice of VCM has the most important impact in the correlation coefficient discrepancies. This is highlighted by the fact that the correlation coefficients are consistent between cases that consider the same VCM even if different transport codes are used. However, some differences can appear between cases that consider different VCM. The VVER-KOZ-6 I-2 submitted results are less complete than the TMI-I or even PB-2 counterparts, resulting in a less than optimal set of data for analysis. Additional investigations and analysis are suggested with more complete correlation coefficient matrices to identify causes for certain features and to determine the impact of the VCM choice used in the lattice calculations. The variations in the group constants are likely to propagate to the core calculations in I-3 and impact the uncertainty of full core parameters.

There were no reported results for the ADF calculation with a 1D model or for the VVER-KOZ-6 minicore colourset lattice calculations.

3.3.3. Exercise I-3: Core physics

As described in Section 3.1.3, the computed uncertainties of the few-group cross sections found in Exercise I-2 are propagated through the neutronics full core calculation in Exercise I-3 to the parameters of interest such as the core *k*-eff and power distribution. As the final exercise of Phase I, this analysis attempts to understand the uncertainty in key output reactor core parameters for the VVER and how improvements could be made to help guide designers during steady-state simulations. The same uncertainty propagation methodologies were used as with the PWR and BWR exercise (see Table 3.1). A more thorough explanation and full list of references for these approaches can be found in (Castro et al., 2018[29]).

The VVER- KOZ-6 core physics model is defined as a core with 163 fuel assemblies and 48 reflector assemblies at the HZP conditions (NEA, 2013[9]). In total, only one set of submitted results were analysed for VVER-KOZ-6 I-3. Figure 3.50 provides the predicted uncertainty in the core eigenvalue, which indicates a value of around 0.56%. This RSD is comparable to the results found from the HZP pin cell and lattice calculations. The estimated mean and RSD are gathered in

Table B.6 of Annex B which includes all the LWR I-3 exercises. The lack of submitted results makes comparisons regarding the impact of different covariance libraries impossible.

Figure 3.50. Calculated *k*-inf for I-3 VVER-KOZ-6 full core at HZP: (a) mean value with uncertainties, (b) RSD grouped by covariance libraries utilised

(a) (b)

Source: NEA data, 2021

By using a sampling-based methods, it allows for the computation of many different output variables such as the radial core power distribution. A relatively unique power distribution can be seen in Figure 3.51, with peak assembly powers at six peripheral locations and with the minimum assembly power in the centre. Generally, the relative uncertainties for the assembly power are higher near the low power regions of the core, which is a similar trend found in the other LWR as well. The maximum assembly power in this case is 2.08 $\pm$ 1.1% and the uncertainties increase up to 5.3% in the centre.

Figure 3.52 shows the axial power distribution and the associated uncertainties within the VVER, with a discretisation of 10 axial nodes that divide the KOZ-6 core height. The axial power profiles indicate the shifted cosine shapes typical of a VVER. The RSD seems to inversely follow the power peaking of the axial nodes, as it is less extreme at high power axial nodes due to the larger nominal value. Further analysis, including additional cases, is suggested for the VVER I-3 exercise in order to conduct a thorough comparative analysis on the unique full core physics of VVER reactors.

Figure 3.51. Compressed radial assembly power distribution for I-3 VVER-KOZ-6 full core at HZP from case 5 (a) mean and (b) RSD

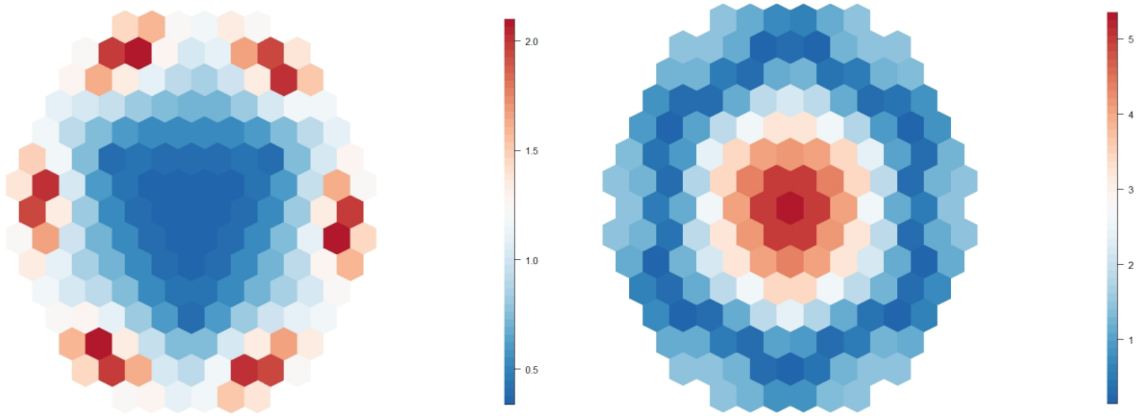

(a) (b)

Source: NEA data, 2021

Figure 3.52. Calculated axial core power distribution for I-3 VVER-KOZ-6 full core at HZP from case 5 (a) mean and (b) RSD

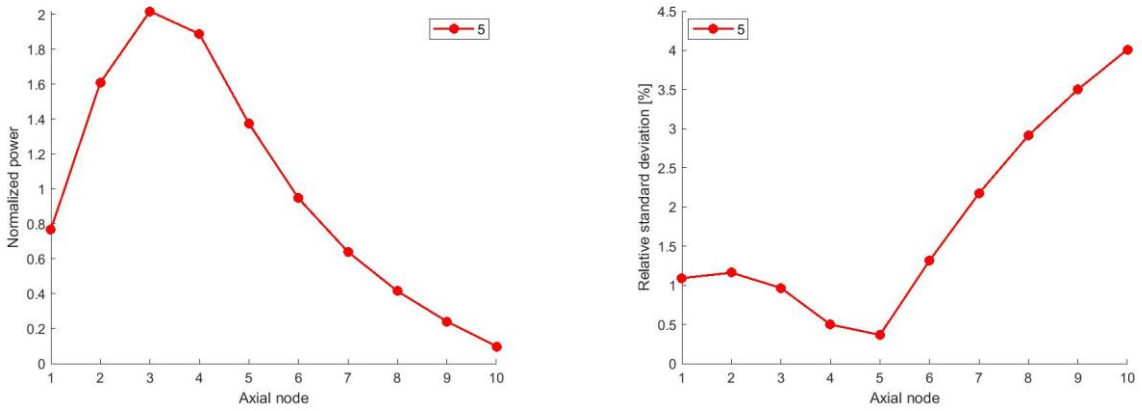

(a) (b)

Source: NEA data, 2021

3.4. Generation III reactor exercises: GEN-III

3.4.1. Exercise I-1: Cell physics

As for the other reactor types in Exercise I-1, the following results were requested from participants: calculated *k*-inf and its associated uncertainty, the top five neutron-nuclide reactions that contribute the most uncertainty to *k*-inf, and covariances of selected one-group cross sections generated in the pin cell calculation.

A 2D PWR MOX fuel pin was selected as the representative GEN-III test problem. It has 9.8% Pu composition and the HFP condition is modelled. More information about this exercise's details can be found in (NEA, 2013[9]). This exercise differs from the previously studied LWR exercises due to the presence of Pu. This was done to enhance the differences between the neutronics exercises. In total, 8 sets of results have been submitted for the HFP condition and Figure 3.53 shows the predicted *k*-inf and associated uncertainties. The nominal value of *k*-inf spans a range of ~1 500 pcm around the value of 1.105 resulting from the differences existing among base nuclear data libraries and the transport codes used. A significant increase of the predicted RSD compared to the previous LWR exercises is observed for the SCALE 6.0/6.1 covariance libraries (excluding the one outlier) of almost doubling of the uncertainty from ~0.5% to ~0.95%. For the SCALE 6.2 library, this does not occur with an RSD of 0.60%, a result similar to the other exercises. This increase for the SCALE 6.0/6.1 VCM is related to the Pu composition of the MOX fuel. More information about the estimated mean and RSD for each covariance library can be found in Table B.1 of Annex B. In Figure 3.54 the 235U and 239Pu nu-bar cross sections are plotted for the SCALE 6.1 44G and SCALE 6.2 56G covariance libraries. We can deduce that the increased predicted RSD in the SCALE 6.0/6.1 cases arises from the increased nu-bar uncertainty of ^{239}Pu compared to the ^{235}U (1.05 % vs 0.31% in the thermal group) and thus the higher the Pu composition the higher will be the *k*-inf RSD when these libraries are used. In the SCALE 6.2 covariance library, the ^{239}Pu nu-bar uncertainty is reduced significantly to 0.18% while the ^{235}U nu-bar uncertainty is increased to 0.39%. Therefore, the SCALE 6.2 cases do not show significant changes in the predicted RSD compared to the other LWR exercises. The limited number of submitted results restricts us to a preliminary analysis without the possibility to completely generalise for all the VCMs.

Figure 3.53. Calculated *k*-inf for I-1 GEN-III at HFP: (a) mean value with uncertainties, (b) RSD grouped by covariance libraries utilised

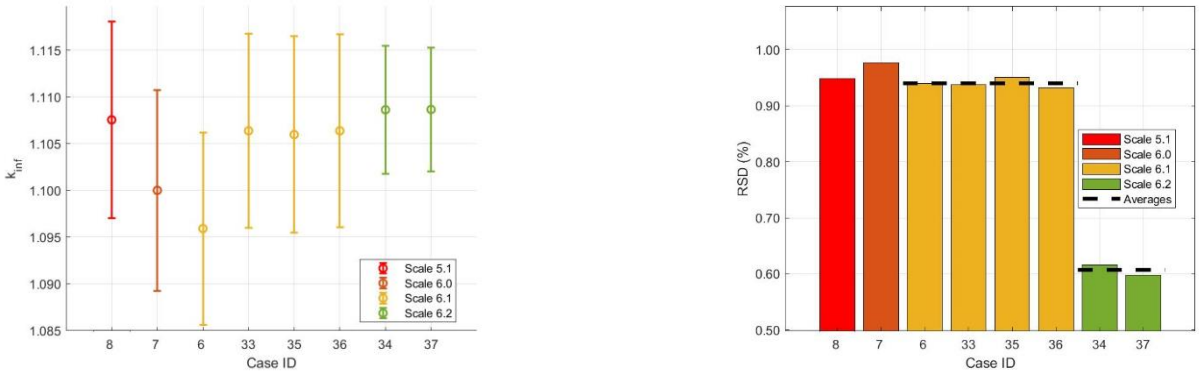

(a) (b)

Source: NEA data, 2021

Figure 3.54. RSD of 235U and 239Pu nu-bar multi-group cross sections from SCALE 6.1 44G and SCALE 6.2 56G covariance libraries

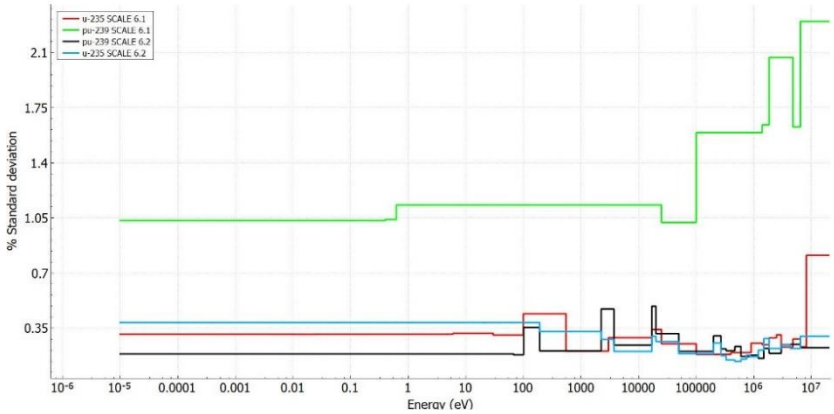

Source: NEA data, 2021

It is convenient to use the PT method to compute the sensitivity coefficients of output variables with respect to nuclear data as compared with the sampling approach, thus making it possible to determine the most influential nuclide-reaction pair to the predicted *k*-inf uncertainties by sorting them from greatest to least variance fraction. For the GEN-III HFP study, 5 sets of submitted results include such information and Figure 3.55 shows the occurrence of various nuclide-reaction pairs as the top five contributors. Although a certain degree of diversity can be found in the ranking as it includes up to seven nuclide-reaction pairs, some reactions dominate the contribution to the uncertainty of *k*-inf, such as ^{239}Pu nu-bar, ^{238}U inelastic scattering and ^{238}U capture.

We observe significant differences compared to the previous LWR exercises arising from the Pu composition of the GEN-III MOX fuel. For example, the ^{235}U nu-bar is not present among the top five contributors to the *k*-inf uncertainty. For the SCALE 6.0 and 6.1 cases, the ^{239}Pu nu-bar is always ranked first something consistent with the previous justification for the increased predicted RSD in these cases due to the increased uncertainty of ^{239}Pu nu-bar cross section in the SCALE 6.1 VCM. For the lower ranks of SCALE 6.0/6.1 cases, the ^{238}U capture is ranked second in most of the cases mainly because the *k*-inf is quite sensitive to the ^{238}U capture cross section, especially in the unresolved resonance regions, where the evaluated cross sections exhibit large uncertainties (Trkov et al., 2005[26]). In the third rank the ^{239}Pu fission mainly occurs and for the lower ranks other ^{239}Pu

and ^{242}Pu cross sections appear. Only one result for the SCALE 6.2 is submitted so it is difficult to generalise the conclusions. In this result, ^{238}U is ranked first, probably due to the ^{235}U composition (natural uranium composition) in the MOX fuel. This is the reason why ^{235}U does not appear in the top five ranks for the SCALE 6.2 VMC, even if its uncertainty was increased compared to SCALE 6.1 VCM. In the second and third rank, the ^{239}Pu fission and ^{239}Pu capture respectively reflect some small differences between the SCALE 6.1 and 6.2 VCMs.

Figure 3.55. Ranking of the five nuclide-reaction pairs with the highest contribution to the *k*-inf uncertainty for I-1 GEN-III at HFP [X.Y = SCALE X.Y covariance libraries]

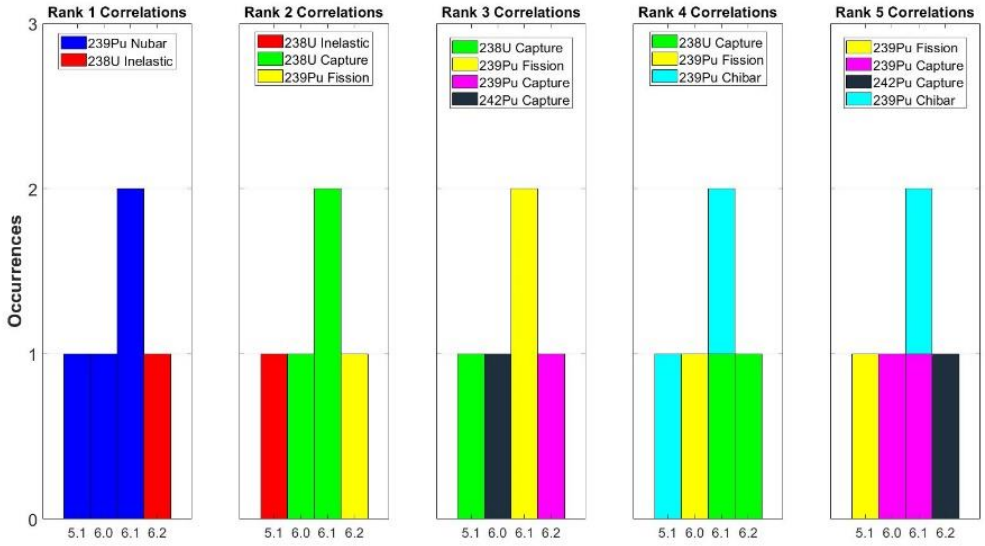

Source: NEA data, 2021

3.4.2. Exercise I-2: Lattice physics

The I-2 exercise, as for the other LWR cores, focuses on propagating nuclear data uncertainties through lattice calculations to determine the uncertainty of specific output variables such as *k*-inf, group constants like cross sections, diffusion coefficients and discontinuity factors.

For the GEN-III core, four different types of assemblies were modelled in 2D lattice calculations. The GEN-III assemblies are in a 17×17 lattice consisting of 265 fuel rods and 24 guide tubes. Assembly T1 is a UOX assembly with a mixed fuel composition of 2.1% and 4.2% ^{235}U enrichment and without UO_2-Gd_2O_3 rods. Assembly T2 is a UOX assembly with 4.2% ^{235}U enrichment for the UO_2 fuel rods and 12 UO_2-Gd_2O_3 rods with 2.2% ^{235}U enrichment. Assembly T3 is a UOX assembly with 3.2% ^{235}U enrichment for the UO_2 fuel rods and 20 UO_2-Gd_2O_3 rods with 1.9% ^{235}U enrichment. Assembly T4 is a MOX assembly including fuel rods with three different Pu composition: 3.7%, 6.5% and 9.8. The assemblies were modelled at HFP conditions and unrodded. A total of 5 sets of results were submitted from cases 33-37. Figure 3.56 and Figure 3.57 show the predicted uncertainty in *k*-inf for the four assemblies. A relative constant spread of ~500 pcm for the mean values is observed for each assembly. A similar trend to the previous exercise is observed for the RSD. For the UOX assemblies SCALE 6.2 predicts a RSD of ~0.60%, a similar trend observed in the other LWR exercises. For the MOX assembly SCALE 6.1 predicts larger RSD of ~0.95% due to mainly the higher ^{239}Pu nu-bar uncertainty as was explained in the previous exercise. More information about the estimated mean and RSD for each covariance library can be found in Table B.2 of Annex B. Concerning the ranking of the important reactions, for the UOX the trend follows again the other LWR exercises with the dominant cross sections being ^{238}U capture and ^{235}U nu-bar, while for the

MOX similar trend to the previous exercise is found with ^{239}Pu nu-bar and ^{238}U inelastic scattering being the dominant ones.

Figure 3.56. Calculated *k*-inf for I-2 GEN-III at HFP unrodded: (a) mean value with uncertainties for T1, (b) RSD for T1 (c) mean value with uncertainties for T2, (d) RSD for T2

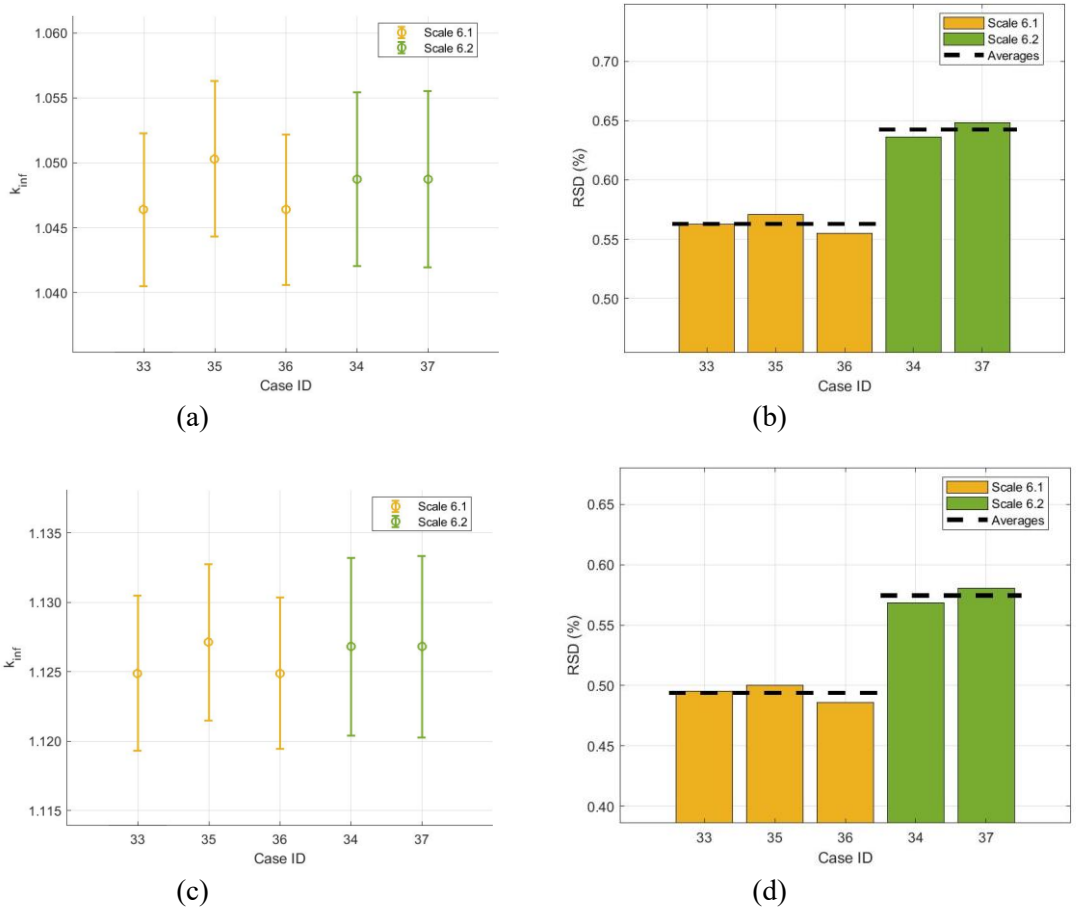

Source: NEA data, 2021

Figure 3.57. Calculated *k*-inf for I-2 GEN-III at HFP unrodded: (a) mean value with uncertainties for T3, (b) RSD for T3 (c) mean value with uncertainties for T4, (d) RSD for T4

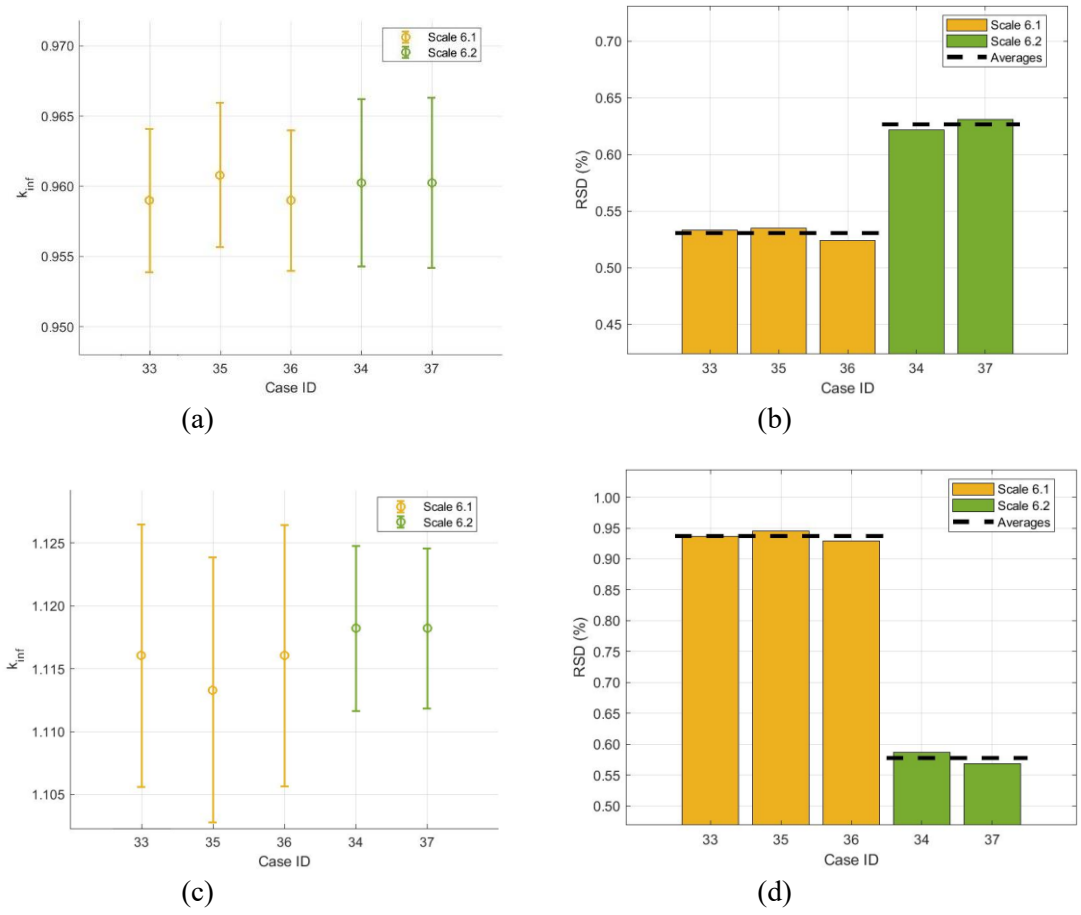

Source: NEA data, 2021

The homogenised two-group nu-fission cross sections and the diffusion coefficients are analysed and organised by the choice of VCM and the results for the MOX assembly are presented in Figure 3.58 and Figure 3.59. For the diffusion coefficient, the general trend found in the other LWR is observed here as well with higher uncertainties for the fast group at the order of ~2.50% indicating that the Pu composition does not have any significant effect. However, for nu-fission cross section a large impact of the Pu is observed for the same reasons with the *k-inf*. We observe larger predicted uncertainties by the SCALE 6.1 VCM but now for the thermal group with a RSD of ~ 1.07%, which is almost double compared to the other LWR exercises. This doubling of the uncertainty in the thermal group is consistent with the almost doubling of the k-inf uncertainty. More information about the average RSD for each covariance library can be found in Table B.4 and Table B.5 of Annex B.

Figure 3.58. RSD of predicted $\nu\Sigma_f$ for I-2 GEN-III T4 assembly and HFP unrodded study: (a) fast group, (b) thermal group

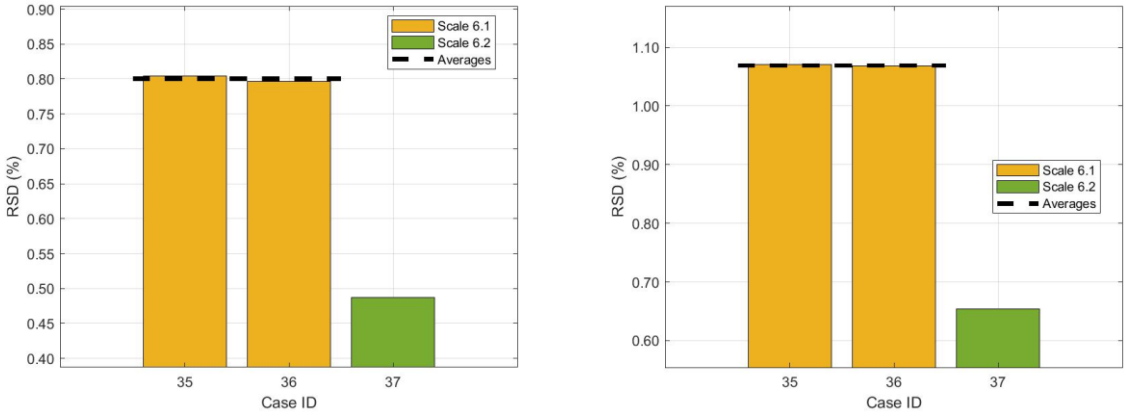

(a) (b)

Source: NEA data, 2021

Figure 3.59. RSD of predicted D for I-2 GEN-III T4 assembly and HFP unrodded study: (a) fast group, (b) thermal group

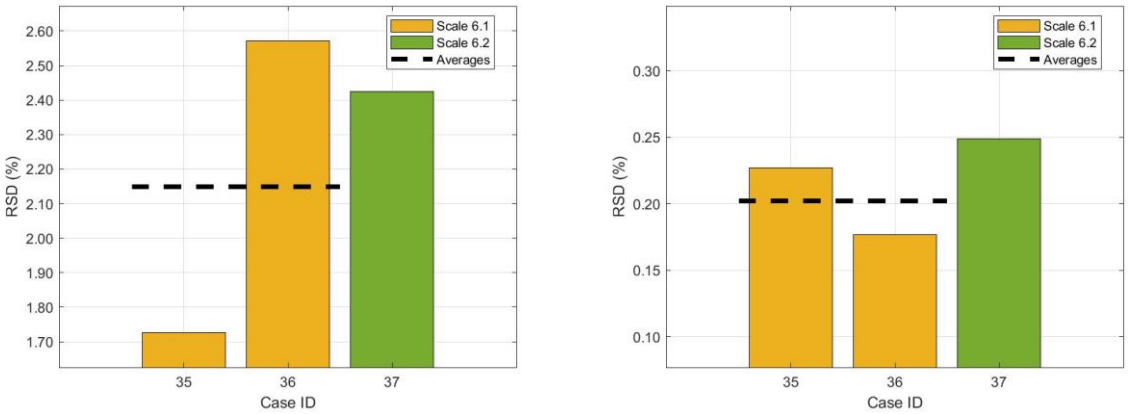

(a) (b)

Source: NEA data, 2021

For the parameters of interest such as *k-inf*, flux, and group constants (cross sections, diffusion coefficients, and assembly discontinuity factors), the relationship between them in the two-group representation can be understood by computing the correlation coefficients between variables. Similar to the other LWR exercises, specific correlation coefficient matrices are presented in Figure 3.60 for the MOX assembly, where the red and blue colour map represents positive and negative correlation between the case parameters, respectively, while a correlation close to zero appears as white.

Figure 3.60. Correlation coefficient matrix of the two-group homogenised cross sections of the unrodded T4 MOX HFP lattice from (a) case 36 with SCALE 6.1 and (b) case 37 with SCALE 6.2

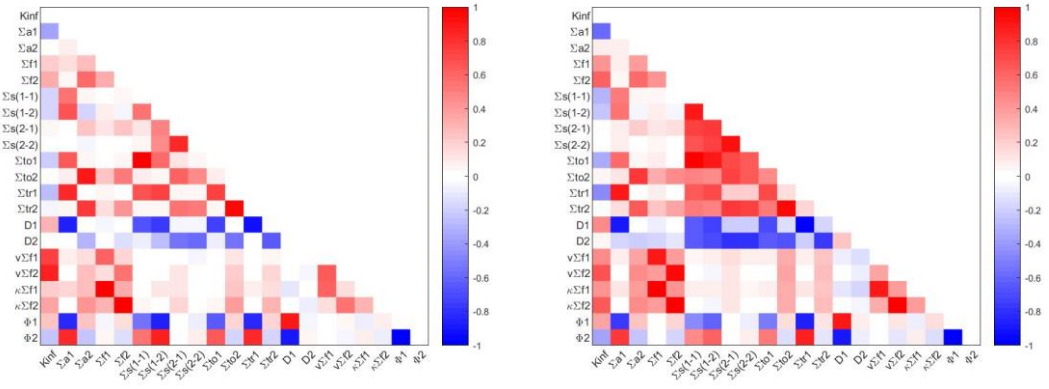

(a) (b)

Source: NEA data, 2021

As in the other reactor exercises, the correlation coefficient matrices seem to show reasonable agreement, with common trends appearing in both of the selected cases. This can be observed by noting the negative correlation between the Group 1 absorption and the *k*-inf, as well as the positive correlation between *k*-inf and the Group 2 nu-fission cross section. The same unique trends of case 37 are also observed here, with strong positive correlation between the scattering and transport cross sections of both thermal and fast group. Once again, the GEN-III I-2 submitted results are less complete than the TMI-I or even PB-2 counterparts, resulting in a less than optimal set of data for analysis. Additional investigations and analysis are suggested with more complete correlation coefficient matrices to identify causes for certain features and to determine the impact of the VCM choice used in the lattice calculations. The variations in the group constants are likely to propagate to the core calculations in I-3 and impact the uncertainty of full core parameters.

3.4.3. Exercise I-3: Core physics

The computed uncertainties of the few-group cross sections found in Exercise I-2 are propagated through the neutronics full core calculation in Exercise I-3 to the parameters of interest such as the core *k*-eff and power distribution. As the final exercise of Phase I, this analysis attempts to understand the uncertainty in key output reactor core parameters for two GEN-III cores. The first is a UOX core consisting of the 241 UOX assemblies and the second is a mixed UOX/MOX core with MOX assemblies in the periphery and UOX assemblies in the centre for a total of 241 assemblies. Both cores are surrounded by a stainless steel heavy reflector and water. The cores are modelled at both HZP and HFP conditions. The same uncertainty propagation methodologies were used as with the PWR and BWR exercise (see Table 3.1). More details about the core can be found in (NEA, 2013[9]). It should be noted once again that the propagation methodologies approaches follow typical reactor simulation methodology, which develops the homogenised group constants, simplifies core geometry (spatial discretisation), and applies lower-order neutronic solvers such as nodal diffusion.

The *k*-eff results are presented in Figure 3.61 for the UOX and UOX/MOX cores at HFP conditions. For both cores the spread of the mean values is ~250 pcm and the predicted RSD is ~0.55% similar to the other LWR exercises. The UOX/MOX core does not show an increased RSD as in the I-1 and I-2 exercises due to the small number of MOX assemblies in the core (about 20% of the total number of assemblies). Similar trends are observed for the HZP cases as well. More information about the estimated mean and RSD for each covariance library can be found in Table B.6 of Annex B.

From the available results, only two cases included results for the power distribution. The power distribution uncertainty propagation results are presented in Figure 3.62 for the UOX core at HFP of case 37 and in Figure 3.63 for UOX/MOX core at HFP of case 36. The mean results highlight the strong effect of the stainless steel reflector as it is shown that for both cases the power is increased in the periphery. The hot spots are located in the regions with less UO_2-Gd_2O_3 rods. The RSD results indicate a larger uncertainty compared to the other LWR exercises, with values >5 % for the UOX core and >12% for the UOX/MOX core. The RSD results for the HZP are even larger, reaching up to 18% for the UOX/MOX core. The uncertainties are in general larger towards the centre of the core, low in the middle and they increase again towards the periphery. Larger uncertainties are observed for the case 36 that uses SCALE 6.1 VCM in the UOX/MOX core and for the case 37 that uses SCALE 6.2 VCM in the UOX core. This might be related to the I-1 and I-2 results but is difficult to generalise from the limited available results. Further analysis needs to be performed in order to understand the exact sources of these uncertainties and why, although the fuel assemblies loading pattern in the central part of both cores is similar, they lead to very different results in terms of predicted RSD in these regions. One potential explanation could be the combined effect of ^{239}Pu producing 2.9 neutrons per fission on average with high uncertainty, while ^{235}U produces 2.4 neutrons per fission on average with lower uncertainty, and of the stainless steel on the periphery reflecting more neutrons produced in the higher uncertainty MOX assemblies compared to the UOX assemblies.

Figure 3.61. Calculated *k*-inf for I-3 GEN-III cores at HFP: (a) mean value with uncertainties for UOX, (b) RSD for UOX (c) mean value with uncertainties for UOX/MOX, (d) RSD for UOX/MOX

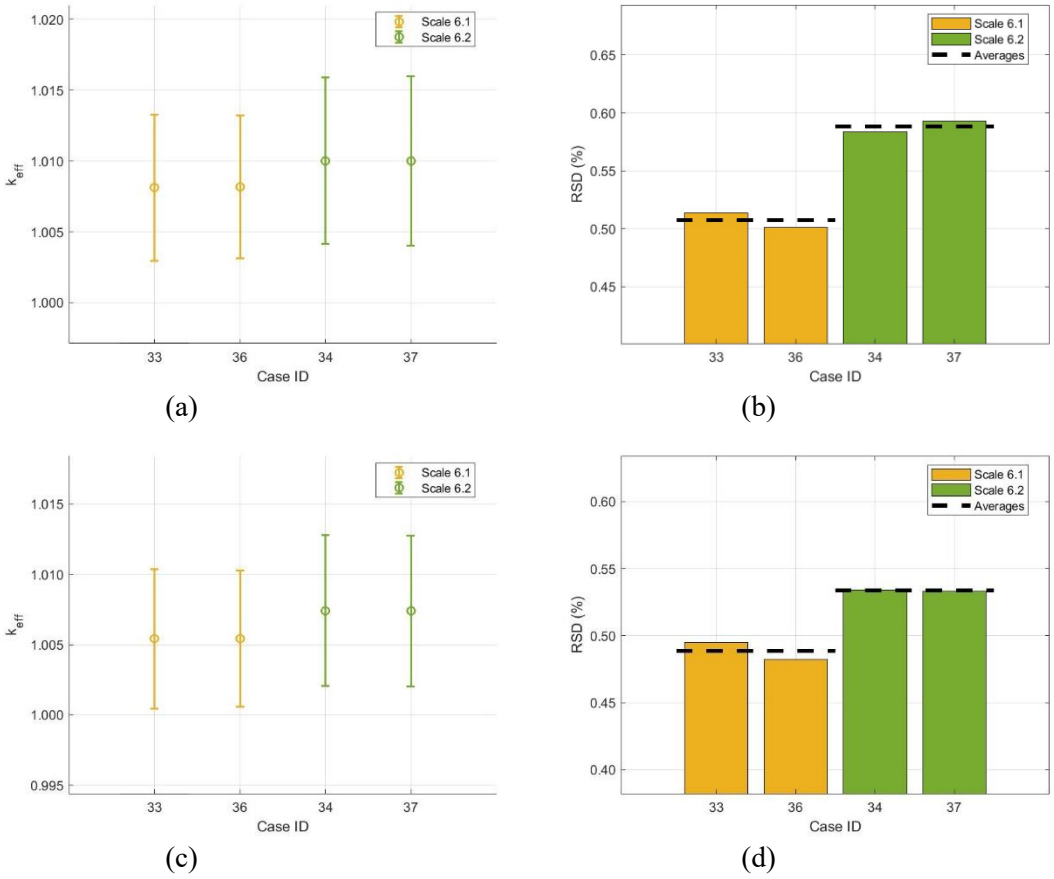

Source: NEA data, 2021

Figure 3.62. Calculated radial assembly power distribution for I-3 GEN-III UOX full core at HFP from case 37 (a) mean and (b) RSD

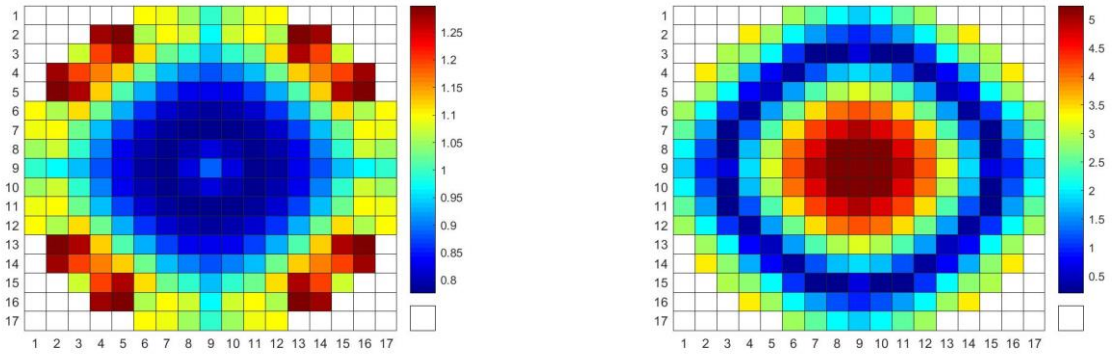

Source: NEA data, 2021

Figure 3.63. Calculated radial assembly power distribution for I-3 GEN-III UOX/MOX full core at HFP from case 36 (a) mean and (b) RSD

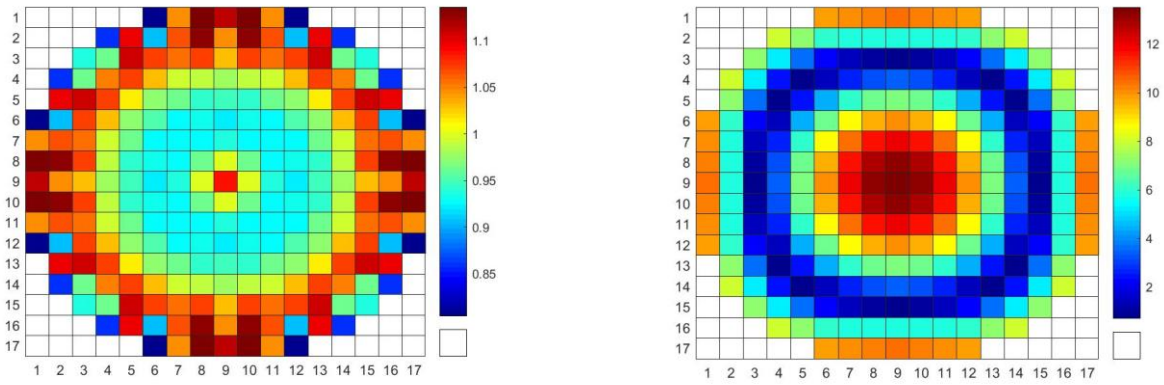

(a) (b)

Source: NEA data, 2021

The results concerning the axial power distribution show very small uncertainties (below 1%) and thus are not plotted. Figure 3.64 presents the results for the mean values for the two cores and shows the typical cosine shape with the two cases having a very good agreement.

Figure 3.64. Calculated axial core power distribution for I-3 GEN-III cores at HFP (a) UOX mean, (b) UOX/MOX mean

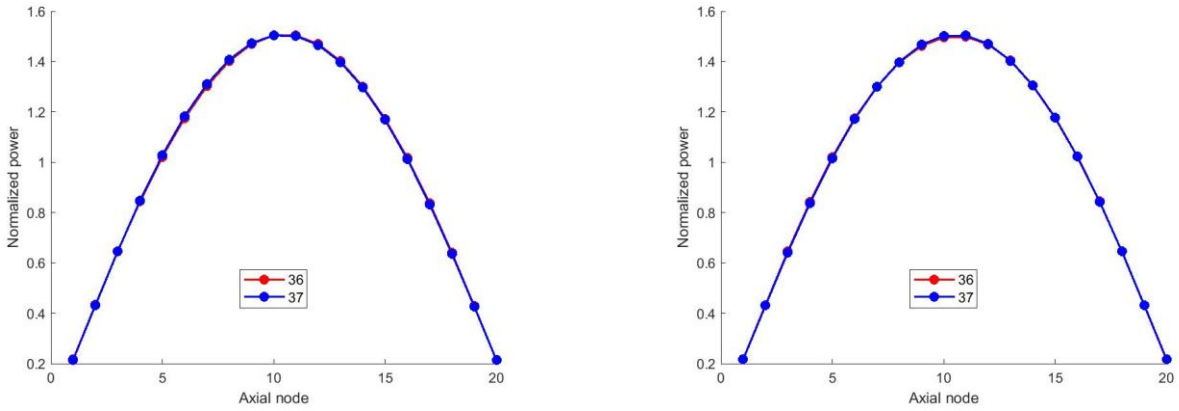

(a) (b)

Source: NEA data, 2021

4. Comparative analysis of experimental results

In the previous exercises, different numerical studies were performed for different LWR reactors. The LWR-UAM benchmark expanded the application of uncertainty quantification methods for experimental tests for the pin cell, assembly lattice and full core exercises.

For the I-1 and I-2 exercises, the KRITZ-2 LEU critical experiments are used. More specifically, three different experiments are included in the benchmark: KRITZ-2:1, KRITZ-2:13 and KRITZ-2:19. The experiments consist of critical lattices of fuel rods at cold and hot conditions. KRITZ-2:1 and KRITZ-2:13 consist of 44×44 and 40×40 lattices of UO_2 fuel rods with ^{235}U enriched to 1.86%. The two experiments are similar to PWR and BWR lattices with the main difference between the two being the pitch size and thus the amount of moderation. For KRITZ-2:1 the pitch size is 1.485 cm and for KRITZ-2:13 it is 1.635 cm. The third experiment, KRITZ-2:19, is a 25×24 lattice of MOX fuel rods with 1.5% PuO2 and 91.41 at.% ^{239}Pu. In I-1 exercise, one pin cell from each experiment and at the two conditions is studied with reflective boundaries, while in I-2 the critical lattice calculation of the experiments is studied for each experiment and at the two conditions.

For the I-3 exercises, results were obtained for two experimental cores. The first is the reactor in the B&W Research Centre. The central region of the core resembled a 3×3 array of PWR fuel assemblies with fuel rods arranged in a 15×15 lattice (similar to TMI-1 core). Loading 2 is selected for the purposes of the OECD LWR-UAM benchmark. The second is the experimental zero-power LR-0 VVER type of reactor. The core consisted of 6 VVER-1000 fuel assemblies and the experiments were carried out at atmospheric pressure and "room" temperature. Case 3 is selected for the purposes of the OECD LWR-UAM benchmark.

For all the experimental exercises, the participants were asked for similar sets of results as for the numerical studies, including the multiplication factor, ranking of the important nuclide-reaction pairs and the relative power distribution.

4.1. Exercise I-1: Cell physics - KRITZ-2 critical experiments

A set of eight results were submitted for the KRITZ-2 experimental pin cell calculations. The uncertainty propagation results for the *k*-inf are presented in Figure 4.1 for KRITZ-2:1, in Figure 4.2 for KRITZ-2:13 and in Figure 4.3 for KRITZ-2:19. For the predicted mean value, the UO_2 experiments show a spread of ~1 000 pcm, while the MOX experiment shows a spread of ~500 pcm. For KRITZ-2:1 at cold conditions, the mean is 1.^{239} with an RSD of 0.61%. We observe a larger predicted RSD for the SCALE 6.2 VCM due to the larger uncertainty of ^{235}U nu-bar as in the PWR numerical exercise. For KRITZ-2:1 at hot conditions, the mean reduces to 1.193 due to the moderator and Doppler effects, with a RSD of 0.66%. The RSD slight increase can be attributed to the increase of the ^{238}U capture importance due to the Doppler and the fact that less neutrons will be moderated to the thermal group and thus more neutrons could be captured in the resonances. The uncertainty of ^{238}U capture is larger than ^{235}U nu-bar, as can be seen in Figure 3.17, leading to this RSD increase at hot conditions.

Figure 4.1. Calculated k-inf for I-1 KRITZ-21: (a) mean value with uncertainties for Cold, (b) RSD for Cold (c) mean value with uncertainties for Hot, (d) RSD for Hot

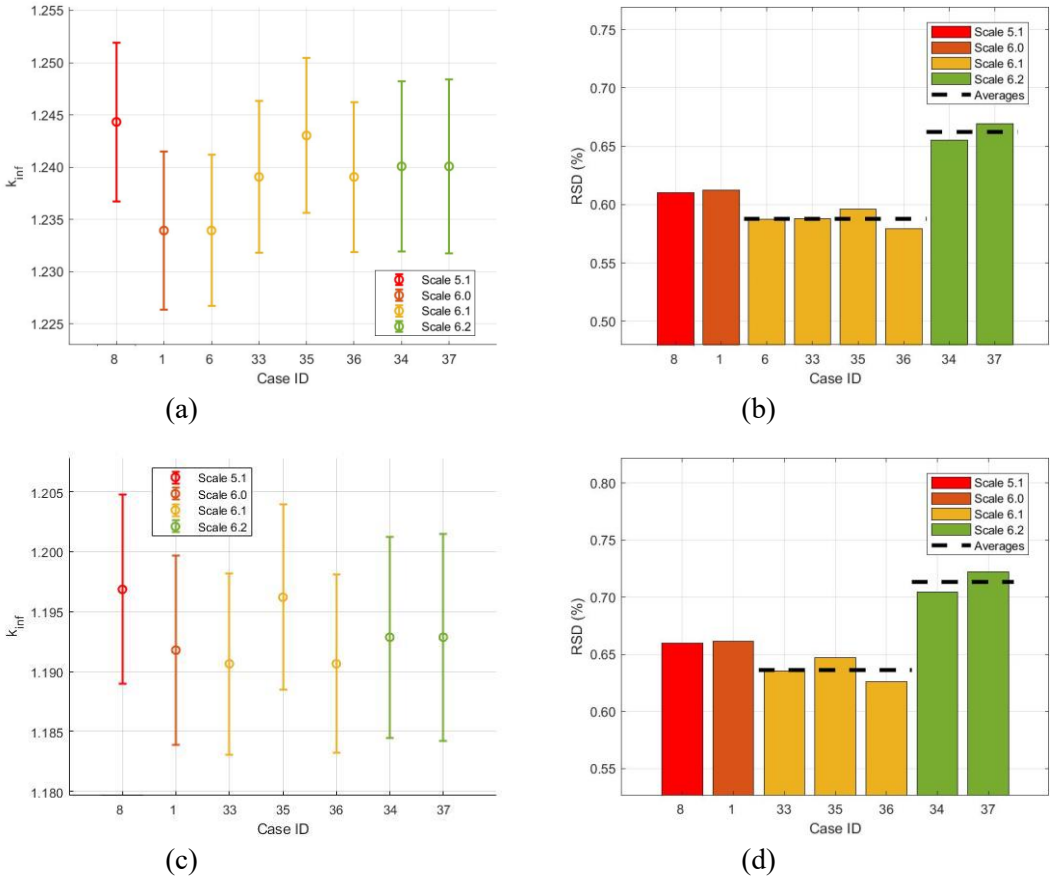

Source: NEA data, 2021

The KRITZ-2:13 experiment has a larger pitch than KRITZ-2:1 and thus more moderation. This leads to larger predicted *k*-inf mean values and lower RSD due to the increase of the ^{235}U nu-bar importance, since more neutrons reach the thermal group that has a lower uncertainty compared to ^{238}U capture. The predicted mean at cold condition is 1.270 with a RSD of 0.57%. The predicted mean at hot condition reduces to 1.242 and the RSD increases to 0.59% due to the same phenomenon as in the KRITZ-2:1 experiment. Again, a larger predicted RSD is shown for the SCALE 6.2 VCM.

Figure 4.2. Calculated k-inf for I-1 KRITZ-213: (a) mean value with uncertainties for Cold, (b) RSD for Cold (c) mean value with uncertainties for Hot, (d) RSD for Hot

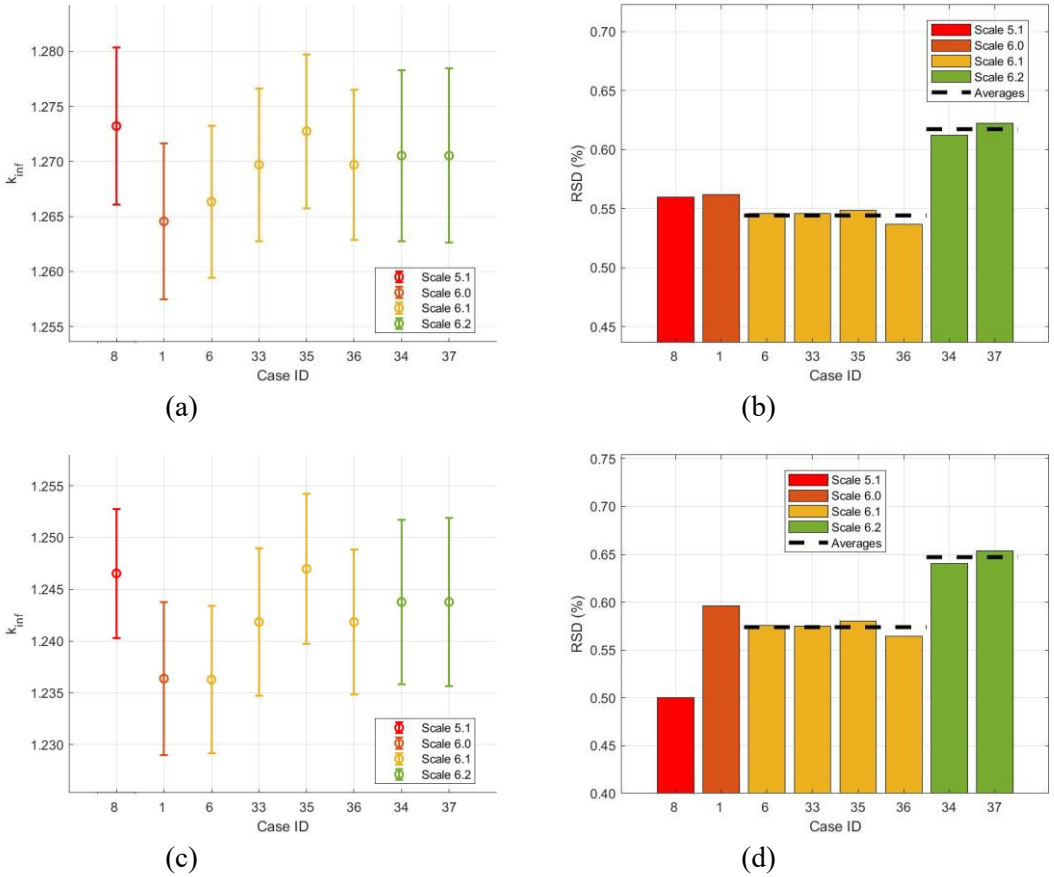

Source: NEA data, 2021

The KRITZ-2:19 experiment is a MOX fuel rod and thus very different from the two previous experiments. The predicted mean at cold condition is 1.283 with a RSD of 0.99% and the predicted mean at hot condition is 1.301 with a RSD of 0.98%. The main difference with the previous experiments' results is the doubling of the predicted RSD for the SCALE 6.0/6.1 VCMs. This effect was also observed in the GEN-III numerical exercise and is attributed to the increases in ^{239}Pu nu-bar uncertainty compared to the ^{235}U nu-bar, as can be seen in Figure 3.54. In the SCALE 6.2 VCM, the two uncertainties are much closer and thus there is not an increased RSD. More information about the estimated mean and RSD for each covariance library can be found in Table B.1 of Annex B.

Figure 4.3. Calculated k-inf for I-1 KRITZ-219: (a) mean value with uncertainties for Cold, (b) RSD for Cold (c) mean value with uncertainties for Hot, (d) RSD for Hot

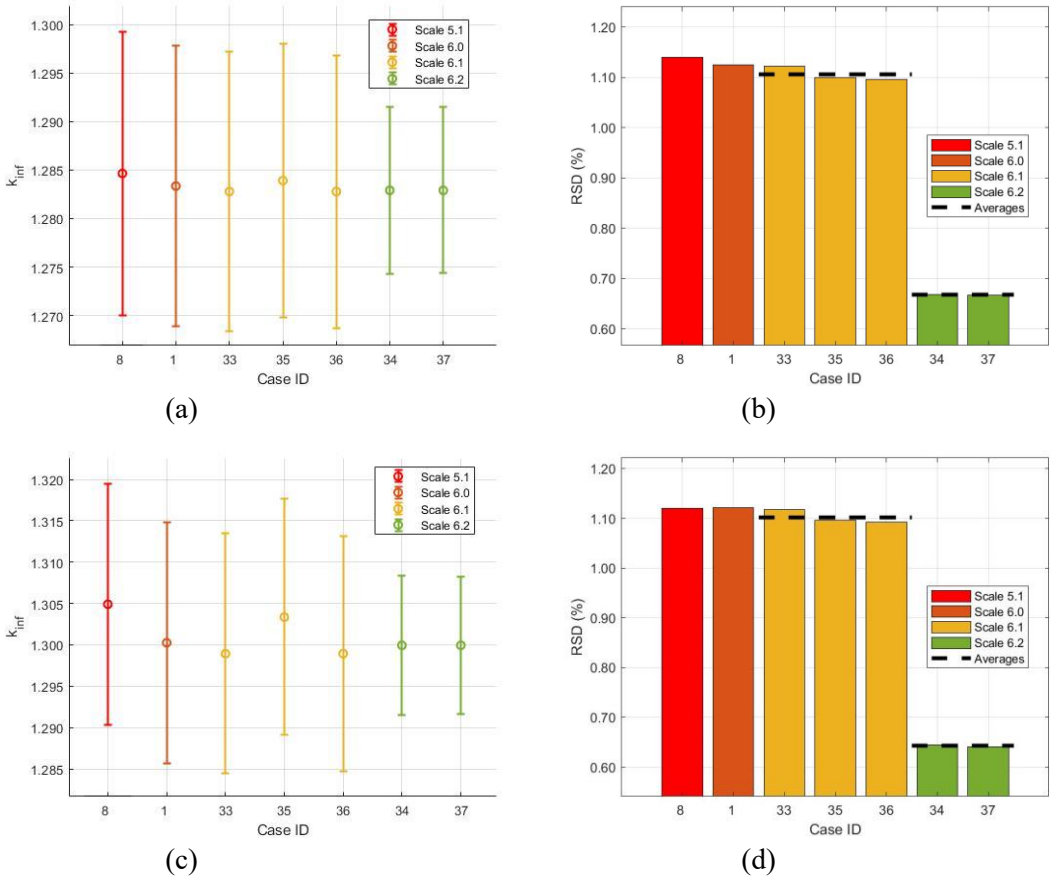

Source: NEA data, 2021

Five participants provided results for the ranking of the top five contributors to the *k*-inf uncertainty. Figure 4.4 presents the results for the KRITZ-2:13 at hot condition. They are representative of the cold condition and the KRITZ-2:1 experiment as well. The observed behaviour is similar to the PWR and BWR exercises with ^{238}U capture, ^{235}U nu-bar and ^{235}U capture being the most important reactions. Figure 4.5 displays the results for the KRITZ-2:19 experiment at hot condition that are also representative of the cold condition. We observe a similar trend with the GEN-III exercise, with ^{239}Pu nu-bar and ^{239}Pu fission being the most important reactions. We can see also the justification of the RSD increase in the SCALE 6.0/6.1 cases since they all rank ^{239}Pu nu-bar as first while the SCALE 6.2 VCM ranks it as fifth.

Figure 4.4. Ranking of the five nuclide-reaction pairs with the highest contribution to the k-inf uncertainty for I-1 KRITZ-213 at Hot condition [X.Y = SCALE X.Y covariance libraries]

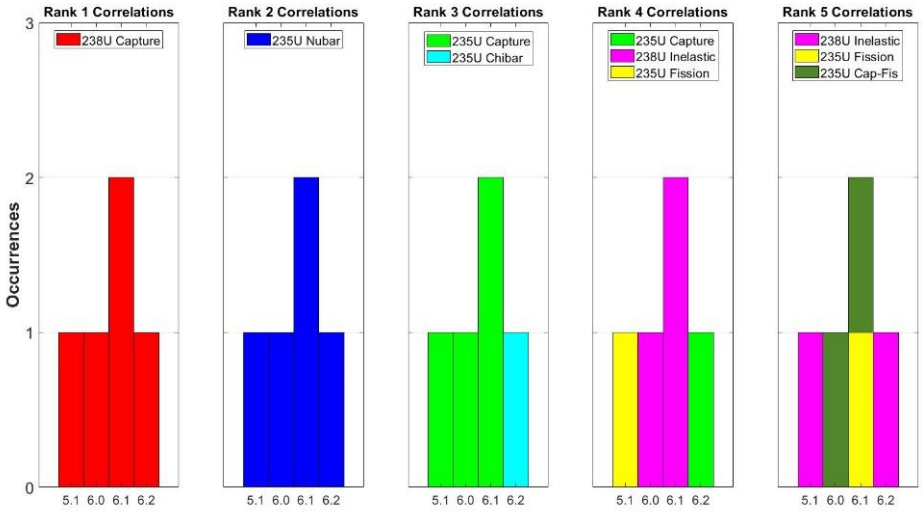

Source: NEA data, 2021

Figure 4.5. Ranking of the five nuclide-reaction pairs with the highest contribution to the k-inf uncertainty for I-1 KRITZ-219 at Hot condition [X.Y = SCALE X.Y covariance libraries]

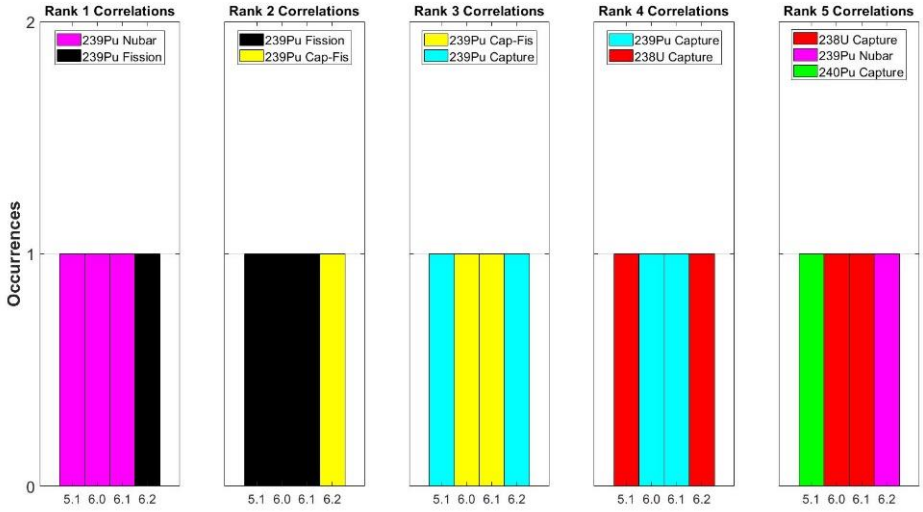

Source: NEA data, 2021

4.2. Exercise I-2: Lattice physics - KRITZ-2 critical experiments

Four sets of results were submitted for the three KRITZ-2 criticality experiments. The k_{eff} uncertainty propagation results are presented through Figure 4.6, Figure 4.7 and Figure 4.8. They show the same behaviour with I-1 exercise regarding the doubling of the predicted RSD by the SCALE 6.1 VCM for the MOX fuel assembly. In general, the *k*-eff mean predictions are better for MOX fuel, with the largest discrepancy being 160 pcm. The KRITZ-2:1 and KRITZ-2:13 at hot conditions underpredict significantly the *k*-eff with discrepancies up to 750 pcm and 450 pcm respectively. The cold conditions seem to show smaller discrepancies, probably indicating that the main reason for the large discrepancies has to do with the 238U capture cross section. More information about the estimated mean and RSD for each covariance library can be found in Table B.2 of Annex B. Further investigation, including different NDL and different numbers of energy groups, should be carried out to better understand the sources of these discrepancies.

Figure 4.6. Calculated *k*-eff for I-2 KRITZ-21: (a) mean value with uncertainties for Cold, (b) RSD for Cold (c) mean value with uncertainties for Hot, (d) RSD for Hot

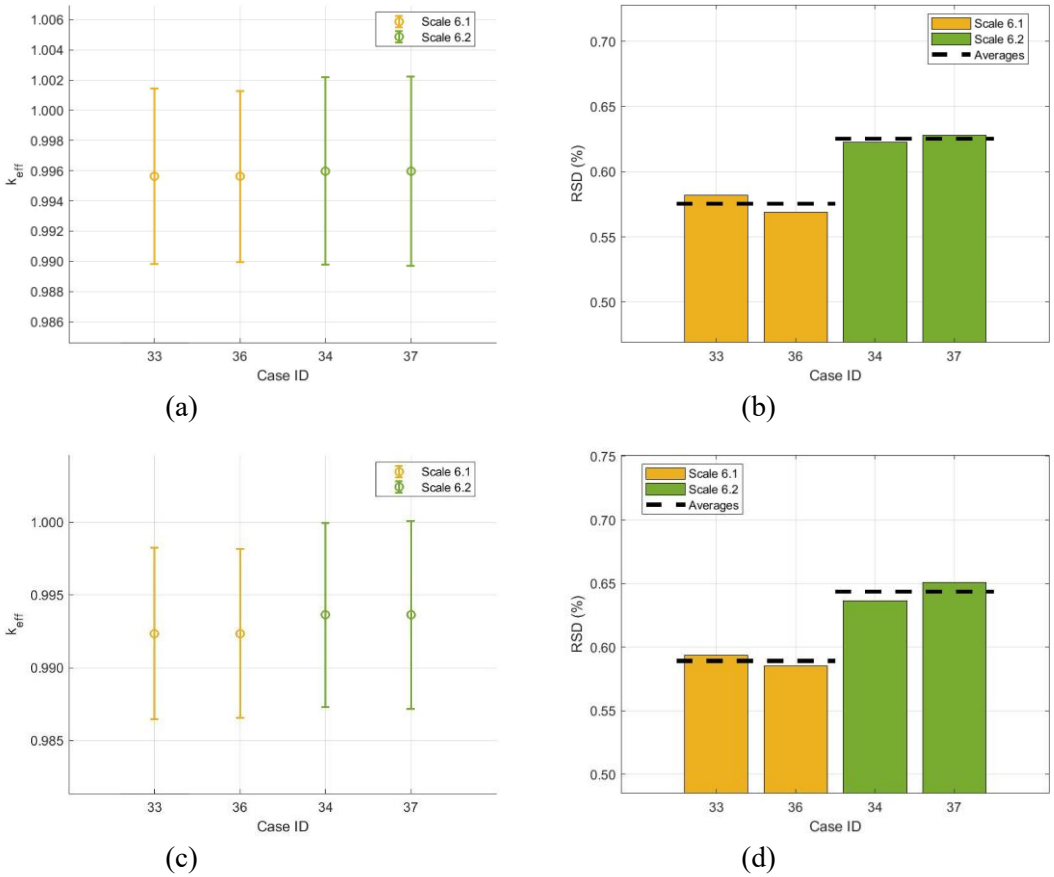

Source: NEA data, 2021

Figure 4.7. Calculated *k*-eff for I-2 KRITZ-213: (a) mean value with uncertainties for Cold, (b) RSD for Cold (c) mean value with uncertainties for Hot, (d) RSD for Hot

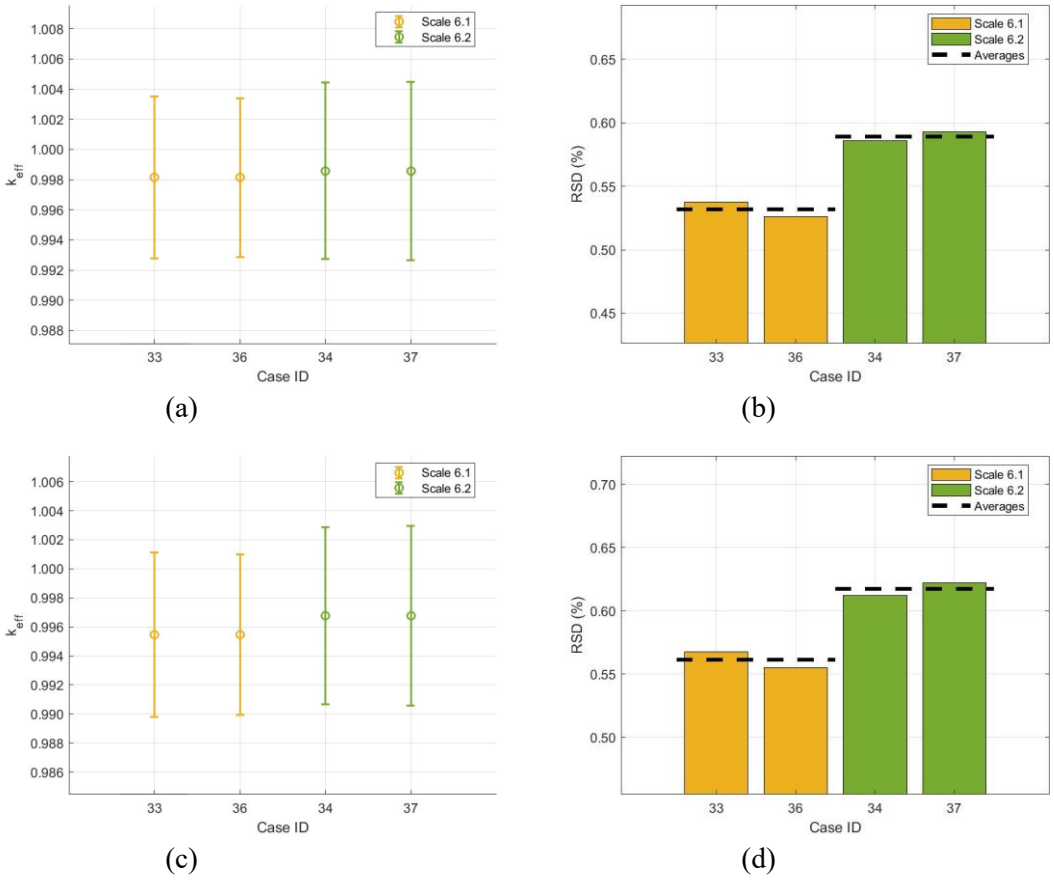

Source: NEA data, 2021

Figure 4.8. Calculated *k*-eff for I-2 KRITZ-213: (a) mean value with uncertainties for Cold, (b) RSD for Cold (c) mean value with uncertainties for Hot, (d) RSD for Hot

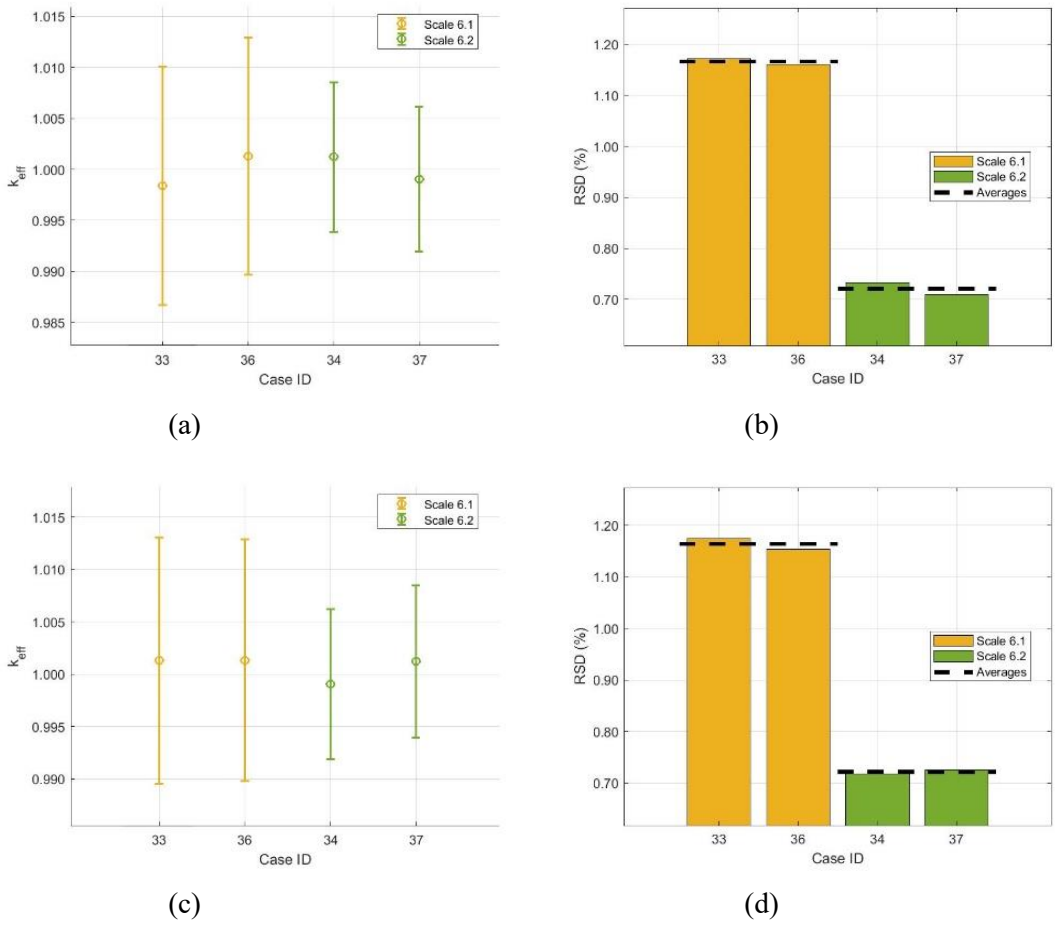

Source: NEA data, 2021

4.3. Exercise I-3: Core physics

4.3.1. B&W PWR

Four sets of results were submitted for the B&W experimental core uncertainty quantification. The results for the k_{eff} are presented in Figure 4.9. The predicted mean has a 250 pcm discrepancy with uncertainties at the order of ~0.50% that cover the criticality. The same trend with the PWR and BWR numerical exercises is observed regarding the impact of the VCM libraries, with SCALE 6.2 predicting a larger RSD due to its larger 235U nu-bar uncertainty. More information about the estimated mean and RSD for each covariance library can be found in Table B.6 of Annex B.

Figure 4.9. Calculated *k*-eff for I-3 B&W PWR: (a) mean value with uncertainties, (b) RSD

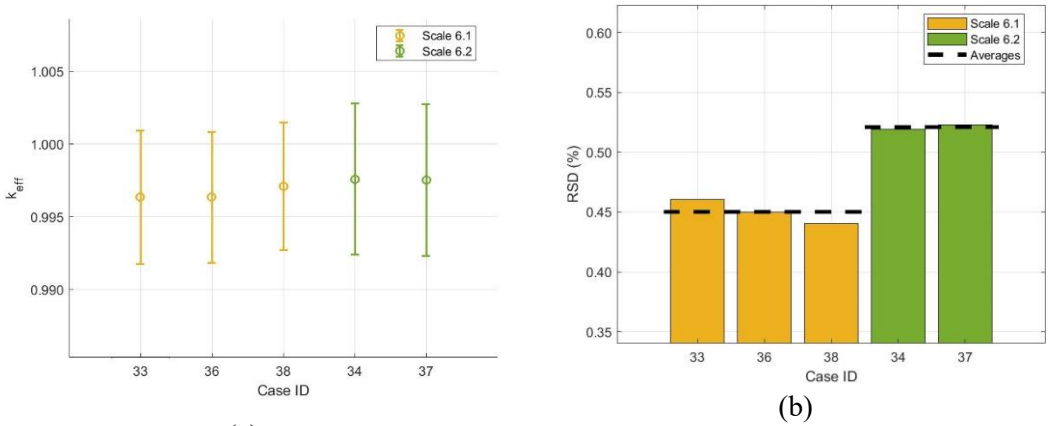

(a) (b)

Source: NEA data, 2021

There were no results concerning the power distribution in the core but one participant provided results for the fission rates' distribution in the central assembly, which are presented in Figure 4.10. Larger fission rates can be observed towards the centre of the assembly, with uncertainties that vary in the range of 0.56%-0.65%, consistent with the k_{eff} uncertainty.

Figure 4.10. Calculated fission rates distribution in the central assembly for I-3 B&W PWR core from case 38 (a) mean and (b) RSD

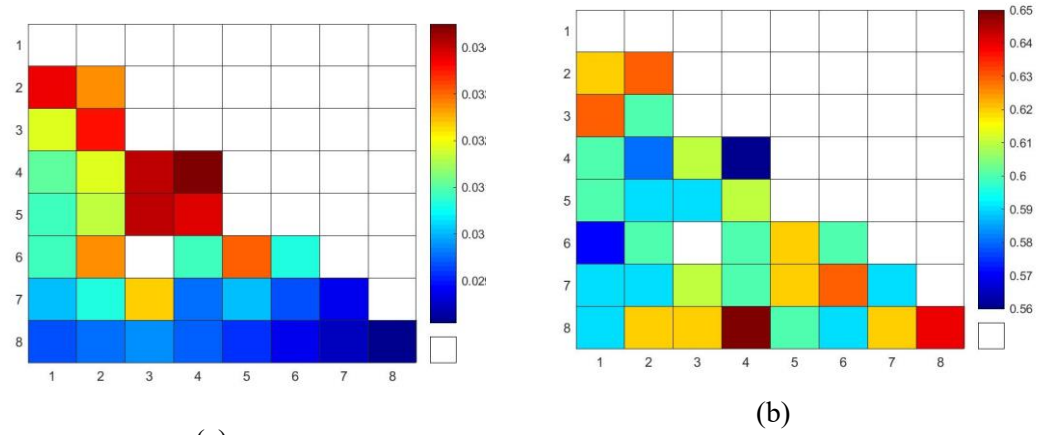

(a) (b)

Source: NEA data, 2021

4.3.2. LR0-VVER

A total of two sets of results were submitted for the LR-0 experimental core uncertainty quantification. This limited number of available results restricts the possible analyses and conclusions that could be drawn. The results for the *k*-eff are presented in Figure 4.11. The predicted mean has a 400 pcm discrepancy with a RSD of 0.57% that cover the criticality. The same trend with the PWR and BWR numerical exercises is observed regarding the impact of the VCM libraries, with SCALE 6.2 predicting a larger RSD compared to SCALE 6.1 due to its larger 235U nu-bar uncertainty. More information about the estimated mean and RSD for each covariance library can be found in Table B.6 of Annex B. No results were obtained concerning the power distribution and the fission rates. Further investigation should be pursued in experimental exercises such as this one, since they add more value to the uncertainty analysis, they can lead to a better understanding and quantification of the biases and errors in the core modelling and can be used to estimate uncertainties related to the numerical modelling.

Figure 4.11. Calculated *k*-eff for I-3 of LR0 VVER: (a) mean value with uncertainties, (b) RSD

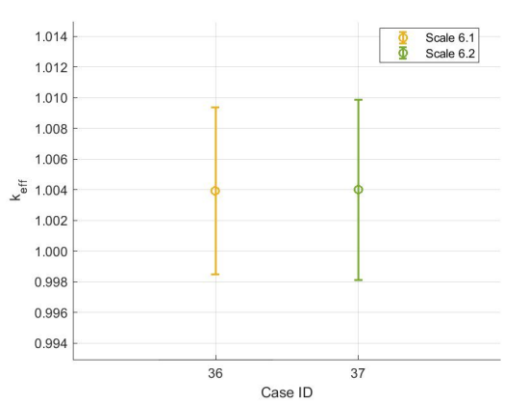

(a)

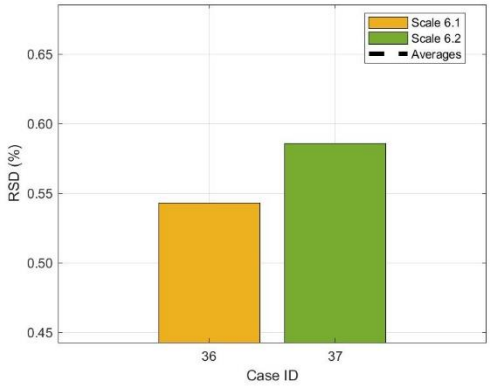

(b)

Source: NEA data, 2021

5. Cross-exercise analysis and results

Throughout this report, the analysis of three scale exercises (I-1, I-2, I-3) for four types of LWRs (PWR, BWR, VVER, GEN-III), including experimental and numerical studies, yielded interesting and often similar results across the exercises. In this section, a cross-comparison is performed of the exercises across the different reactors and conditions in order to draw some general conclusions. The quantity most studied in this work is the multiplication factor, whether it is the *k*-inf for I-1 and I-2 or *k*-eff for I-3 exercises. A general trend was observed for the multiplication factor among most of the PWR, BWR, VVER and GEN-III numerical and experimental exercises, which is a predicted RSD of ~0.5%. This result was obtained at all three scales: pin cell, assembly lattice and full core. For these cases, discrepancies were found around 0.5% related to the VCM package used by the different participants. The predicted RSD was found to progressively increase from SCALE 6.0/6.1 to SCALE 6.2 and to ENDF/B-VII.1. It was found that this behaviour is related to the larger ^{235}U nu-bar uncertainty in the different VCMs. The uncertainty in the thermal group is ~0.31% in SCALE 6.1, ~0.39% in SCALE 6.2 and ~0.7% in ENDF/B-VII.1. For the latter, the mismatch between the prompt ^{235}U nu-bar and the ^{235}U nu-bar can lead to very different results across participants. The ranking of the most important contributors highlighted that the ^{238}U capture and ^{235}U nu-bar are the two dominant inputs consistently ranked in the first two ranks. These two reactions guided another observation concerning the impact of the enrichment and moderation. When one of these two effects leads to an increase in ^{235}U nu-bar importance, either directly through higher enrichment or indirectly through more moderation, the RSD was found to decrease. This is attributed to the fact that ^{235}U nu-bar uncertainty in most of the VCMs is smaller than the ^{238}U capture uncertainty, which can become very large, especially in the unresolved resonances. That is why the RSD is higher in cases with less enrichment, such as in the BWR or VVER fuel rods, and in cases where less moderation occurs, such as in the BWR HFP conditions with 40% void fraction, and when there are smaller pitch sizes (KRITZ-2:1 vs KRITZ:2:13). A second important observation concerning the multiplication factor was found for the MOX fuel experiments in I-1 and I-2 exercises for the GEN-III numerical results and for the KRITZ:2:19 experimental ones. In these exercises, the predicted RSD from the SCALE 6.0/6.1 cases almost doubles from ~0.5% to ~ 1%, while the predicted RSD by SCALE 6.2 is not impacted significantly. This effect is related to the Pu composition of the MOX fuel, because the ^{239}Pu nu-bar uncertainty is much larger than the ^{235}U nu-bar one. This is justified by the ranking of the top contributors to the multiplication factor obtained for the different participants, where the major reactions for the MOX fuel were the ^{239}Pu nu-bar, ^{239}Pu fission and ^{238}U inelastic scattering. Although there were no comparative studies between different Pu compositions, it is anticipated that the higher the concentration in Pu, the higher the multiplication factor uncertainty will be. This RSD for the MOX fuel rods is not observed in the I-3 UOX/MOX core studied in this benchmark, mainly because ~80% of the assemblies are UOX assemblies, which also are positioned in the centre of the core and thus their effect dominates the MOX assemblies effect on the multiplication factor.

From I-1 to I-2 and I-3, the uncertainties are propagated through group constants condensed in energy and homogenised in space. For the uncertainty propagation in I-3 exercises, the typical two-step approach samples directly from the assembly group constants. The uncertainty quantification of the group constants in I-2 exercises is crucial since the uncertainties will be propagated to the core calculations in I-3 exercises. The group constants uncertainty quantification consists of their RSD and the correlations between the different group constants. This work emphasises the results of the two-group nu-fission cross section and the diffusion coefficient. The former is strictly related to the multiplication factor and thus is impacted by the same effects previously described. The latter is more related to the two-group solution in the core and from the available results, it does not exhibit any significant variations related to the different reactor types, conditions and VCMs. A general

trend was observed for these two-group constants and for most of the rest as well, with higher uncertainties for the fast group compared to the thermal group. In some cases, there was an order of magnitude of difference as can be seen in Figure 3.15. These differences arise from the fact that, for most of the reactions, the VCM have higher uncertainties in the higher energy, mainly because at higher energies there are fewer measurements available. Concerning the correlation matrices, strong correlations are observed through the lattice calculations with the more characteristic example being the strong positive correlation between the total cross section, the absorption and the scattering matrix. The correlation matrices may differ case by case, indicating a dependence on the methods used by the transport codes for the condensation and homogenisation processes and on the selected NDLs. It will be interesting in future studies to quantify the impact of these differences in the core calculations when a two-step uncertainty quantification approach is used.

In the I-3 exercises, full core calculations are performed with an emphasis on the radial and axial power distribution in the core. For PWR, VVER and GEN-III cores, similar trends were observed for the radial distribution, with higher mean values towards the periphery and corresponding higher uncertainties towards the centre, where the power is lower. In the BWR core, the opposite occurs, with higher mean values towards the centre and higher uncertainties towards the periphery, again at the locations of low power. The observed maximum RSD in the radial power distribution for PWR, BWR, VVER and GEN-III UOX cores is ~5%. This RSD increases to >18% in the GEN-III UOX/MOX cores, indicating a strong impact of the Pu uncertainties. Concerning the axial variation, the trend of higher uncertainties in the low power regions is observed again with the values reaching up to ~5% for PWR and VVER, up to 10% for BWR and values <1% for the GEN-III cores, although for the last case a very limited number of results was submitted. Further analysis is suggested on the impact of uncertainty propagation on radial and axial power calculations, specifically on the uncertainty results in the most limiting locations within each of the reactor types.

Finally, a set of experimental exercises for I-1, I-2 and I-3 were studied by a limited number of participants, restricting the possible analyses. From these results, a bias of ~500 pcm in the k_{eff} prediction was observed for SCALE 6.1 and 6.2 VCMs in the UOX cases for all the scales. The predicted RSD matches the one predicted in the numerical cases ~0.5%. These results indicate that for some cases the bias is as large as the uncertainty. For the MOX cases the bias decreases significantly to ~150 pcm, while the RSD increases due to the Pu presence up to 1% as in the numerical cases. This bias/uncertainty quantification is very important and can be captured only through experimental exercises such as these ones. For this reason, further investigation is suggested using different experimental exercises in order to better quantify the biases and uncertainties in the core calculations, something that can help quantify better the model and numerical errors induced by the codes and separate them from the fundamental uncertainties.

6. Conclusions and future work

This study summarises the results of the standalone neutronics exercises in Phase I of the LWR-UAM benchmark, which mainly are concerned with the propagation of input uncertainties through the standard two-step LWR simulation procedure to key core parameters, such as the multiplication factor. The uncertainties on nuclear data are propagated in the TMI-1 PWR, PB-2 BWR, KOZ-6 VVER and GEN-III UOX and UOX/MOX numerical studies and in KRITZ-2, B&W PWR and LR-0 VVER experimental studies. It was observed that the uncertainty estimates for the system eigenvalue due to nuclear data in all scales (the pin cell, lattice, and core) are similar for the UOX cases with a relative standard deviation of approximately 0.5% Δk/k. Larger uncertainties were obtained for the MOX cases with a relative standard deviation of approximately 1% Δk/k. Overall, the VVER results most closely match those from the PWR results, with the BWR exhibiting some unique behaviour, especially for the HFP and rodded cases due to the hardening of the neutron spectrum in the presence of void. Comparative analyses of all submitted results were then carried out to investigate the dependence of the predicted uncertainties of crucial core parameters on the choice of solution methods, nuclear data libraries and VCMs, etc. It was found that the *k*-inf (k_{eff}) uncertainty strongly depends on the VCM and the results generated using the VCM of ENDF/B-VII.1 and SCALE 6.2 lead to significantly larger values than those using other VCMs in the UOX cases. The sensitivity analysis suggests that the large difference of the ^{235}U nu-bar uncertainty in the thermal energy range is responsible for the disagreements in the results. In the MOX cases, the ^{239}Pu nu-bar is the most important cross section and the SCALE 6.1 VCM led to higher uncertainties due to increased uncertainty of ^{239}Pu nu-bar. Another conclusion concerning the multiplication factor results is that the hardening of the spectrum seems to create a small increase of the predicted uncertainty due to the increased importance of ^{238}U capture that exhibits very large uncertainties in the resonances. Finally, in all the studied exercises a significant bias of the best estimate values is found among the participants. The bias is typically at the order of the average RSD, with a few results showing even larger biases. These discrepancies can have various sources that can be traced back to:

- Differences in modelling approaches between neutronic codes (i.e. lattice, core and depletion calculations).
- The choice of base nuclear data library.
- Uncertainty propagation methods. An example is the procedure involving the self-shielding treatment: some methods perturb the self-shielding factors while others perturb directly the cross sections after the self-shielding.
- Data processing and interpretation across the participants.

It is important thus in future analyses to investigate both biases and uncertainties more thoroughly to understand better their sources and reduce both through code verification and validation.

The I-2 assembly lattice exercises highlighted a general trend regarding the group constants, with higher predicted uncertainties for the fast group than the thermal group. The differences can reach one order of magnitude. These fast groups' larger uncertainties are attributed to the fact that most of the cross sections in the different VCMs have higher uncertainties in high energies due to the lack of available measurements in these regions, especially if resonances are present. The correlation matrices obtained for the I-2 exercises showed that they share some major trends such as a high positive correlation between total, absorption and scattering cross sections. However, differences are found in case-by-case comparisons, indicating an impact of the aspects already mentioned in I-1, but also of the methods specifically used in lattice transport calculations for the condensation and homogenisation.

In the I-3 exercises, the full core calculations for PWR, VVER and GEN-III show similar trends for the power radial distribution, with higher mean values towards the periphery and corresponding higher uncertainties towards the centre, where the power is lower due to the lower mean values. In the BWR core, the opposite occurs, with higher mean values towards the centre and higher uncertainties towards the periphery, again at the locations of low power. The observed larger RSD in the radial power distribution for PWR, BWR, VVER and GEN-III UOX cores is ~5%. This RSD increases to >18% in the GEN-III UOX/MOX cores, indicating a strong impact of the Pu uncertainties. Concerning the axial variation, the trend of higher uncertainties in the low power regions is observed again, with the values reaching up to ~5% for PWR and VVER, up to 10% for BWR and values <1% for the GEN-III cores, although for the last case a very limited number of results were submitted. The large number of results for PWR and BWR facilitate understanding of the above-mentioned phenomena. However, because a limited number of results were submitted for the VVER and GEN-III, there is a need for further investigation for these types of reactors.

The experimental exercises for the pin cell, assembly lattice and core calculations indicate that for the UOX the observed bias can be at the order of the predicted uncertainty. This is an accordance with the numerical results and highlights the need for more experimental exercises to better quantify the bias/uncertainties and to be able to separate the model and numerical errors induced by the codes from the fundamental uncertainties.

Finally, the conclusions of this work give a picture of the state of knowledge in this area and serve as a reliable foundation for proceeding to Phase II (Core Phase) of the LWR-UAM benchmark. As new evaluations and methods are available (e.g. methods to propagate angular distributions in transport calculations), new assessments should be performed and the conclusions should be updated.

7. References

Baccou, J. et al. (2018), "SAPIUM: A Systematic Approach for Input Uncertainty Quantification", Best Estimate Plus Uncertainty International Conference (BEPU 2018), Conference Proceeedings. [7]

Cabellos, O. (2013), "Presentation and Discussion of the UAM/Exercise I-1b: "Pin-Cell Burn-Up Benchmark" with the Hybrid Method", *Science and Technology of Nuclear Installations*, Vol. 2013, pp. 1-12, http://dx.doi.org/10.1155/2013/790206. [28]

Castro, E. et al. (2018), "Impact of the homogenization level, nodal or pin-by-pin, on the uncertainty quantification with core simulators", *Progress in Nuclear Energy*, Vol. 104, pp. 218-228, http://dx.doi.org/10.1016/j.pnucene.2017.10.001. [29]

Iooss, B. and P. Lemaître (2015), "A Review on Global Sensitivity Analysis Methods", in *Uncertainty Management in Simulation-Optimization of Complex Systems, Operations Research/Computer Science Interfaces Series*, Springer US, Boston, MA, http://dx.doi.org/10.1007/978-1-4899-7547-8_5. [17]

Krzykacz, B., E. Hofer and M. Kloos (1994), "A software system for probabilistic uncertainty and sensitivity analysis of results from computer models", Proc. Int. Conf. Probabilistic Safety Assessment and Management (PSAM-II), San Diego, CA. [15]

Little, R. et al. (2008), "Low-fidelity Covariance Project", Nuclear Data Sheets, pp. 2828-2833, http://dx.doi.org/10.1016/j.nds.2008.11.018. [21]

Marshall, W. et al. (2013), "Validation of criticality safety calculations with SCALE 6.2", Proceedings of ANS NCSD 2013 - Criticality Safety in the Modern Era: Raising the Bar, Wilmington, NC, United States. [24]

Marshall, W. et al. (2015), "Development and testing of neutron cross-section covariance data for SCALE 6.2", International Conference on Nuclear Criticality Safety (ICNC 2015), Charlotte, NC, United States. [20]

Members of JNDC (1992), "Japanese Evaluated Nuclear Data Library, Version-3, JENDL-3", in *Nuclear Data for Science and Technology, Research Reports in Physics*, Springer Berlin Heidelberg, Berlin, Heidelberg, http://dx.doi.org/10.1007/978-3-642-58113-7_223. [27]

NEA (2021), "International Criticality Safety Benchmark Evaluation Project (ICSBEP) Handbook", OECD Publishing, Paris, https://www.oecd-nea.org/jcms/pl_20291/icsbep-handbook. [10]

NEA (2021), "International Handbook of Evaluated Reactor Physics Benchmark Experiments (IRPhE)", OECD Publishing, Paris, https://www.oecd-nea.org/jcms/pl_20279/international-handbook-of-evaluated-reactor-physics-benchmark-experiments-irphe. [11]

NEA (2016), "PREMIUM: A Benchmark on the Quantification of the Uncertainty of the Physical Models in System Thermal-hydraulic Codes", NEA,CSNI/R(2016)9, OECD Publishing, Paris. [6]

NEA (2013), "Barcelona Workshop Proceedings OECD/CSNI Workshop on Best Estimate Methods and Uncertainty Evaluations, hosted by Technical University of Catalonia (UPC) with the support [5]

from Spanish Nuclear Safety Council (CSN) Barcelona, Spain, 16-18 November 2011", NEA/CSNI/R(2013)8, OECD Publishing, Paris.

NEA (2013), "Benchmark for Uncertainty Analysis in Modelling (UAM) for the Design, Operation and Safety Analysis of LWRs - Specification and Support Data for Neutronics Cases (Phase I)", NEA/NSC/DOC(2013)7, OECD Publishing, Paris. [9]

NEA (2003), "Manual for ANGELO2 and LAMBDA codes", Software Package NEA-1264/05, OECD Publishing, Paris. [22]

NEA (1998), "Report of the Uncertainty Method Study for Advanced Best Estimate Thermal Hydraulic Code Applications", NEA/CSNI/R(97)35, OECD Publishing, Paris. [4]

Pusa, M. (2012), "Perturbation-Theory-Based Sensitivity and Uncertainty Analysis with CASMO-4", *Science and Technology of Nuclear Installations*, Vol. 2012, pp. 1-11, http://dx.doi.org/10.1155/2012/157029. [14]

Rearden, B. et al. (2009), "TSUNAMI Primer: A Primer for Sensitivity/Uncertainty Calculations with SCALE", Oak Ridge National Laboratory, ORNL/TM-2009/027. [13]

Rohatgi, U. and J. Kaizer (2020), "Historical perspectives of BEPU research in US", *Nuclear Engineering and Design*, Vol. 358, p. 110430, http://dx.doi.org/10.1016/j.nucengdes.2019.110430. [3]

Roy, C. and W. Oberkampf (2011), "A comprehensive framework for verification, validation, and uncertainty quantification in scientific computing", *Computer Methods in Applied Mechanics and Engineering*, Vol. 200/25-28, pp. 2131-2144, http://dx.doi.org/10.1016/j.cma.2011.03.016. [12]

Serot, O. and A. Chebboubi (eds.) (2019), "JEFF-3.3 covariance application to ICSBEP using SANDY and NDAST", *EPJ Web of Conferences*, Vol. 211, p. 07003, http://dx.doi.org/10.1051/epjconf/201921107003. [25]

Smith, R. (2013), *Uncertainly Quantification: Theory, Implementation, and Applications*, Society for Industrial and Applied Mathematics (SIAM), ISBN 978-1-611973-21-1. [18]

Sobes, V. et al. (2019), *ENDF/B-VIII.0 Covariance Data Development and Testing for Advanced Reactors*, Office of Scientific and Technical Information (OSTI), http://dx.doi.org/10.2172/1502567. [23]

Trkov, A. et al. (2005), "Revisiting the238U Thermal Capture Cross Section and Gamma-Ray Emission Probabilities from239Np Decay", *Nuclear Science and Engineering*, Vol. 150/3, pp. 336-348, http://dx.doi.org/10.13182/nse05-a2520. [26]

United States Nuclear Regulatory Commission (2012), "State of the Art Reactor Consequence Analyses (SOARCA) Report", *NUREG-1935*. [8]

United States Nuclear Regulatory Commission (1975), "Reactor Safety Study-An Assessment of Accident Risks in U.S. Commercial Nuclear Power Plants", Report WASH-1400 (NUREG-75/014). [1]

United States Nuclear Regulatory Commission (1990-1991), "Severe Accident Risks: An Assessment for Five U.S. Nuclear Power Plants", Report NUREG-1150, Vols. 1-3, Office of Nuclear Regulatory Research, Division of Systems Research. [2]

Wieselquist, W., R. Lefebvre and M. Jessee (2020), "SCALE Code System", Oak Ridge National Laboratory, Oak Ridge, ORNL/TM-2005/39, Version 6.2.4. [19]

Williams, M. et al. (2013), "A statistical sampling method for uncertainty analysis with SCALE and XSUSA", *Nuclear technology*, Vol. 183(3), pp. 515-526. [16]

Yankov, A. et al. (2012), "A Two-Step Approach to Uncertainty Quantification of Core Simulators", *Science and Technology of Nuclear Installations*, Vol. 2012, pp. 1-9, http://dx.doi.org/10.1155/2012/767096. [30]

Zeng, K. et al. (2019), "Uncertainty Quantification and Propagation of Multiphysics Simulation of the Pressurized Water Reactor Core", *Nuclear Technology*, Vol. 205/12, pp. 1618-1637, http://dx.doi.org/10.1080/00295450.2019.1580533. [31]

Annex A. Additional details for the contributors

Table A.1. Additional information about the submitted results of standalone neutronics cases for LWR-UAM Phase I benchmark.

Case	Establishment	Name(s) of Participant(s)	Lattice code	Core code	Calculation method	UQ method	NDL	VCM	Additional information
1	Nuclear and Industrial Engineering (NINE)	Baiocco Giorgio, Cherubini Marco, Petruzzi Alessandro	SERPENT 2	-	Monte Carlo	Deterministic	ENDF/ B-VI	SCALE 6.0	
2	Nuclear and Industrial Engineering (NINE)	Baiocco Giorgio, Cherubini Marco, Petruzzi Alessandro	SCALE 6.0	-	Deterministic	Deterministic	ENDF/ B-V	SCALE 6.0	
3	Hungarian Academy Of Sciences Centre For Energy Research (MTA EK)	István Panka, András Keresztúri	MULTICELL	-	Deterministic	Sampling	ENDF/ B-VI	SCALE 5.1	Only nuclear data
4	Hungarian Academy Of Sciences Centre For Energy Research (MTA EK)	István Panka, András Keresztúri	MULTICELL	-	Deterministic	Sampling	ENDF/ B-VI	SCALE 5.1	With manufacturing uncertainty
5	Hungarian Academy Of Sciences Centre For Energy Research (MTA EK)	István Panka, András Keresztúri	-	KIKO3D	Deterministic	Sampling	ENDF/ B-VI	SCALE 5.1	
6	Karlsruhe Institute of Technology (KIT)	L. Mercatali, V. Sanchez	XSDRNPM	-	Deterministic	Deterministic	ENDF/ B-VII.0	SCALE 6.1	-
7	VTT Technical Research Centre of Finland (VTT)	Maria Pusa	CASMO4	SIMULATE3	Deterministic	Deterministic/ Sampling	ENDF/ B-VI	SCALE 6.0	
8	Paul Scherrer Institut (PSI)	Mathieu Hursin, Olivier Leray, Hakim Ferroukhi, Alexander Vasiliev	CASMO-5MX	-	Deterministic	Sampling	ENDF/ B-VII.0	SCALE 5.1	
9	Nuclear Energy Corporation of South Africa (NECSA)	Suzanne Groenewald	NEWT	-	Deterministic	Deterministic (TSUNAMI)	ENDF/ B-VII.0	SCALE 6.1	
10	Nuclear Energy Corporation of South Africa (NECSA)	SA Groenewald, RH Prinslo and PM Bokov	-	MGRAC	Deterministic	Sampling	ENDF/ B-VI	SCALE 6.1	

Case	Establishment	Name(s) of Participant(s)	Lattice code	Core code	Calculation method	UQ method	NDL	VCM	Additional information
11	Universidad Politécnica de Madrid (UPM)	Óscar Cabellos, Chiara Ceresio, Jesús S. González, Carlos J. Díez	MCNP5	-	Monte Carlo	Deterministic (SUSD3D)	ENDF/ B-VII	SCALE 6.0	Only UO_2 isotopes nuclear data uncertainties
12	Universidad Politécnica de Madrid (UPM)	Nuria Garcia-Herranz, Ana Martínez-Campo	NEWT	-	Deterministic	Deterministic (TSUNAMI)	ENDF/ B-VII.0	SCALE 6.1	
13	Universidad Politécnica de Madrid (UPM)	Nuria Garcia-Herranz, Santiago Sanchez-Cervera, Emilio Castro	NEWT	-	Deterministic	Sampling (SAMPLER)	ENDF/ B-VII.1	SCALE 6.2	
14	Universidad Politécnica de Madrid (UPM)	Nuria Garcia-Herranz, Santiago Sanchez-Cervera, Emilio Castro	-	COBAYA	Deterministic	Sampling	ENDF/ B-VII.1	SCALE 6.2	Nodal diffusion without ADF
15	Universidad Politécnica de Madrid (UPM)	Nuria Garcia-Herranz, Santiago Sanchez-Cervera, Emilio Castro	NEWT	COBAYA	Deterministic	Sampling (SAMPLER)	ENDF/ B-VII.1	SCALE 6.2	Nodal diffusion with ADF
16	Universidad Politécnica de Madrid (UPM)	Nuria Garcia-Herranz, Santiago Sanchez-Cervera, Emilio Castro	NEWT	COBAYA	Deterministic	Sampling (SAMPLER)	ENDF/ B-VII.1	SCALE 6.2	Pin by Pin diffusion
17	Universidad Politécnica de Madrid (UPM)	Nuria Garcia-Herranz, Santiago Sanchez-Cervera, Emilio Castro	NEWT	COBAYA	Deterministic	Sampling (SAMPLER)	ENDF/ B-VII.1	SCALE 6.2	Nodal diffusion
18	McMaster University	Michael Tucker, David Novog	POLARIS	-	Deterministic	Sampling (SAMPLER)	ENDF/ B-VII.1	SCALE 6.2	
19	McMaster University	Michael Tucker, David Novog	NEWT	-	Deterministic	Sampling (SAMPLER)	ENDF/ B-VII.1	SCALE 6.2	
20	McMaster University	Michael Tucker, David Novog	NEWT	-	Deterministic	Sampling (SAMPLER)	ENDF/ B-VII.0	SCALE 6.2	
21	Japan Nuclear Regulation Authority (NRA)	Tatsuya Fujita	CASMO5	SIMULATE5	Deterministic	Sampling	JENDL-4.0	JENDL-4.0	
22	North-West University (NWU)	GP Nyalunga, VV Naicker	NEWT	-	Deterministic	Deterministic (TSUNAMI)	ENDF/ B-VII.0	SCALE 6.2	
23	North-West University (NWU)	GP Nyalunga, VV Naicker	NEWT	-	Deterministic	Sampling (SAMPLER)	ENDF/ B-VII.0	SCALE 6.2	
24	North-West University (NWU)	GP Nyalunga, VV Naicker	NEWT	-	Deterministic	Sampling (SAMPLER)	ENDF/ B-VII.0	SCALE 6.2	
25	Seoul National University (SNU)	Dong Hyuk Lee	McCARD	-	Monte Carlo	Deterministic	ENDF/ B-VII.1	ENDF/ B-VII.1	

Case	Establishment	Name(s) of Participant(s)	Lattice code	Core code	Calculation method	UQ method	NDL	VCM	Additional information
26	Ulsan National Institute of Science and Technology (UNIST)	Yunki Jo, Deokjung Lee	MCS	-	Monte Carlo	Deterministic	ENDF/B-VII.1	ENDF/B-VII.1	
27	Ulsan National Institute of Science and Technology (UNIST)	Yunki Jo, Deokjung Lee	MCS	-	Monte Carlo	Deterministic	ENDF/B-VII.1	SCALE 6.1	
28	Ulsan National Institute of Science and Technology (UNIST)	Yunki Jo, Deokjung Lee	MCS	MCS	Monte Carlo	Deterministic	ENDF/B-VII.1	ENDF/B-VII.1	
29	Ulsan National Institute of Science and Technology (UNIST)	Yunki Jo, Deokjung Lee	MCS	MCS	Monte Carlo	Deterministic	ENDF/B-VII.1	SCALE 6.1	
30	Ulsan National Institute of Science and Technology (UNIST)	Woonghee Lee, Deokjung Lee	STREAM	-	Deterministic	Deterministic	ENDF/B-VII.1	SCALE 6.2	
31	Ulsan National Institute of Science and Technology (UNIST)	Woonghee Lee, Deokjung Lee	STREAM	-	Deterministic	Deterministic	ENDF/B-VII.1	ENDF/B-VII.1	
32	Ulsan National Institute of Science and Technology (UNIST)	Woonghee Lee, Deokjung Lee	STREAM	-	Deterministic	Sampling	ENDF/B-VII.1	ENDF/B-VII.1	
33	Gesellschaft für Anlagen-und Reaktorsicherheit (GRS) gGmbH	-	NEWT	SCALE	Deterministic (for I-1, I-2) /Monte Carlo for (I-2 Exp, I-3)	Deterministic (TSUNAMI)	ENDF/B-VII.0	SCALE 6.1	
34	Gesellschaft für Anlagen-und Reaktorsicherheit (GRS) gGmbH	-	NEWT	SCALE	Deterministic (for I-1, I-2) /Monte Carlo for (I-2 Exp, I-3)	Deterministic (TSUNAMI)	ENDF/B-VII.1	SCALE 6.2	
35	Gesellschaft für Anlagen-und Reaktorsicherheit (GRS) gGmbH	-	HELIOS2	-	Deterministic	Sampling (XSUSA)	ENDF/B-VII.1	SCALE 6.1	
36	Gesellschaft für Anlagen-und Reaktorsicherheit (GRS) gGmbH	-	NEWT	SCALE	Deterministic (for I-1, I-2) /Monte Carlo for (I-2 Exp, I-3)	Sampling (XSUSA)	ENDF/B-VII.0	SCALE 6.1	
37	Gesellschaft für Anlagen-und Reaktorsicherheit (GRS) gGmbH	-	NEWT	SCALE	Deterministic (for I-1, I-2) /Monte Carlo for (I-2 Exp, I-3)	Sampling (XSUSA)	ENDF/B-VII.1	SCALE 6.2	

Case	Establishment	Name(s) of Participant(s)	Lattice code	Core code	Calculation method	UQ method	NDL	VCM	Additional information
38	Oak Ridge National Laboratory (ORNL)	Matthew Jessee, Mark Williams, Mark DeHart, Ron Ellis, Brad Rearden, Harold Smith, Doro Wiarda	NEWT/ TRITON (for I-1b)	SCALE	Deterministic	Deterministic (TSUNAMI) / Sampling (SAMPLER) for I-1b, I-3	ENDF/ B-VII / ENDF/ B-VI for I-1	SCALE 6.1	
39	JACOBS	G Alford, B Lindley	WIMS	-	Deterministic	Sampling (LHS)	JEFF-3.1.2	WIMS[1]	
40	Valencia Polytechnic University (UPV)	Antonella Labarile	NEWT	-	Deterministic	Sampling (SAMPLER)	ENDF/ B-VII.0	SCALE 6.2	
41	Valencia Polytechnic University (UPV)	Antonella Labarile	NEWT	-	Deterministic	Sampling (SAMPLER)	ENDF/ B-VII.1	SCALE 6.2	
42	JACOBS	Ben Lindley, Glynn Hosking	WIMS	PANTHER	Deterministic	Sampling (LHS)	JEFF-3.1.2	WIMS[1]	Only nuclear data uncertainties
43	JACOBS	Ben Lindley, Glynn Hosking	WIMS	-	Deterministic	Sampling (LHS)	JEFF-3.1.2	WIMS[1]	Nuclear data and enrichment uncertainties
44	JACOBS	Ben Lindley, Glynn Hosking	WIMS	-	Deterministic	Sampling (LHS)	JEFF-3.1.2	WIMS[1]	Nuclear data, enrichment and densities uncertainties
45	Tsinghua University (THU)	Kan Wang, Yishu Qiu, Guanlin Shi	-	RMC	Monte Carlo	Sampling	ENDF/ B VII.0	SCALE 6.2/6.1[2]	
46	North Carolina State University (NCSU)	Kaiyue Zeng, Jason Hou, Kostadin Ivanov	POLARIS	PARCS	Deterministic	Sampling	ENDF/ B-VII.1	SCALE 6.2	
47	North Carolina State University (NCSU)	Christopher Sedota, Scott Palmtag	MPACT	-	Deterministic	Sampling	ENDF/ B-VII.1	ENDF/ B-VII.1	
48	FRAMATOME GmbH	Carlos J. Díez, Oliver Buss, Axel Hoefer	TRITON	-	Deterministic	Sampling (NUDUNA)	ENDF/ B-VII.1	ENDF/ B-VII.1	Nuclear data uncertainties for selected fuel isotopes and fission products

[1]Covariance data were collected from various sources, including JEFF-3.2, ENDF/BV-II.1, JENDL-4.0 and TENDL-2011. For comparison purposes it will be considered as ENDF/B-VII.1.
[2]SCALE 6.2 is used for the PWR exercises and SCALE 6.1 for the BWR exercises.

Source: NEA data, 2021

Annex B. Phase I additional results

Table B.1. Results for k-inf in I-1 exercises

k-inf			SCALE 5.1		SCALE 6.0/6.1		SCALE 6.2		JENDL-4.0		ENDF/B-VII.1		Total	
			Mean	RSD	Mean	RSD	Mean	RSD	Mean	RSD	Mean	RSD	Mean	RSD
PWR	HZP		1.431	0.512%	1.428	0.474%	1.431	0.544%	1.432	0.502%	1.431	0.614%	1.430	0.529%
	HFP		1.413	0.522%	1.411	0.486%	1.414	0.552%	1.413	0.512%	1.415	0.638%	1.413	0.545%
BWR	HZP		1.346	0.556%	1.346	0.522%	1.348	0.579%	1.348	0.561%	1.347	0.514%	1.345	0.540%
	HFP		1.229	0.656%	1.231	0.611%	1.233	0.684%	1.2333	0.646%	1.233	0.533%	1.232	0.628%
VVER	HZP		1.350	0.579%	1.348	0.518%	1.349	0.573%	-	-	1.354	0.414%	1.349	0.530%
	HFP		-	-	1.330	0.527%	1.332	0.581%	-	-	1.338	0.409%	1.332	0.532%
GEN-III	HFP		1.108	0.948%	1.103	0.947%	1.109	0.607%	-	-	-	-	1.105	0.862%
KRITZ	21-Cold		1.244	0.610%	1.[238]	0.593%	1.240	0.662%	-	-	-	-	1.[239]	0.612%
	21-Hot		1.197	0.660%	1.192	0.643%	1.193	0.713%	-	-	-	-	1.193	0.665%
	213-Cold		1.273	0.560%	1.269	0.548%	1.270	0.617%	-	-	-	-	1.270	0.567%
	213-Hot		1.247	0.500%	1.241	0.578%	1.244	0.647%	-	-	-	-	1.242	0.586%
	219-Cold		1.285	1.140%	1.283	1.111%	1.283	0.668%	-	-	-	-	1.283	0.989%
	219-Hot		1.305	1.120%	1.300	1.107%	1.300	0.643%	-	-	-	-	1.301	0.976%

Source: NEA data, 2021

Table B.2. Results for *k*-inf in I-2 exercises

k-inf		SCALE 5.1		SCALE 6.0/6.1		SCALE 6.2		JENDL-4.0		ENDF/B-VII.1		Total	
		Mean	RSD	Mean	RSD	Mean	RSD	Mean	RSD	Mean	RSD	Mean	RSD
PWR	HZP Unr	1.412	0.506%	1.414	0.466%	1.418	0.540%	1.418	0.488%	1.416	0.617%	1.415	0.503%
	HZP Rod	-	-	1.079	0.493%	1.089	0.566%	1.080	0.494%	1.072	0.628%	1.080	0.525%
	HFP Unr	-	-	1.399	0.475%	1.403	0.536%	1.401	0.496%	1.398	0.562%	1.399	0.511%
	HFP Rod	-	-	1.064	0.502%	1.074	0.575%	1.063	0.504%	1.057	0.632%	1.064	0.533%
BWR	HZP Unr	-	-	1.108	0.505%	1.108	0.592%	1.110	0.583%	1.107	0.573%	1.108	0.544%
	HZP Rod	-	-	0.860	0.496%	0.864	0.587%	0.860	0.543%	0.862	0.548%	0.861	0.537%
	HFP Unr	-	-	1.079	0.544%	1.082	0.634%	1.081	0.591%	1.079	0.575%	1.080	0.570%
BWR	HFP Rod	-	-	0.790	0.581%	0.795	0.686%	0.784	0.590%	0.795	0.590%	0.791	0.614%
VVER	HZP Unr	1.306	0.570%	1.343	0.499%	1.335	0.564%	-	-	-	-	1.332	0.536%
	HZP Rod	1.040	0.549%	1.022	0.500%	1.020	0.581%	-	-	-	-	1.024	0.536%
	HFP Unr	-	-	1.328	0.507%	1.330	0.576%	-	-	-	-	1.328	0.530%
	HFP Rod	-	-	1.008	0.509%	1.005	0.590%	-	-	-	-	1.007	0.541%
GEN-III	T1 Unr	-	-	1.048	0.563%	1.049	0.642%	-	-	-	-	1.048	0.600%
	T2 Unr	-	-	1.126	0.494%	1.127	0.575%	-	-	-	-	1.126	0.526%
	T3 Unr	-	-	0.960	0.531%	0.960	0.626%	-	-	-	-	0.960	0.569%
	T4 Unr	-	-	1.115	0.937%	1.118	0.578%	-	-	-	-	1.116	0.793%
KRITZ	21-Cold	-	-	0.996	0.576%	0.996	0.625%	-	-	-	-	0.996	0.601%
	21-Hot	-	-	0.992	0.589%	0.994	0.644%	-	-	-	-	0.993	0.616%
	213-Cold	-	-	0.998	0.532%	0.999	0.589%	-	-	-	-	0.998	0.561%
	213-Hot	-	-	0.996	0.561%	0.997	0.617%	-	-	-	-	0.996	0.589%
	219-Cold	-	-	1.000	1.167%	1.000	0.721%	-	-	-	-	1.000	0.944%
	219-Hot	-	-	1.001	1.164%	1.000	0.721%	-	-	-	-	1.001	0.943%

Source: NEA data, 2021

Table B.3. Results for k-inf of minicore coloursets in I-2 exercises

k-inf		SCALE 5.1		SCALE 6.0/6.1		SCALE 6.2		JENDL-4.0		ENDF/B-VII.1		Total	
		Mean	RSD	Mean	RSD	Mean	RSD	Mean	RSD	Mean	RSD	Mean	RSD
PWR	HZP	-	-	1.386	0.458%	1.389	0.528%	1.389	0.486%	-	-	1.387	0.486%
	HFP	-	-	1.370	0.464%	1.373	0.534%	1.371	0.494%	-	-	1.371	0.492%
BWR	HZP	-	-	0.994	0.491%	0.996	0.584%	0.995	0.561%	-	-	0.995	0.532%
	HFP	-	-	0.946	0.541%	0.947	0.642%	0.942	0.580%	-	-	0.945	0.576%

Source: NEA data, 2021

Table B.4. RSD results for νΣf in I-2 exercises at HFP and unrodded conditions (except VVER, which is HZP and unrodded)

?Sf	SCALE 5.1		SCALE 6.0/6.1		SCALE 6.2		JENDL-4.0		ENDF/B-VII.1		Total	
	Fast	Thermal	Fast	Thermal	Fast	Thermal	Fast	Thermal	Fast	Thermal	Fast	Thermal
PWR	-	-	0.541%	0.455%	0.619%	0.492%	0.547%	0.458%	0.907%	0.737%	0.670%	0.553%
BWR	-	-	0.979%	0.448%	1.318%	0.500%	1.018%	0.458%	-	-	1.042%	0.457%
VVER	-	-	0.692%	0.448%	0.903%	0.495%	-	-	-	-	0.798%	0.472%
GEN-III T4	-	-	0.801%	1.069%	0.487%	0.654%	-	-	-	-	0.696%	0.931%

Source: NEA data, 2021

Table B.5. RSD results for diffusion coefficient D in I-2 exercises at HFP and unrodded conditions (except VVER, which is HZP and unrodded)

D	SCALE 5.1		SCALE 6.0/6.1		SCALE 6.2		JENDL-4.0		ENDF/B-VII.1		Total	
	Fast	Thermal	Fast	Thermal	Fast	Thermal	Fast	Thermal	Fast	Thermal	Fast	Thermal
PWR	-	-	1.590%	0.187%	2.623%	0.295%	1.848%	0.341%	2.158%	0.324%	1.923%	0.262%
BWR	-	-	1.668%	0.209%	2.525%	0.310%	1.753%	0.345%	-	-	1.825%	0.249%
VVER	-	-	2.034%	0.225%	2.496%	0.301%	-	-	-	-	2.265%	0.263%
GEN-III T4	-	-	2.149%	0.202%	2.425%	0.249%	-	-	-	-	2.241%	0.218%

Source: NEA data, 2021

Table B.6. Results for *k*-inf in I-3 exercises

k_{eff}	SCALE 5.1		SCALE 6.0/6.1		SCALE 6.2		JENDL-4.0		ENDF/B-VII.1		Total	
	Mean	RSD	Mean	RSD	Mean	RSD	Mean	RSD	Mean	RSD	Mean	RSD
PWR	-	-	1.006	0.459%	1.002	0.517%	1.007	0.469%	1.006	0.701%	1.004	0.526%
BWR	-	-	0.978	0.507%	-	-	0.974	0.585%	0.981	0.592%	0.977	0.562%
VVER	1.001	0.555%	-	-	-	-	-	-	-	-	1.001	0.555%
GEN-III UOX	-	-	1.008	0.508%	1.010	0.589%	-	-	-	-	1.009	0.548%
GEN-III UOX/MOX	-	-	1.005	0.489%	1.007	0.534%	-	-	-	-	1.006	0.511%
B&W PWR	-	-	0.997	0.450%	0.998	0.521%	-	-	-	-	0.997	0.479%
LR0-VVER	-	-	1.004	0.543%	1.004	0.586%	-	-	-	-	1.004	0.565%

Source: NEA data, 2021